THÈSE

Pour obtenir le grade de

Docteur

l

Délivré par l'Université de Montpellier

Préparée au sein de l'école doctorale SPSA
Et de l'unité de recherche UMR IATE

Spécialité: Biochimie, chimie et technologie des aliments

Présentée par Guilherme DE OLIVEIRA REIS

Study of the mechanism of acid coagulation of *Hevea* latex and of the rheological properties of resulting gels

Soutenue le 10/12/2015 devant le jury composé de

Mr. Christophe CHASSENIEUX, Professeur, Université du Maine	Rapporteur
Mr. Fréderic PIGNON, Directeur de recherche, CNRS Grenoble	Rapporteur
Mr. Giuseppe FOFFI, Professeur, Université Paris-Sud	Examinateur
Mr. Frédéric BONFILS, Chercheur, CIRAD	Directeur de thèse
Mr. Christian SANCHEZ, Professeur, Université de Montpellier	Directeur de thèse
Mr. Paul MENUT, Maître de conférence, Montpellier Supagro	Encadrant de thèse

Study of the mechanism of acid coagulation of *Hevea* latex and of the rheological properties of resulting gels

by

Guilherme DE OLIVEIRA REIS

Mr. Christophe CHASSENIEUX, Professor, Université du Maine	*Reporter*
Mr. Fréderic PIGNON, Research director, CNRS Grenoble	*Reporter*
Mr. Giuseppe FOFFI, Professor, Université Paris-Sud	*Examiner*
Mr. Frédéric BONFILS, Researcher, CIRAD	*Thesis director*
Mr. Christian SANCHEZ, Professor, Université de Montpellier	*Thesis director*
Mr. Paul MENUT, Ass. professor, Montpellier Supagro	*Supervisor*

2015, December 10

Abstract

Natural rubber latex is mainly composed by rubber particles whose core is made of *cis*-1,4-polyisoprene and the shell of non-isoprene compounds. It stability in the tree is provided by the negative charge of the shell due to the presence of proteins and lipids. Natural rubber latex coagulates after acidification to form a colloidal gel that is the first step of its transformation into natural rubber.

In this PhD thesis, we studied this acid-induced aggregation and gelation and the properties of the resulting gels. For this, a commercial natural rubber latex composed by rubber particles (1 µm in diameter), was used. Aggregation was induced by hydrolysis of a compound called glucono-delta-lactone (GDL). The aggregation was followed by different techniques based on light scattering (turbidimetry, DWS, SLS). Gelation was followed *in situ* by rheology. Then, the rheological properties of colloidal gels formed at pH 4 were characterized in the linear and non-linear regimes.

Dependence to the volume fraction and the pH of the onset of aggregation was observed. The non-redispersion of aggregates proves the strong interactions between rubber particles. Three different state behaviors (stable solution, phase separation and gel) can be predicted from a state diagram pH-volume fraction that was established over 5 weeks. The gel state exhibited a fractal structure, characterized by a power law relationship between the elastic modulus *G'* and the volume fraction. At high deformations, an irreversible reorganization under stress resulted in an irreversible strain hardening of the material. We observed by rheo-ultrasound that above 50 % deformation, a homogenous destructuration occurred in the gel.

Keywords: natural rubber latex, aggregation, fractal colloidal gel, irreversible strain hardening

Résumé

Le latex d'*Hevea brasiliensis* est composé principalement de particules de caoutchouc dont le noyau est constitué de *cis*-1,4-polyisoprène et la membrane de composés dit non-isoprène. Sa stabilité dans l'arbre est assurée par les charges négatives de la membrane en raison de la présence de protéines et de lipides. Le latex d'*Hevea brasiliensis* coagule après acidification pour former un gel colloïdal qui est la première étape de sa transformation en caoutchouc naturel.

Dans cette thèse, nous avons étudié l'agrégation et la gélification induite par ajout d'un acide et les propriétés des gels obtenus. Pour cela, un latex de caoutchouc naturel commercial constitué par des particules de caoutchouc (1 µm de diamètre), a été utilisé. L'agrégation a été induite par l'hydrolyse d'un composé appelé glucono-delta-lactone (GDL). Cette agrégation a été suivie par différentes techniques basées sur la diffusion de la lumière (turbidimétrie, DWS, SLS). La gélification a été suivie *in situ* par rhéologie. Ensuite, les propriétés rhéologiques de gels colloïdaux formés à pH 4 ont été caractérisées dans les régimes linéaires et non-linéaires.

La dépendance à la fraction volumique et le pH d'apparition de l'agrégation ont été observé. La non-redispersion des agrégats montre les interactions fortes entre les particules de caoutchouc. Trois état différents (solution stable, séparation de phase et gel) peuvent être prédits à partir d'un diagramme d'état fraction volumique-pH qui a été établi sur une durée de 5 semaines. L'état de gel présente une structure fractale, caractérisée par une relation de loi de puissance entre le module élastique *G'* et la fraction volumique. Pour des fortes déformations, une réorganisation irréversible sous contrainte a abouti à un durcissement irréversible du matériau. Nous avons observé par rheo-ultrasons qu'au-dessus de 50 % de déformation, une déstructuration homogène se produit dans le gel.

Mots-clés: latex d'*Hevea*, agrégation, gel colloidal fractal, durcissement irréversible

Contents

List of figures

Chapter 1 State of the art

Chapter 2 Materials & Methods

Chapter 3 Acid-induced aggregation and gelation of natural rubber particles

Chapter 4 Irreversible restructuration of natural rubber latex gels during hardening under stress

Chapter 5 Gelation under an oscillatory shear: influence of the strain amplitude on the structural properties

Chapter 6 Discussion & Conclusions

Introduction

Natural rubber latex is extracted from *Hevea brasiliensis* tree, and is mainly produced in Southeast Asia, which represents 95 % of the global production (Vaysse *et al.* 2012; Ngo Kinh 2013). Natural rubber is an important social-economic issue in the producing countries. For example, in Thailand more than 7 million peoples depend on this culture, which represents around 10 % of the population, plantations being essentially family farms. In the recent years, the number of *Hevea* plantations increased, which generated an environmental risk due to the replacement of other plantations and virgin forests.

Items made from natural rubber and natural rubber latex have been used since decades. They are present in different products such as, for instance, tires, gloves and condoms. Tires are the most important market, and represent about 70 % of the natural rubber market. In recent decades, natural rubber accounts for over 41 % of global elastomer consumption despite the development of synthetic counterparts (Vaysse *et al.* 2012). These synthetics elastomers, obtained from petrochemical industry, cannot replace natural rubber in many applications, as in aircraft tires which still must be composed predominantly of natural rubber. Indeed, natural rubber exhibit unique properties such as high elasticity, high resistance to deformation and fracture, low heat build-up and slower crack propagation. These exceptional properties are attributed to the existence of a complex associative structure, not yet precisely determined, formed between the polyisoprene chains and the others natural compound (Tanaka 2001; Vaysse *et al.* 2009). These compounds, called non-isoprene, are mainly proteins, lipids, sugars and minerals (Wititsuwannakul 2001).

Natural rubber latex is composed by rubber particles and non-isoprene compounds suspended in an aqueous phase. These rubber particles are composed by a core of *cis*-1.4-polyisoprene and a mixed monolayer membrane composed mostly by proteins and lipids (Blackley 1996; Cornish *et al.* 1999; Nawamawat *et al.* 2011; Berthelot *et al.* 2014). Negatively charged at a native pH 7 in the tree, the rubber particles will aggregates when the pH of the suspension decreases. Depending on the grade of natural rubber, this could be caused by the action of bacteria, in “natural coagulation”, or by addition of a weak acid, in “acid coagulation”. The coagulation is anyway the first step of transformation of the latex into natural rubber, a dense *cis*-1.4-polyisoprene network, obtained after several mechanical transformations and drying of the coagulated latex.

Although natural rubber latex is used to make different products for over a century, dynamics of its structuration over the various processing steps involved in its transformation in rubber are still unclear. This structuration, from the tree until final products, occurring at different scales (micro, meso and macro) and will affect the properties of the final material. Since many decades, biochemical approaches were used to follow the transformation of the different compounds of the latex and their impact on the final properties of the natural rubber. However, the structure of the colloidal gel (resulting from the coagulation) and its impact on the natural rubber properties was never studied before.

In the last decade**,** there have been several advances in the study of turbid suspensions and the formation of gels, especially in the field of soft matter physics, resulting in a better description of their rheological response and links to their structure. In this PhD work, we used such approach from the physics of colloidal systems to investigate the formation of natural rubber latex gels and their viscoelastic properties. Our aim was to identify and characterize the structuration of the network of rubber particles during an acid-induced gelation of a commercial natural rubber latex. We used mostly light scattering and rheology to characterize aggregation, gelation and the final viscoelastic properties of the network formed by particles percolation. With an initial average size of rubber particles centered at 1 µm, the system is colloidal, but the aggregation rapidly result in the formation of clusters which larger dimension suggest a granular-like behavior.

This manuscript is divided in 6 chapters:

Chapter 1 – this chapter presents a **state of the art** divided into three main parts. First, a presentation of the raw material used for this study, with a focus on the origin, composition and properties of natural rubber and natural rubber latex. Second, an introduction about the behavior of colloidal systems studied in terms of interactions, aggregation and gelation. Third, we develop a focus about rheological measurements of the viscoelastic behavior.

Chapter 2 – this chapter presents the **materials and methods** used during this work, with a focus on the light scattering and rheological methods. The materials and methods used in chapter 3, 4 and 5 are completed in their own section.

Chapter 3 – in this chapter, we study the **early stages of the aggregation and then the gelation of natural rubber latex**. For this, we used a combination of light scattering techniques to determine the onset of aggregation in a large range of volume fraction ($1.0x10^{-4}$ to $2.0x10^{-1}$). **A state diagram pH-volume fraction** has then established and its time-dependence characterized. In this state diagram, **three different states** were observed: *i*) **stable suspension**, *ii*) a **macroscopic phase separation** between a suspension and *iii*) a **gel**. The viscoelastic properties of the gels formed at pH 4 demonstrated a typical **fractal colloidal gel** behavior.

Chapter 4 – in this chapter, we focus on the rheological characterization of the gels. **The viscoelastic properties were characterized in the linear and non-linear regimes**. In the latter, we evidenced an **original irreversible strain hardening** that we attributed to an **internal reorganization** inside the gel. Moreover, a **critical oscillatory strain** was determined: **if submitted to higher strains**, the network is **progressively degrade** as evidence by a continuous elastic modulus decrease, and eventually brake.

Chapter 5 – in this chapter, we evaluated the **effect of an oscillatory strain imposed during the gelation on the final structure of the gel**. **Four different regimes** were observed **depending on the strain amplitude**. In regime I, corresponding to the **lower strains values**, the viscoelastic properties **were unchanged**. In regime II, for strain values **superior to 10 % a hardening** was observed during gelation, which amplitude was equivalent to in the one

described in chapter 4 for similar strain values. For oscillatory strain higher than the **critical strain of 50 %** identified in chapter 4, a different behavior was observed: when gelation is conducted under an oscillatory strain, **materials first harden and then progressively degrade**. In this regime, material lost their strain hardening behavior. Finally, in regime IV, macroscopically heterogeneous gels were formed.

Chapter 6 – In this last chapter, a **general discussion of the results** and a comparison with those reported in the literature with other types of colloidal gels was done. Moreover, the **conclusions** of this thesis and the **perspective** of this work are also discussed.

References

Berthelot, K., *et al.* (2014). "Hevea brasiliensis REF (Hev b 1) and SRPP (Hev b 3): An overview on rubber particle proteins." Biochimie **106**(0): 1-9.

Blackley, D. C. (1996). Polymer Latices: Science and Technology. London, Chapman & Hall.

Cornish, K., *et al.* (1999). "Rubber particles from four different species, examined by transmission electron microscopy and electron-paramagnetic-resonance spin labeling, are found to consist of a homogeneous rubber core enclosed by a contiguous, monolayer biomembrane." Planta **210**(1): 85-96.

Nawamawat, K., *et al.* (2011). "Surface nanostructure of Hevea brasiliensis natural rubber latex particles." Colloids and Surfaces A: Physicochemical and Engineering Aspects **390**(1–3): 157-166.

Ngo Kinh, L. (2013). Natural rubber industry report 2013, Fpt Securities: Vietnam.

Tanaka, Y. (2001). "Structural characterization of natural polyisoprenes: Solve the mystery of natural rubber based on structural study." Rubber Chemistry and Technology **74**(3): 355-375.

Vaysse, L., *et al.* (2012). Natural rubber in Polymer Science: A Comprehensive Reference. Amsterdam, Elsevier BV.

Vaysse, L., *et al.* (2009). Natural Rubber in Sustainable Solutions for Modern Economies,Coord. Dr Rainer Höfer, The Royal Society of Chemistry. Cambridge, UK**:** 339-367.

Wititsuwannakul, D. a. W., R. (2001). Biochemistry of Natural Rubber and Structure of Latex. Weiheim, Germany.

Chapter 1

State of the art

1.1 Natural rubber latex and natural rubber

Originally from Amazonian forest but mainly produced in Southeast Asia (94 % of world production), natural rubber latex (NRL) and natural rubber (NR) are widely used in many everyday products around the world. It represents more than 41 % of the elastomer market. Gloves, condoms, anti-vibration parts, vehicle (car, bus, truck) tires are made, at least partly, from natural rubber latex or natural rubber. The tires industry remains the major consumer of NR and represent more than 75 % of the total consumption (Vaysse *et al.* 2012). The consumption of NR increased in last year's with a demand of 12.15 million tons in 2014. It is expected to reach 16.5 million tons in 2023 according the International Rubber Study Group (IRSGReport 2015).

Despite the fact that the natural rubber latex can be obtained from other plant sources, such as *Taraxacum brevicorniculatum* (Dandelion), *Parthenium argentatum* (Guayule), *Euphorbia lactiflua* and *Ficus elastica*, it is mainly extracted from the *Hevea brasiliensis* tree (Mooibroek and Cornish 2000). When the tree bark is tapped, it defends itself by flowing a white liquid named latex. The natural rubber is obtained after several transformation of the natural rubber latex as shown in Figure 1.1. NRL can be collected in liquid or solid states. The solid state (Intapun *et al.* 2010) is obtained either by controlled coagulation (acid-induced coagulation) or by natural coagulation (the latex coagulate naturally in the cup) (Figure 1.1). The controlled coagulation is made by addition of a weak acid such as acetic acid or formic acid (Blackley 1996). Instead, the natural coagulation results from the action of microorganism. A colloidal gel is then obtained from the latex by the percolation of the particle-particle aggregates.

To avoid the natural aggregation of the NRL and collect it in its liquid state, an ammonia (NH_3) solution is added to rise the pH of the suspensions. This liquid latex can be concentrated, after addition of a supplemental dose of ammonia, to prepare the different types of systems used in gloves industry. The latex can be concentrated by different techniques: evaporation, creaming, electrodecantation or centrifugation (Blackley 1996). However, the centrifugation is the most widely used. The latex is stabilized by addition of ammonia and concentrated to around 60 %wt. The concentrated latex can be classified, depending on the amount of ammonia added, in high ammonia latex or low ammonia latex with $NH_3 > 0.6$ % and < 0.3 %, respectively.

Once the latex is coagulated, the NRL colloidal gel is subjected to a succession of mechanical stresses to prepare the dry forms of commercial dry NR (Figure 1.1). Dry NR sheets are obtained after drying sheets with hot air or smoke (Figure 1.1). Other types of commercial dry natural rubbers, especially the technically specified rubber (TSR) or crumb rubber, are obtained mostly from natural coagulation. The coagula are pressed to remove water and processed through various equipments. The TSR and the NR sheets (mainly Ribbed Smoked Sheet (RSS)) are the most important products with around 70 % and 20 % of the world production, respectively. These solid products represent about 90 % of the market while the concentrated latex represents the remaining. The latex composition, the processing and other factors (season, *Hevea brasiliensis* genotypes, etc.) influence the final properties of the natural rubber. A dynamic structuration occurs during the processing and the storage of the natural rubber. Indeed, the amount of non-isoprene compounds decreases during the processing but remains a key parameter in the structuring of raw NR.

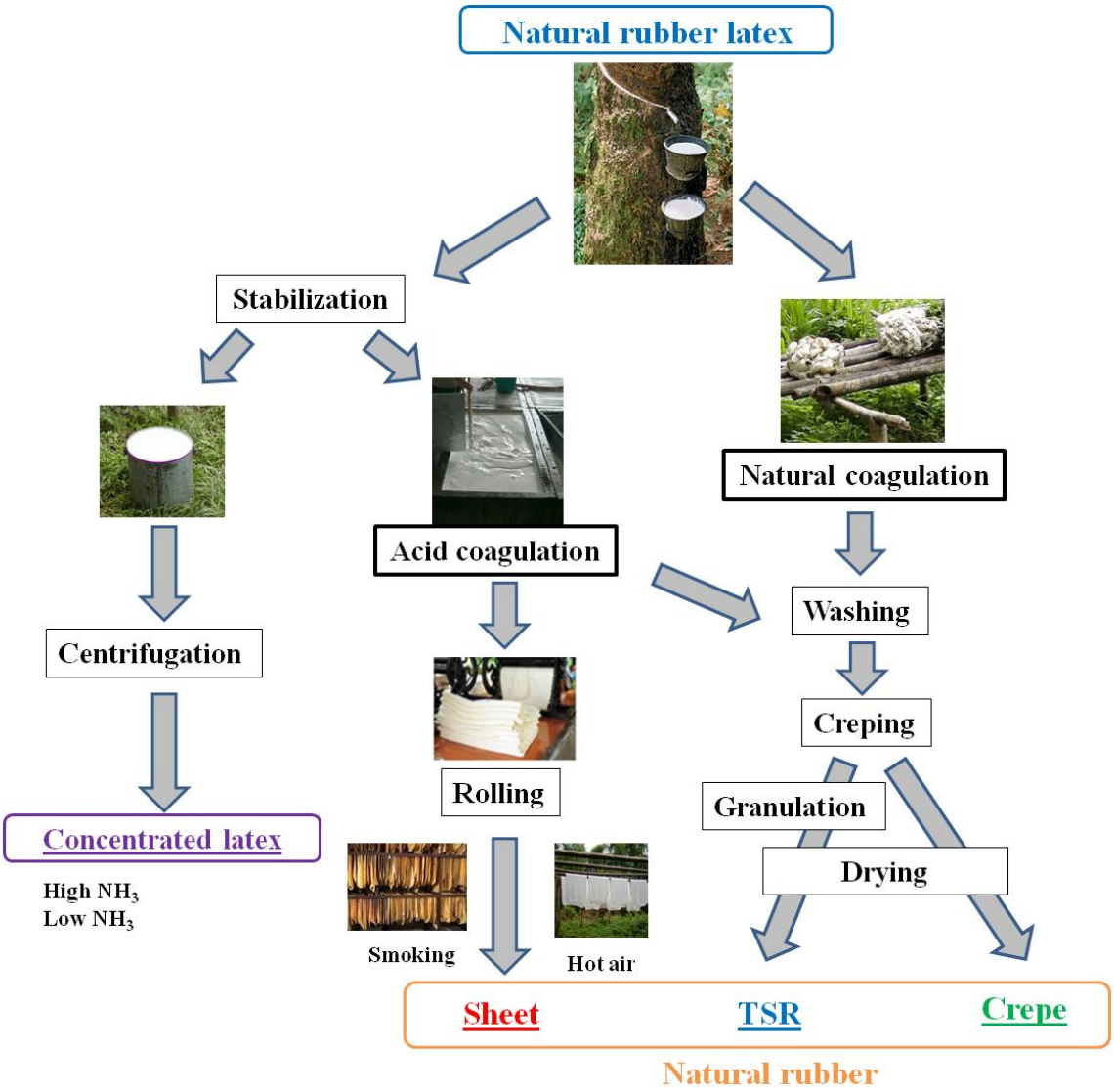

Figure 1.1: Illustration of the processing to obtain concentrated latex and the main natural rubber commercial forms. Pictures made by the rubber team of CIRAD.

1.1.1 Natural rubber latex (NRL)

The NRL is a complex suspension composed by 30-45 %wt of *cis*-1,4-polyisoprene particles and by 5-6 %wt of non-isoprene compounds, both suspended in an aqueous phase, called serum phase (Jacob *et al.* 1993; Wititsuwannakul 2001). Other intrinsic particles formed by non-isoprene compounds such as lutoids and Frey Wyssling particles and extrinsic particles like bacteria or yeast, are also present in suspensions (Southorn 1960). The non-isoprene compounds present in the latex are proteins, lipids, carbohydrates, minerals, and others. The average composition of the natural latex and dry natural rubber are shown in Table 1.1. Some non-isoprene compounds are removed during processing but some are still present in the dry rubber. The composition varies according to several natural parameters such as season, age of the tree, the genotype (clones), etc.

Different clones of *Hevea brasiliensis* obtained from several breeding programs using controlled pollination exist. The composition and final properties of raw NR change depending on the type of clone (Wisunthorn *et al.* 2012). However, end-use products made from NR are obtained from raw NR from a mix of different clones.

The stability of latex is provided by the repulsion of negatives charged surrounding the particles (Ho *et al.* 1996; Sansatsadeekul *et al.* 2011). This repulsion avoids the adhesion between the particles. The native pH of field latex is around 7 with a density between 0.9 and 0.98 (Blackley 1996). If the isoelectric pH (pH_i) is reached, the repulsion forces between particles decrease. The pH_i of the NRL particles is estimated to be between 4 and 4.7 (Ho *et al.* 1996). However, if a chemical treatment is performed in the NRL, the pH_i decreases due to the changes in membrane composition (Ho 1989). Furthermore, the pH_i decreases with the storage of the NRL (Ho 1989).

The coagulation (destabilization) can occur for many reasons, the main one being a decrease of the pH of the latex promoting particle-particle aggregation. Other mechanisms were proposed to explain latex coagulation: *i*) the neutralization of anions on the particle membrane (liberated by hydrolysis of some lipid compounds) and the divalent cations Mg^{2+} or Ca^{2+} (present in the latex) or *ii*) formation of links between particles due to the action of *hevein* protein present in the latex (Gidrol *et al.* 1994).

Table 1.1 - NRL and NR average composition

	NRL (%w/w)[a]	**Dry NRL (%w/w)[b]**	**NR (%w/w)[c]**
***cis*-1,4 polyisoprene**	~30-45	~87	94
Lipids	~1.5	~3.2	~3.4
Proteins	~1.5	~3.7	~2.2
Others	< 2	~4	< 1

a: (Wititsuwannakul 2001) b: calculated from a and c: (Sainte Beuve J. 2006)

1.1.2 Rubber particles

Rubber particles are of core-shell type with a core of polyisoprene and a complex membrane composed of lipids and proteins charged negatively at native pH (Ho *et al.* 1996). Particles display high polydispersity with diameters comprised between 0.2 and 1 µm (Wood and Cornish 2000). The thickness of the membrane was estimated between 1 – 20 nm according to the different authors (Nawamawat *et al.* 2011; Gaboriaud *et al.* 2012; Rochette *et al.* 2013). Around 20-30 % of proteins and most of the lipids present in the latex are localized in this complex membrane. Recently, the presence of 186 different proteins on the rubber particles was demonstrated (Dai *et al.* 2013). Moreover, the presence of two principal proteins present on the membrane, the small rubber particles proteins (SRPP) and the rubber elongation factor (REF) was reported. Both proteins are described as co-factors of the biosynthesis of the natural rubber latex (Berthelot *et al.* 2014). The lipids in the latex are neutral lipids (around 50

%), glycolipids (around 25 %), and phospholipids (around 25 %) (Hasma and Subramaniam 1986; Liengprayoon *et al.* 2011). Today, the nature and the organization of the lipids and proteins on the membrane are still on debate. Some authors proposed a membrane organized in mixed monolayers and others in a double layer (Cornish *et al.* 1999; Wood and Cornish 2000; Nawamawat *et al.* 2011; Gaboriaud *et al.* 2012; Rochette *et al.* 2013). Blackley *et al.* (Blackley 1996) proposed a double layer membrane with a lipid layer around the core of rubber particle and an external layer of proteins (Figure 1.2a). This external proteins layer was also proposed for particles from the *Parthenium argentatum* latex (Cornish *et al.* 1999). Later, with the evolution of the measurement techniques, new models were proposed. Nawamawat *et al.* (Nawamawat *et al.* 2011), using atomic force microscopy and confocal microscopy, proposed a rubber particle surrounded by a mixed layer of lipids and proteins under the form of patches (Figure 1.2b). Rochette *et al.* (Rochette, Crassous et al. 2013) proposed a stratified layer of proteins and lipids around the rubber particles using electrokinetic measurements and transmission electron microscopy (Figure 1.2c).

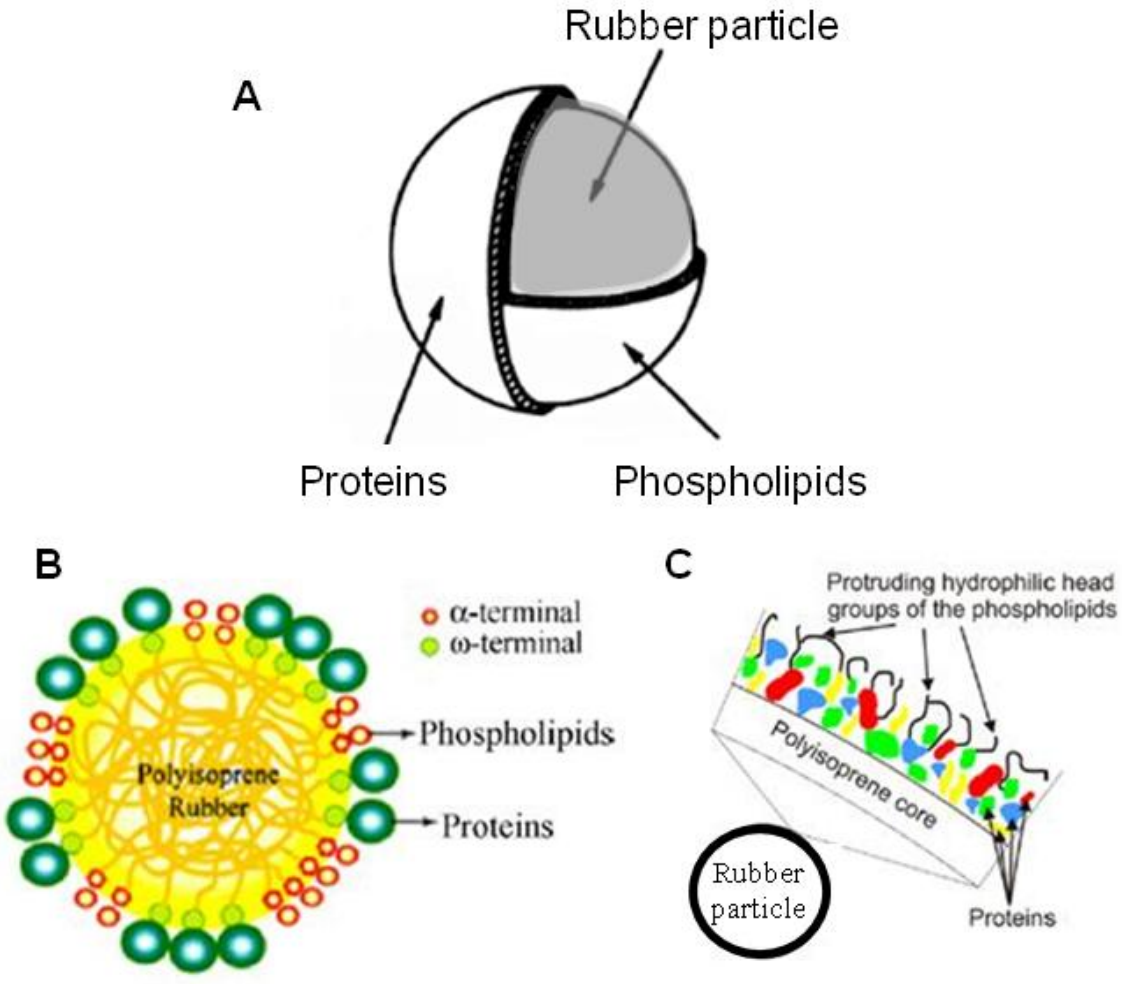

Figure 1.2: Three different propositions of organization of the membrane on the rubber particles in natural rubber latex proposed by (a) Blackley *et al.*, (b) Nawamawat *et al.* and (c) adapted from Rochette *et al.*

Recently, the presence of two main proteins, namely small rubber particles proteins (SRPP) and rubber elongation factor (REF), on these complex membrane was proposed using different biophysical techniques (Berthelot *et al.* 2014). Moreover, Hillebrand *et al.* (Hillebrand *et al.* 2012) proposed that SRPP would play a role in stability of rubber particles towards aggregation for the *Taraxacum brevicorniculatum* (Dandelion) latex. Concerning *Hevea brasiliensis* latex, it was demonstrated a dependence of the nature and organization of the membrane with the size of the rubber particles (Berthelot *et al.* 2014). Firstly, the SRPP is usually present in the small rubber particles membrane and the REF in the largest rubber particles as shown in Figure 1.3. Secondly, they proposed a double layer membrane with the SRPP adsorbed on a monolayer of lipids while the REF would be inserted in the monolayer of lipids.

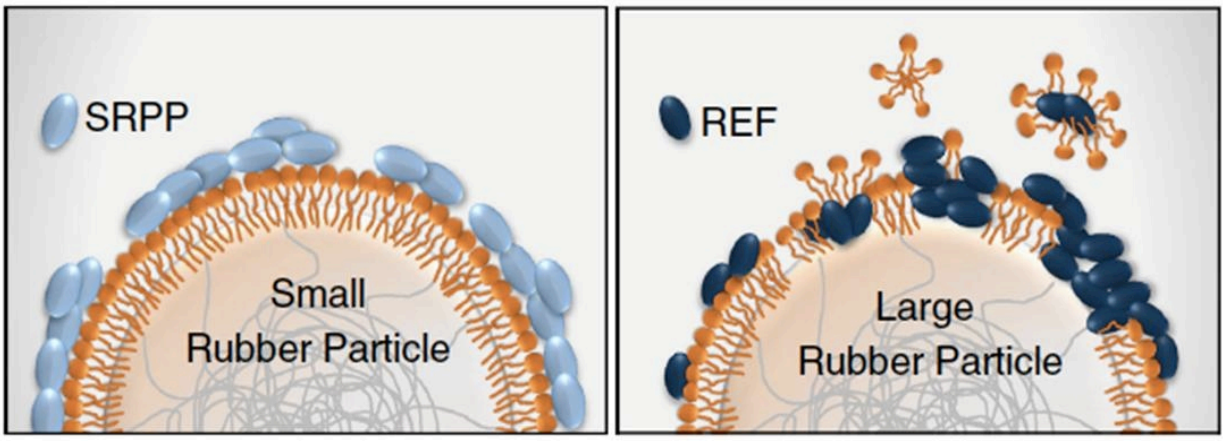

Figure 1.3: Illustration of the models of small (left) and large particle (right) proposed by (Berthelot *et al*. 2014). In light blue: SRPP and in dark blue: REF. In orange: the lipids.

In addition, chemical modifications in the latex can change the nature of the membrane. Liberation of fatty acids when the ammonia is added to the natural rubber latex was demonstrated (Blackley 1996). Then, changes in the electrokinetic properties of natural rubber latex with chemical modifications were demonstrated (Ho, Kondo et al. 1996). In this study, they proposed that for ammonia natural rubber latex, after chemical modifications the membrane contains 86 % of free fatty acids and 14 % of proteins.

1.1.3 Natural rubber (NR)

The natural rubber is still irreplaceable in many areas due to its unique properties such as high elasticity, strain-induced crystallization, low heat build-up at high temperature, high tack and high green strength (Vaysse *et al.* 2009). These unique properties would be related to the specific associative structure of NR due to links between the polyisoprene chains and certain non-isoprene compounds (Vaysse *et al.* 2009). The presence of the bonds formed between the polyisoprene chains and these non-isoprene compounds is demonstrated by the formation of an insoluble macroscopic gel or “macrogel”, chemical and physical, when the NR is dissolved in a good solvent for polyisoprene (Tarachiwin *et al.* 2005; Kim *et al.* 2008; Tanaka and

Tarachiwin 2009; Wisunthorn *et al.* 2012). The presence of this macroscopic gel is correlated with the physical properties of natural rubber (Bonfils *et al.* 2005; Ehabé *et al.* 2005).

In order to obtain end-use products, like tires, the NR is cured, or vulcanized, by addition of vulcanizing agent such as sulfur and other additives. Thereafter, the formation of sulfur links between the polyisoprene chains takes place and increases the mechanical properties. However, vulcanization can be done directly with the concentrated latex in liquid state (Blackley 1996). This treatment, namely pre-vulcanization, would generate sulfur-polyisoprene links inside the rubber particles. In this treatment, the latex is heated with a sulfur dispersion, one or more vulcanization accelerators and in most cases zinc oxide. The advantage is that the pre-vulcanization is carried out at lower temperatures than those for vulcanization of raw dry NR.

1.2 Colloidal suspensions

A colloidal system is a mixture consisting of at least one dispersed phase into a suspending medium, the dispersed phase being characterized by a size ranging from a few nm to a few µm. Depending on the nature of both phases, the colloids can be separated into different groups. If the dispersed phase is liquid, it is called an emulsion, and if the dispersed phase is solid it is called a suspension.

In general, colloidal systems are not monodisperse but polydisperse and exhibit a range of sizes that can be approximated by for instance a Gaussian distribution. Depending on the nature or physicochemical conditions, the shapes of colloidal particles can be spherical, ellipsoidal, rod-like, disc-like, etc. Latex and emulsions contains spherical particles while some proteins and viruses present a non-spherical shape. To measure particles size, optical techniques can be used despite the resolution limit. The electron or confocal microscopy techniques can be used to observe directly the particles (Shaw 1992). The static and dynamic light (SLS, DLS), X-ray (SAXS) or neutron scattering techniques (SANS) are also used to estimate the particle size and shape from the scattered intensity at small angles (Hamley 2013).

Colloidal particles diffuse in a liquid *via* Brownian motion throughout all the space. For particles larger than 100-500 nm, the gravitational force can become significant and can cause sedimentation or creaming depending on the density difference between phases. In addition, for the complete characterization of a colloidal suspension, interactions with other particles should also be considered as it can result in their aggregation.

1.2.1 Interactions in colloidal suspensions

The stability of colloids is very important in the conception of many products used every day such as foods, paints, cosmetic or pharmaceutical products. For example, the stability of beer is important to avoid changes in the sensory characteristics like flavor, foam consistency or color. The different interactions between dispersed (particles) and dispersion (medium) phases are one of the critical points determining the behavior and stability of colloids. These interactions that control the properties of the colloid depend on the number of particles and their distance. The physical and chemical properties will impact those interactions. For colloidal dispersion, several interactions exist such as the repulsion between the double layers, attractive Van der Walls interactions.

For charged particles, the electric double layer is a high ionic density zone formed around each colloidal particle immersed in a liquid, and is illustrated in Figure 1.4. An electric double layer is formed by two zones of different ion densities around the colloid: *i*) the Stern layer, closest to the particle, positively charged (when the surface of the colloidal particle is negatively charged) or negatively charged (when the surface of the colloidal particle has a positive charge) comprises ions adsorbed to the surface of the colloidal particle; *ii*) the second layer, diffuse or Gouy-Chapman layer, is formed by free ions and counterions homogeneously distributed. All ions contained in the region of the electrical double layer accompany the Brownian motion of the colloidal particle. The potential in this layer is called the zeta potential (ζ) and is of great significance in the stability behavior of colloidal particles. Thereby, the stability increases when the absolute zeta potential increases. Indeed, if the zeta potential is larger than ± 40 mV a good stability of suspensions is ensured while for values of zeta potential lower than ± 30 mV, the suspensions is less stable. The ionic strength also affects the aggregation through a strong impact in the electrostatic barrier. The repulsive forces between colloidal particles decrease by the addition of salt on the solution. The impact of the salt on the stability of negatively colloidal particles was demonstrated (Holthoff *et al.* 1996; Montes Ruiz-Cabello *et al.* 2015).

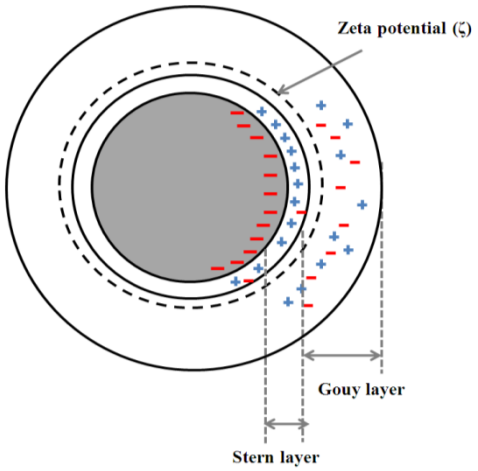

Figure 1.4: Illustration of the electric double layer around a colloidal particle charged negatively.

Repulsion can be enhanced by adding polymers that are adsorbed on the particles surface and which generate a repulsion between the polymer chains and consequently between the particles. This phenomenon is the factor determining, for example, the action of protective polymers. Repulsions of this nature tend to stabilize a system by steric effect (or entropic). When the polymers are polyelectrolyte, repulsion becomes extremely effective, and in this case is called electrosteric. In case of the electrostatic and steric forces the repulsive forces increases when the particles approach each other due to the presence of both charges and polymer brushes on the particles surface (Figure 1.5).

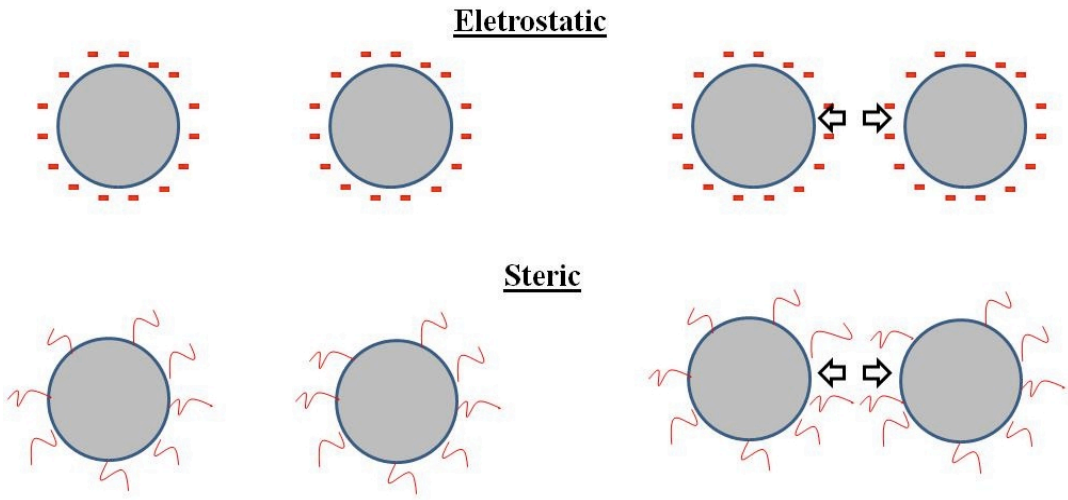

Figure 1.5: Illustration of the colloidal stabilizer electrostatic and steric. The repulsion increase when particles approach to each other (left to the right) due to the ions and branch.

The attractive van der Walls forces act at short distances and can induce the aggregation of the system when particles approach each other, even in presence of some repulsions interactions between particles. Therefore, the stability of a colloidal suspension is determined by long and short-range interactions between colloidal particles. The total energy interaction (V_T) of the system depends on the contribution of the attractive van der Waals forces (V_w) and the electrical repulsive forces (V_e) as illustrated in Figure 1.6. This is the base of the Deryagin-Landau-Verwey-Overbeek (DLVO) theory which a quantitative description of the colloidal stability. The observation of various types of deviant from the theory DLVO led to the proposition of other important factors affecting colloidal stability. Among them, these factors such as surface hydration, depletion and hydrodynamic interactions can introduce a delay factor to the particle-particle adhesion (Shaw 1992).

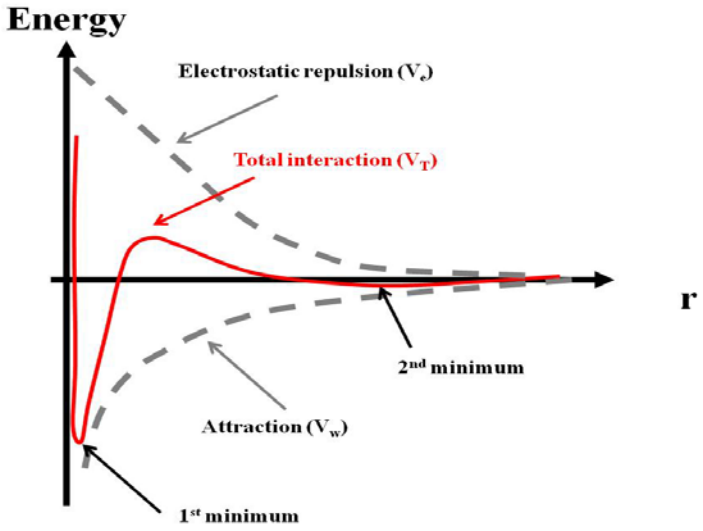

Figure 1.6: Illustration of energy of interaction in function of the distance r between particles. The total energy (red curve) is the resultant of the attractive and repulsive forces (dashed curves).

The depletion consists of a mechanism of instability of colloidal particles caused by polyelectrolyte, other colloidal particles, or in most case by polymers. Destabilization occurs when these species are excluded from the interparticle region, resulting in an osmotic pressure promoting aggregation (Figure 1.7). The volume available for polymers increases when the depletion zone overlaps. These distances are known as thickness depletion layer and depend on the diameter of the depletants (rigid species surrounding the particles).

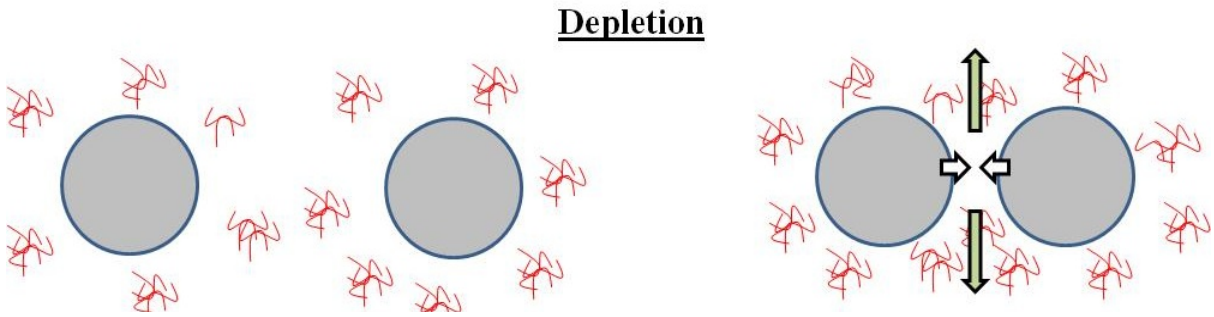

Figure 1.7: Illustration of the colloidal destabilization due to the depletion. The attraction can occur when particles approach to each other (left to the right) due to the expulsion of depletants between particles.

The external forces due to the gravity or shear also influence the interactions and collisions between particles. Hydrodynamic forces can impact the interactions between particles. Therefore, different forces influence simultaneously system.

1.2.2 Aggregation

If attractive interactions dominate the repulsive ones, particles aggregate. The aggregation is characterized by the adhesion between two or more particles with each other. In the early stages, the particles form small isolate aggregates and then the size of aggregates (clusters) increases. In the last stages, a gel can be formed by percolation of clusters. Figure 1.8 shows the aggregation between particles (doublet and triplet) up to gel formation.

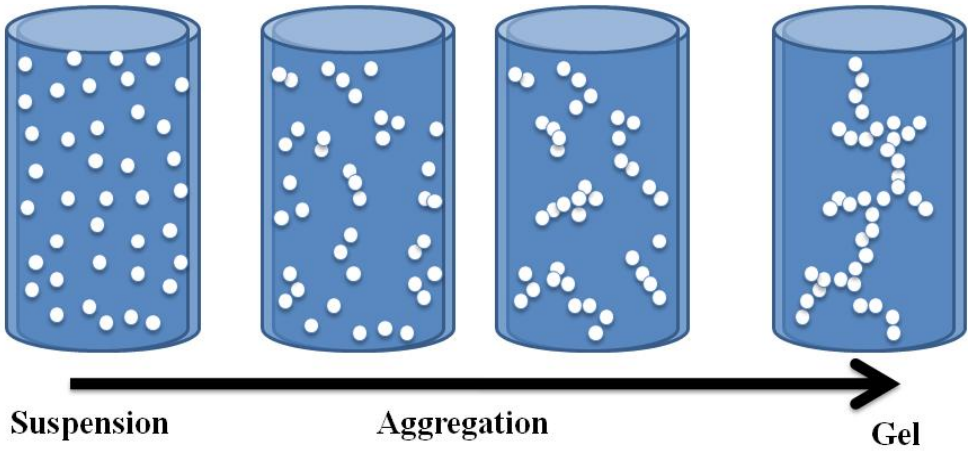

Figure 1.8: Illustration of aggregation of particles: from the stable suspension to a colloidal gel.

1.2.2.1 Cluster aggregation

Particles aggregation will result in the formation of clusters which structure is controlled by the aggregation kinetics. Two kinetics models have been described. In the first case, aggregation occurs immediately after a collision of particles forming a large (open) structure (Figure 1.9, left). This fast aggregation is named *diffusion limited cluster aggregation* (DLCA) (Weitz *et al.* 1985). In the second case, for which the interaction potential exhibit a finite, short-range repulsive barrier, the aggregation only occurs after several collisions between particles and therefore a more dense structure is formed as shown in Figure 1.9 on the right (Lin *et al.* 1990; Lin *et al.* 1990). This slow aggregation is named *reaction limited cluster aggregation* (RLCA) (Weitz *et al.* 1985). Tang *et al.* (Tang *et al.* 2000) demonstrated by image analysis the distinct structures formed by latex particles from these aggregation kinetics (Figure 1.9).

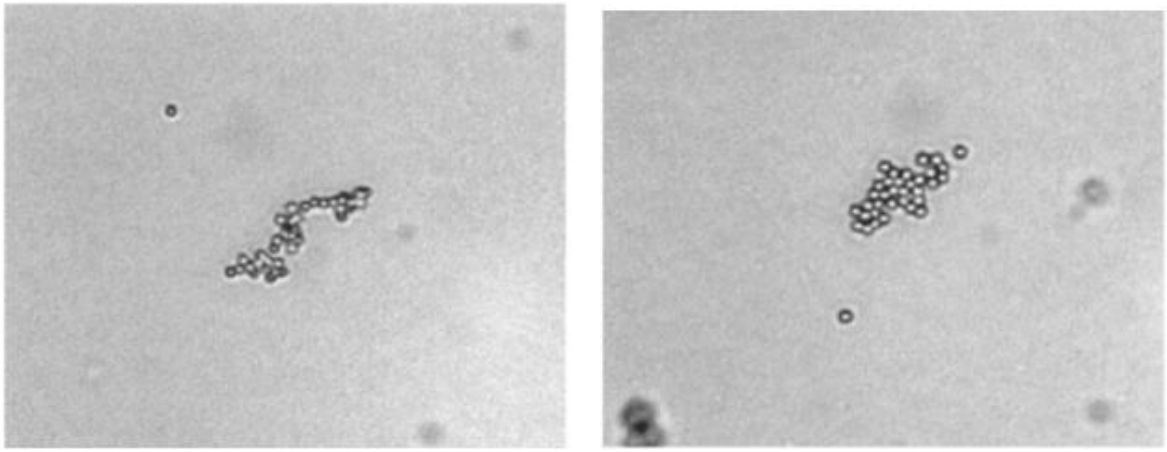

Figure 1.9: Images of structure of aggregates of latex particles formed on DLCA (left) and RLCA (right) from Tang *et al.* (Tang *et al.* 2000).

Clusters resulting from particles aggregation are characterized by a ramified structure in the three dimensions, which can be described using the fractal formalism, namely a fractal dimension (D_f) (R.Jullien 1987). This fractal dimension, between 1 and 3, can be determined directly by light and x-ray scattering, imagery techniques or by numerical simulation (Meakin 1999). The values of D_f obtained with this techniques are typically around 1.8 for DLCA and more than 2.1 for the RLCA (Weitz and Oliveria 1984; Weitz *et al.* 1985). In a fractal structure, the cluster radius (R_c) depend on the number of particles (N), their initial radius a and the value of D_f, as express in equation 1.

$$R_c \sim a\, N^{1/D_f} \qquad \text{Eq. 1}$$

The universality of these mechanisms, was described by Lin *et al.* (Lin *et al.* 1989) and Sandkühler *et al.* (Sandkühler, Lattuada et al. 2005), respectively. Both were described in the literature for colloids such as polystyrene, silica, gold, apple juice particles, etc (Lin *et al.* 1989; Benítez *et al.* 2010). Aggregates formed by DLCA and RLCA can be observed by electron microscopy techniques (SEM or TEM) (Lin *et al.* 1989; García *et al.* 2013), by confocal microscopy (Dinsmore *et al.* 2001) and by atomic force microscopy (AFM) (Liao *et al.* 2003). A 3D-reconstitution can be done by confocal microscopy (Prasad *et al.* 2007). The choice of the technique depends on the size of particles and aggregates formed. Simulation described these mechanisms with a good agreement with experimental results (Kolb *et al.* 1983; Meakin 1983; Lattuada *et al.* 2003).

Recently, a transition from RLCA to DLCA (or from DLCA to RLCA) during the aggregation was proposed (Moncho-Jordá *et al.* 2001; Sandkühler *et al.* 2005; Wu *et al.* 2013). In such case, two distinct stages during the colloidal aggregation of particles were described (Wu *et al.* 2013). In stage 1, clusters grow and form a gel by clusters interconnection in stage 2. A crossover from RLCA to DLCA in aggregation kinetics was

observed using small-angle light scattering method due to the decrease of the exponent of a power law between the intensity and the scattering vector. In another study, the changes of the fractal dimension during the sol-gel transition of irreversible clusters were described (Sorensen and Chakrabarti 2011). These authors proposed the presence of superaggregates with different fractal dimensions depending on the length scale.

1.2.2.2 Effect of external forces on aggregation

Some external forces such as gravitational and hydrodynamics forces can affect the diffusion of particles. During aggregation, the impact of gravitational forces can become considerable when aggregate size increase. Depending on their density, aggregate will tend to sediment or cream. Hydrodynamics interactions are forces between particles *via* the movement of the medium. This movement generates a flow between two particles. The hydrodynamic interactions increase when the concentration of particles increases.

The effect of the gravity coupled with the diffusion on the aggregation and gelation has been demonstrated with a calcium carbonate gel (Allain *et al.* 1995). Colloidal particles grow and will sediment or form a gel depending on the volume fraction (Φ_v) and on the time. Moreover, the gel settling with time will result eventually in its fracture under its own weight. The effect of gravity on the aggregation and coagulation has also been studied more recently (Dukhin *et al.* 2007). The authors proposed a dependence of the gravitational effect with the size of particles and electrostatic barrier. Indeed, the gravity will affect the system for particle sizes > 1 µm and the system can be destabilized if the electrostatic barrier is poor.

Hydrodynamic effects on aggregation were also demonstrated by numerical simulations (Honig *et al.* 1971; Kovalchuk and Starov 2012). It was reported an overestimation of the growth rate of aggregation in the case of absence of hydrodynamic interactions. Indeed, the hydrodynamic interaction between particles induces a decrease of the aggregation rate. Due to the incompressibility of the liquid surrounding the particles, clusters are characterized by a more elongated shape and this lowers the colloid volume fraction threshold for percolation (Furukawa and Tanaka 2010; Whitmer and Luijten 2011; Cao *et al.* 2012). The impact of the hydrodynamics, due to the shear rate, on the structure of the fractal aggregates was also reported (Wessel and Ball 1992). The effect of hydrodynamic interactions depends on the stage of aggregation and on the volume fraction (Tomilov *et al.* 2013). However, the true effect of hydrodynamic forces in the experimental results is still unclear.

1.3 Colloidal gels

As shown previously, attractive particles aggregate and a network is formed if the numbers of particles is enough to percolate in all space. Depending on the volume fraction of the suspension, different network can be formed. At low volume fractions, if the total energy interaction is attractive the particles aggregate and form colloidal fractals gels as described previously. Instead, for very high volume fractions, colloidal particles can form an attractive

glass. A state diagram in the interaction energy – volume fraction is given in Figure 1.10 (Trappe and Sandkühler 2004; Gibaud *et al.* 2012). The physical-chemical conditions (ionic strength, T° and pH) impact the formation of colloidal gels.

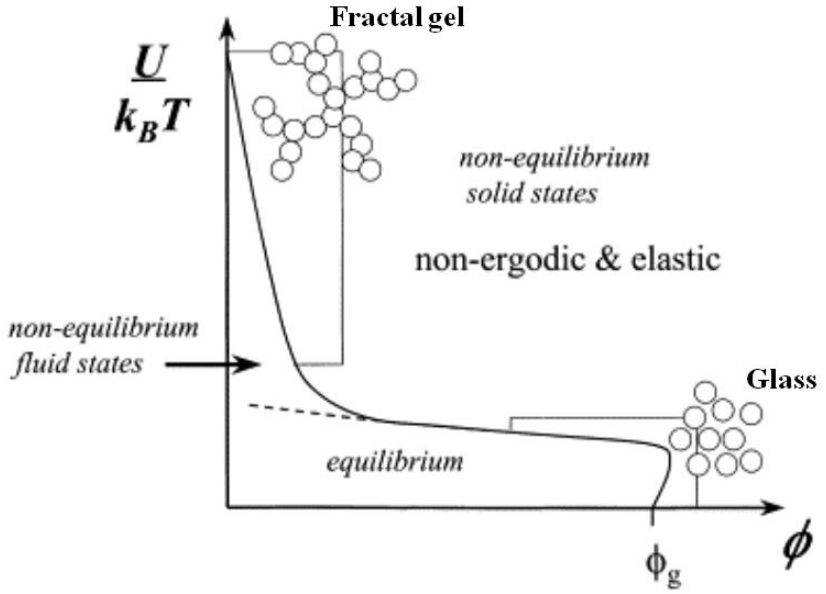

Figure 1.10: State diagram energy of the system function of volume fraction (from Trappe and Sandkühler (Trappe and Sandkühler 2004)).

In colloidal gels, particles form a ramified and continuous network in the 3D space. Figure 1.11 illustrates this ramified network obtained from a suspension of poly(methyl methacrylate) (PMMA) particles (Dinsmore *et al.* 2001). The fractal dimension of the network formed depends on the physical-chemical conditions during the formation of the firsts aggregates. The structure of the network controls the final materials properties. Structures of fractal gels have been studied using scattering techniques from which the fractal dimension can be estimated from scattering data. D_f can be obtained from the exponent of the power law relation between the intensity and the scattering vector if this latter is sufficiently larger (some decades) (Poon and Haw 1997; Lattuada *et al.* 2003). The fractal structure of colloidal gels can also be studied indirectly by rheology. Indeed, D_f can be estimated from scaling law between the elastic modulus and the volume fraction (Shih *et al.* 1990; Hagiwara *et al.* 1997; Gisler *et al.* 1999; Ikeda *et al.* 1999; Wu and Morbidelli 2001; Ould Eleya *et al.* 2004; Pouzot *et al.* 2006). This scaling law obtained by rheology will be discussed in the next sections.

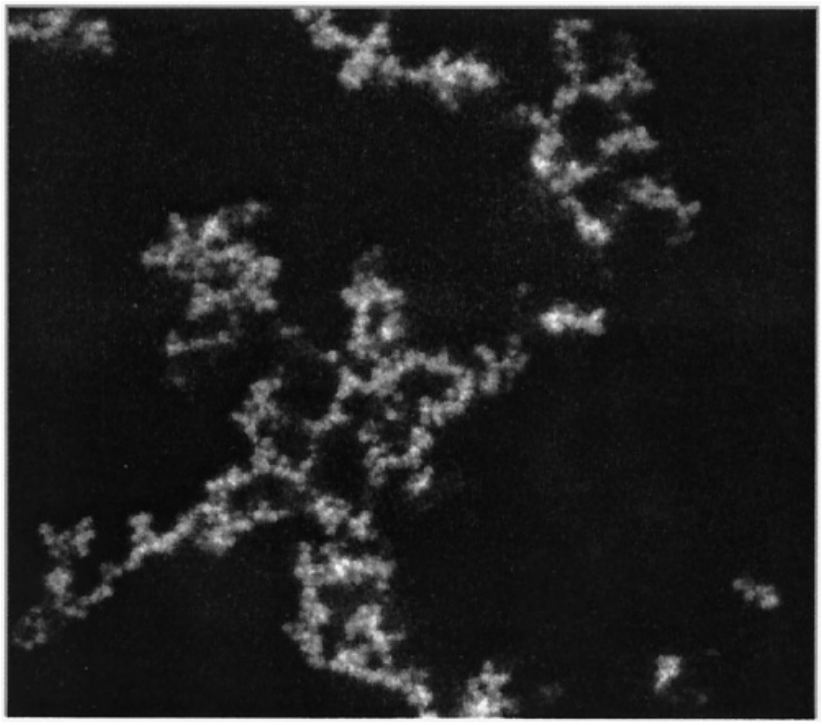

Figure 1.11: Example of a confocal image for a colloidal gel of PMMA from Dinsmore *et al.* (Dinsmore *et al.* 2001).

1.4 Rheological properties of colloidal suspensions and gels

Rheology is the science of the flow and deformation of materials. It is used in several areas to characterize different kind of materials such as liquids, foams, gels and solids. The knowledge of the rheological behaviors of a material is very important, both for their processing and their use. A rheometer is the equipment used to measure several characteristics such as the viscosity (for a liquid) or the viscous and elastic moduli (for a viscoelastic fluid). Depending on the shear applied two distinct tests are possible: rotational and oscillatory. In the rotational measurements, a controlled shear rate (or shear stress) is applied and progressively increase (or decrease) function of time. In this test the flow behavior of materials can be measured. In the oscillatory measurements, the viscoelastic profile of materials is measured. A sinusoidal stress (or strain) is applied to a sample and the response of the material (strain or stress) is measured. These two different measurements will be detail below.

1.4.1 Flow behavior of suspensions

The flow measurements consist in imposing a rotational speed on a sample and record its relation with the shear stress. Having the shear rate (σ) and shear stress ($\dot{\gamma}$), dynamic viscosity (η) of sample can be calculated according to the Newton's postulate (Eq. 2). The dynamic viscosity (η) translates the capacity of the fluid to resist to the flow. The rheological behavior of these suspensions depends on the volume fraction (Φ_v) and the nature of the particles. It can be classified in Newtonian or non-Newtonian behavior. A fluid is called Newtonian if the viscosity is independent of the applied shear rate ($\dot{\gamma}$) or shear stress (σ). On other hands, if the viscosity depends on the shear rate the fluid is non-Newtonian.

$$\eta = \frac{\sigma}{\dot{\gamma}} \qquad \text{Eq. 2}$$

In a suspension, viscosity increases as the particle volume fraction increases. For low volume fraction and in absence of interactions between particles, the suspensions respond like a Newtonian fluid. The evolution of the viscosity in function of particle volume fraction can be described by the Einstein equation (Eq. 3). A viscosity increment parameter is proposed depending on the shape of particle.

$$\eta = \eta_0 \left(1 + {}^{5}/_{2}\, \phi_v\right) \qquad \text{Eq. 3}$$

where η_0 is the viscosity of the medium and Φ_v is the volume fraction. The parameter 5/2 is the viscosity increment for spherical particles.

However, as the particles volume fraction increases, the experimental viscosity diverges from Einstein postulate (Eq. 2) as the volume fraction approaches the maximum packing volume fraction (Φ_{max}). Different models were proposed to fit this behavior. Firstly, Krieger and Dougherty (Krieger and Dougherty 1959) proposed a model for hard spheres. In their model, the fit of the viscosity behavior depends on Φ_{max} and the intrinsic viscosity [η] (Eq. 3). The parameter [η] reflects the hydrodynamic volume of particles. For monodisperse hard spheres, the Φ_{max} =0.58 and [η] =2.5, the same value as the viscosity increment used in the Einstein law.

$$\eta = \eta_0 \left(1 - \frac{\phi_v}{\phi_{max}}\right)^{-[\eta]\phi_{max}} \qquad \text{Eq. 4}$$

Later, to used only one unknown parameter (Φ_{max}) Quemada (Quemada 1977) proposed an extension of the Krieger-Dougherty model. In this model (Eq. 5) the exponent was replaced by the constant -2. This model was validated with experimental results for hard spheres for low and high volume fractions.

$$\eta = \eta_0 \left(1 - \frac{\phi_v}{\phi_{max}}\right)^{-2} \quad \text{Eq. 5}$$

However, for high volume fraction these models previously cited do not fit the behavior of deformable objects.

Recently, a model for soft particles and star polymers has been proposed (Mendoza and Santamaría-Holek 2009; Mendoza 2011). In this model (Eq. 6), an effective volume fraction, which depends on a critical volume fraction (Φ_c), is introduced in the equation. Φ_c is larger than the volume fraction at the random close packing for soft particles due to the deformability of particles (Ohshima 2010).

$$\eta = \eta_0 \left(1 - \frac{\phi_v}{1-k\phi_v}\right)^{-[\eta]} \; where\; k = \frac{1-\phi_c}{\phi_c} \quad \text{Eq. 6}$$

The impact of the polydispersity and the softening of particles was taken into account by Shewan and Stokes (Shewan and Stokes 2015). Their model namely MPQ is based on the models proposed by the Maron and Pierce (Maron and Pierce 1956) and Quemada (Quemada 1977). In the MPQ model (Eq. 7), the maximum volume fraction (Φ_{max}) was replaced by the volume fraction at random close packing (Φ_{rcp}). Φ_{rcp} is determined from the particle size distribution using the model proposed by Farr and Groot (Farr and Groot 2009). This polydispersity parameter is obtained from independently conducted size distribution measurements.

$$\eta = \eta_0 \left(1 - \frac{\phi_v}{\phi_{rcp}}\right)^{-2} \quad \text{Eq. 7}$$

Finally, a visual summary of the relative viscosity in function of the volume fraction for the different models cited previously is shown in Figure 1.12. For the very low volume fraction a good agreement with the Einstein model was observed as expected. Then, the relative viscosity increases with the volume fraction and the models (Eq. 4-7) deviate from the Einstein's theory.

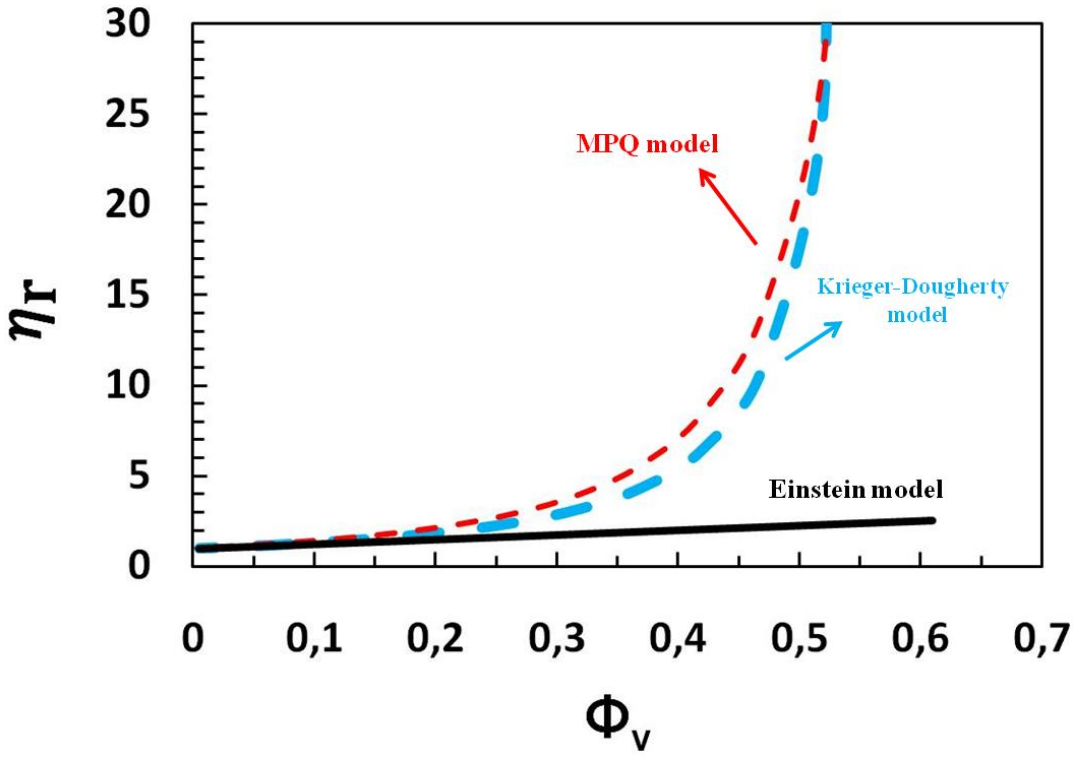

Figure 1.12: Relative viscosity function of volume fraction with the different models: black solid line: Einstein model, blue dashed line: Krieger-Dougherty (Φ_{max} =0.58 and [η] =2.5) and red dashed line: MPQ model (Φ_{rcp} =0.64).

1.4.2 Viscoelastic behavior of colloidal gels

As previously described, in the oscillatory measurement an input sinusoidal strain (or stress) is applied and an output stress (σ) (or strain (γ)) response is measured. The viscoelastic behavior of a material is determined by the phase difference between the input and the output (phase angle δ). The response of a perfect solid is described by the Hook law with δ =0° while from a perfect liquid it is described by the Newton's postulate with δ =90°. For a viscoelastic material, the phase angle is between 0° and 90° (Figure 1.13).

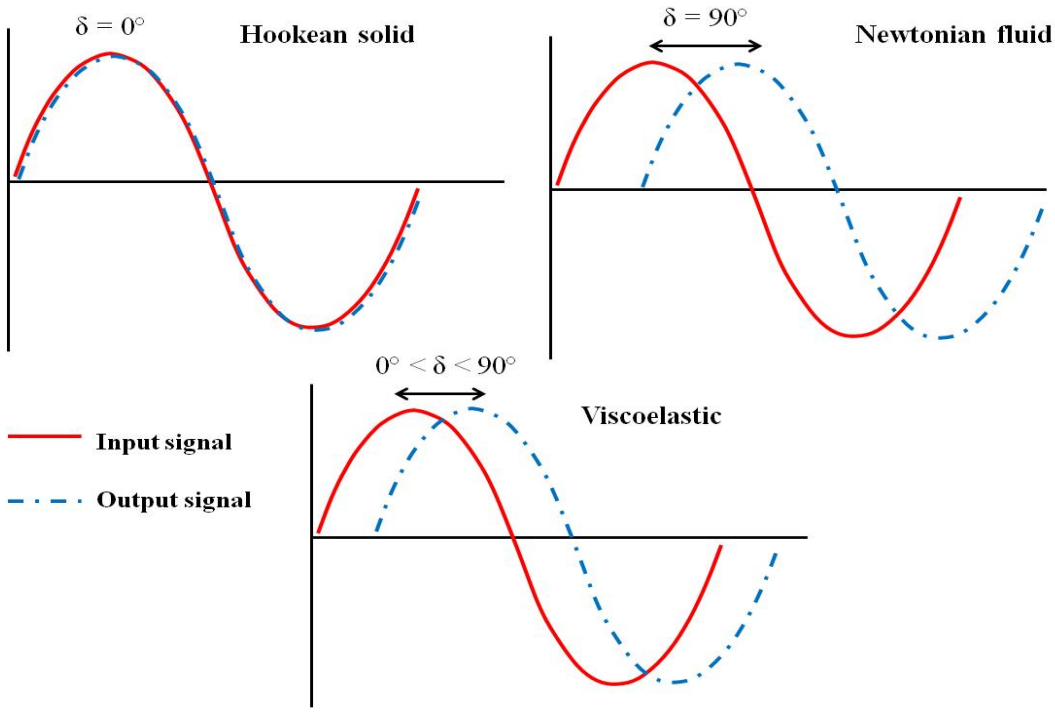

Figure 1.13: Input/output sinusoidal signals for different kinds of materials.

A complex shear modulus which express the resistance of the material to the full deformation can be calculated from the ratio of the stress and the strain (G* =σ/γ). *G** can be separated into two components: an elastic (or storage) modulus, *G'*, and a viscous (or loss) modulus, *G"*. The elastic modulus, which reflects the ability of the material to store energy, and the viscous modulus, which reflects the ability of the material to dissipate energy, are calculated using the Eq. 8 and 9.

$$G' = \frac{\sigma}{\gamma}\cos\delta \qquad \text{Eq. 8}$$

$$G'' = \frac{\sigma}{\gamma}\sin\delta \qquad \text{Eq. 9}$$

The tangent δ, obtained from the ratio *G"/G'*, quantifies the balance between the loss (*G''*) and storage (*G'*) moduli. In this line, the fracture of a material is characterized by a sharp increase of tan *δ* with a sharp decrease of the *G'*.

Colloidal suspensions and colloidal gels usually present a viscoelastic behavior, which can be characterized by rheology. Usually, a frequency sweep and a stress (or strain) sweep are done. The behavior of the elastic modulus *G'* and viscous modulus *G''* during the frequency spectrum reflects the material structure. Unlike a gel whose behavior is almost independent of frequency, some materials exhibit a solid-like or a liquid-like behavior depending on the applied frequency (Figure 1.14).

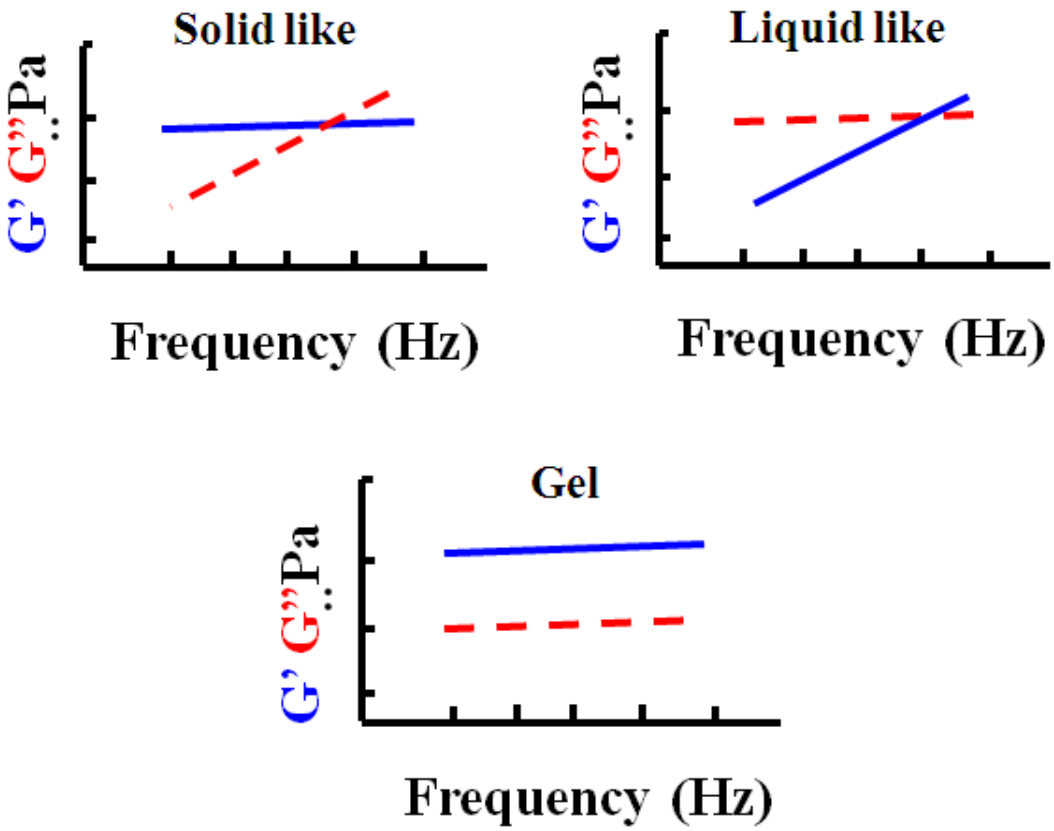

Figure 1.14: Example of frequency spectrum for different kinds of materials.

In the mechanical analyses, for the low values of strain (or stress) a linear response was observed. Indeed, the stress increase linearly with strain, this is called the linear regime. Then, a deviation of the linearity of the stress-strain curve was observed when the strain is increased. In this latter case, the deviation of linearity is called the non-linear regime. In the linear regime, the moduli *G'* and *G"* are constant and the output signal is a perfect sinusoid (Figure 1.15). Instead, in the non-linear regime, *G'* and *G"* vary with the input signal and the output signal is more and more deformed (Figure 1.15). The moduli *G'* and *G"* decrease (breaking of the structure, flow of material…) or increase (for strain hardening cases) depending on the properties of material. The limit of this linearity is normally expressed by the limit of linearity of strain (γ_0). This limit is estimated from the deviation on the stress-strain curves (Hagiwara *et al.* 1997). In general, it takes place at small strain when the sample is mostly solid and at high strain when the sample is mostly liquid.

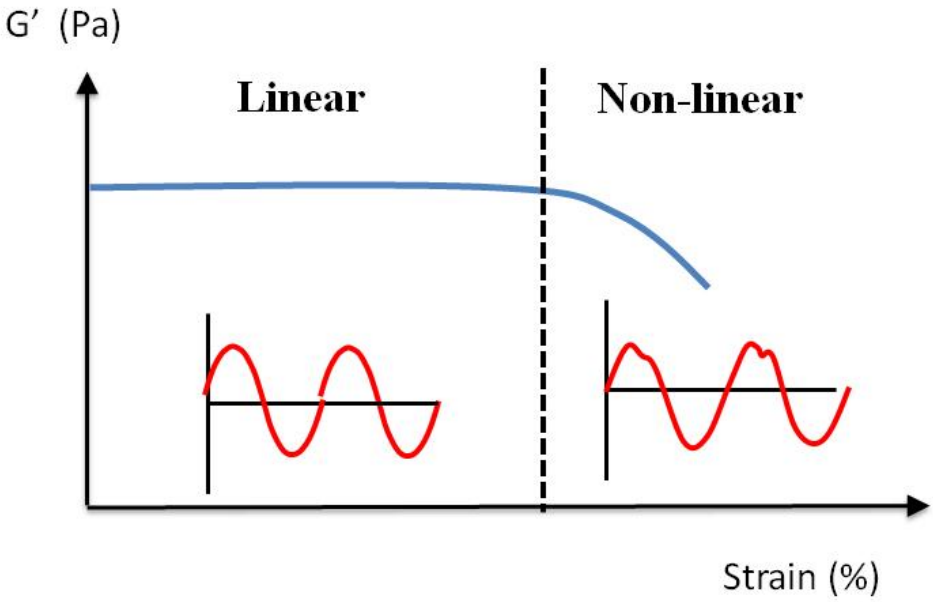

Figure 1.15: Illustration of evolution of *G'* as a function of strain: in the linear and non-linear regimes with corresponding output signals during the strain sweep.

1.4.2.1 Scaling laws and fractality

In the linear regime, the scaling behavior between the elastic modulus *G'* of a colloidal gel and the particles volume fraction has been described by Buscall *et al.* (Buscall *et al.* 1988). The fractal dimension of the structure can be deduced from the relation $G' \sim \Phi_v^{\,A}$, in which the exponent *A* depends on the fractal dimensions of the cluster (D_f) and its backbone (called chemical bond dimension or D_b). The backbone connects two given points separated by an arbitrary distance in 2D (Herrmann *et al.* 1984) (Figure 1.16).

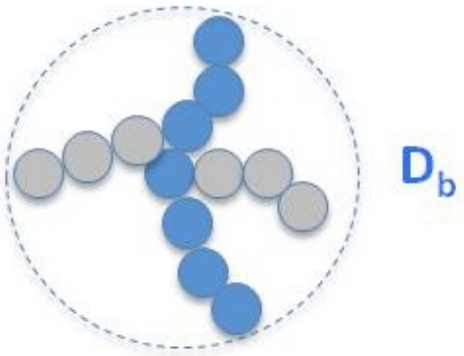

Figure 1.16: Illustration of the backbone fractal dimension on a fractal cluster.

The determination of the exponent *A* of the scaling behavior of the fractal structure can be associated with the kind of fractal structure obtained in the different kinetic regimes of aggregation cited in section 1.2.2.1. The system is in the RLCA regime if *A* is close to 4.5 and

in the DLCA regime if *A* is close to 3.5 (Buscall *et al.* 1988). Then, from the scaling behavior two distinct regimes were proposed to describe the connections between clusters and between particles (Shih *et al.* 1990). It was proposed that a difference of strength of interactions between particle-particle connection inside the clusters and between the clusters will originate in different behaviors. If the connections between clusters yield the regime is called weak link while if the particle-particle connections yield the regime is called strong link. A scaling behavior between the limit of the linearity of strain (γ_0) and the volume fraction was used to determine the regime. Depending on the signal of the exponent of this latter scaling law, the kind of regime can be determined. Indeed, a strong link regime and a weak link regime are characterized by a positive and a negative exponent respectively. Thereby, they proposed different exponent for these scaling laws of *G'* and γ_0 with the volume fraction, depending on the kind of regime as described in Eq. 10 and Eq. 11 in the Euclidean dimensions (D_e =3).

Strong link regime: $$G' \sim \Phi_v^{\frac{(D_e+D_b)}{(D_e-D_f)}} \quad and \quad \gamma_0 \sim \Phi_v^{\frac{(-1+D_b)}{(D_e-Df)}} \qquad \text{Eq. 10}$$

Weak link regime: $$G' \sim \Phi_v^{\frac{(D_e-2)}{(D_e-Df)}} \quad and \quad \gamma_0 \sim \Phi_v^{\frac{1}{(D_e-D_f)}} \qquad \text{Eq. 11}$$

with D_e the Euclidian dimension, D_b the backbone fractal dimensions.

Colloidal gels such as bovine serum albumin (BSA) gels (Hagiwara *et al.* 1998), casein gels (Zhong *et al.* 2004) and other protein gels (Verheul *et al.* 1998; Ikeda *et al.* 1999) were characterized by these models (Eq. 10 and 11). Then, a transition regime between these two regimes was proposed by Wu and Morbidelli (Wu and Morbidelli 2001). The experimental results from the literature were used and a model was proposed to integrate the transition regime between the strong link and weak link regimes. In this model (Eq. 12), they integrated the macroscopic elastic constant (α) in the exponent of the two power law relation cited (Eq. 10 and 11). The values of the elastic constant expressed the type of regime. Indeed, α =0 in the strong link regime, α =1 in the weak link regime and 0 < α < 1 in the transition regime.

$$G' \sim \Phi_v^{\frac{\beta}{(D_e-D_f)}} \quad and \quad \gamma_0 \sim \Phi_v^{\frac{(D_e-\beta+1)}{(D_e-D_f)}} \qquad \text{Eq. 12}$$

$where\ \beta = (D_e + 2) + (2 + D_b)(1 - \alpha)$

The effect of the pH on the fractal structure formed was demonstrated in heat-induced protein gels by Ould Eleya *et al.* (Ould Eleya *et al.* 2004). They used the scaling models proposed previously (Eq. 10-12) to determine the fractal dimension. An impact of the pH on the D_f of the structure was demonstrated. At low and neutral pH the structure of the gel is formed according the DLCA regime while is formed according the RLCA regime for the high pH.

Mellema *et al.* (Mellema *et al.* 2002) related the scaling behavior and the structural rearrangement of casein gels. In their model (Eq. 9), the coefficient (υ) used in the exponent

of the power law is used to determine the kind of strand. The two types of deformation of strand of particles are the bending and stretching modes. The different kind of strand and the corresponding value of υ are listed in the Table 1.2. This coefficient can be estimated close to 4 for almost all fractal colloidal gels in literature (Hagiwara *et al.* 1997; Gisler *et al.* 1999; Ikeda *et al.* 1999; Ould Eleya *et al.* 2004; Pouzot *et al.* 2006). However, its value will depend on the physic-chemistry conditions. For example, the variation of υ with the pH and the ionic strength for the protein gels was demonstrated (Hagiwara *et al.* 1997; Ould Eleya *et al.* 2004). The structural rearrangements can take place at different scales. It is classified in *i*) sub-particle (intraparticle) rearrangements, *ii*) interparticle rearrangements, *iii*) cluster rearrangements and *iv*) syneresis.

$$G' \sim \Phi_v^{\upsilon/(De-D_f)} \qquad \text{Eq. 13}$$

Table 1.2– Different categories of structure of strand and their corresponding type of deformation and the coefficient υ of scaling behavior proposed by Mellema *et al.* (Mellema *et al.* 2002).

Category	Type of strand	Deformation	υ
II	Curved, flexible	Bending	4
III	Hinged, Rigid	Bending	3
IV	Straight, flexible	Stretching	2
V	Rigid	Stretching	1

1.4.2.2 Non-linear regime

1.4.2.2.1 Strain hardening behavior

The strain hardening is a behavior observed at high deformations with colloidal and biological gels. In most cases, when a colloidal gel passes its limit of linearity, the moduli *G'* and *G"* decrease with the strain due to the fracture or the flow of the system. In some cases, a strain hardening appears instead. The strain hardening is characterized by the increases of both *G'* and *G"* up to the fracture or flow of the gel (Figure 1.17). This strain hardening was attributed to the new contacts between the strands of particles due to deformation of clusters under stress (Wessel and Ball 1992). Gisler *et al.* (Gisler *et al.* 1999) established that for polystyrene gels, a master curve of *G'* normalized by the *G'* at plateau, G'_0, in function of the volume fraction can be drawn. In this model, the origin of the strain hardening is the straightening of the backbone of the clusters with the strain. Then, polynomials models were proposed to incorporate the calculation using the Gisler *et al.* model (Gisler *et al.* 1999) using a protein gel (Pouzot *et al.* 2006).

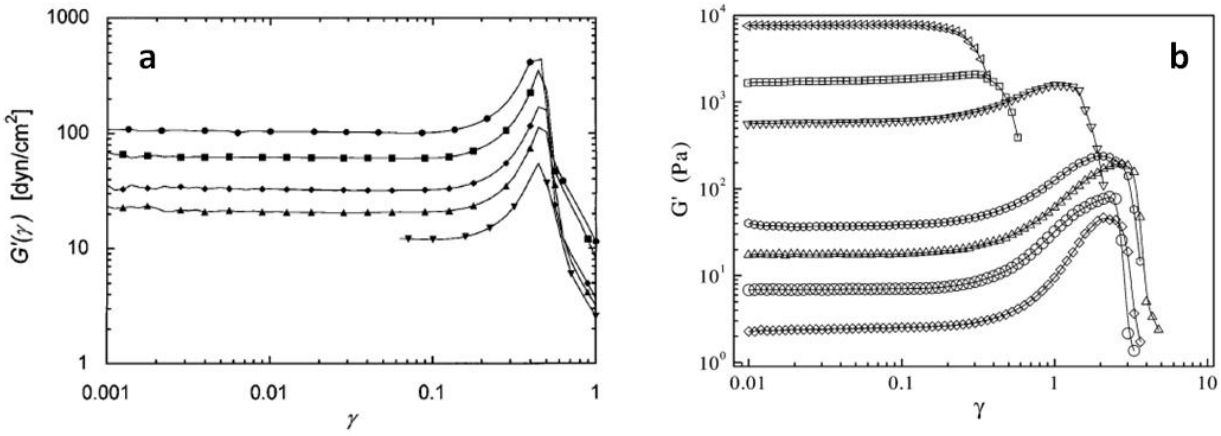

Figure 1.17: Strain hardening behavior observed with polystyrene gels by (a) Gisler *et al.* (Gisler *et al*. 1999) and protein gels by (b) Pouzot *et al.* (Pouzot *et al*. 2006).

Strain hardening behavior was also observed in DNA gels for the physical and chemical gels (Orakdogen *et al.* 2010) and in different protein gels: from fish (Brenner *et al.* 2009), from collagens gels due to the alignment of network chains (Vader *et al.* 2009), from fibrin, polyacrylamide (Storm *et al.* 2005). For the gel sensitive to the physical-chemical conditions, the strain hardening behavior was affected by the pH (Sittikijyothin *et al.* 2007) and by the temperature (Brenner *et al.* 2009).

Recently, Colombo and Del Gado (Colombo and Del Gado 2014) proposed a model to explain the strain hardening behavior and the yielding of a model colloidal gel. In their model, they demonstrated the onset of the strain hardening for values of strain around 10 %. This onset was observed due to the bending forces which push in the direction of the shear. Then, when the strain increases the stretching of the interparticle bonds also increase. During the strain hardening, bond formation dominates over bonds breaking. They proposed that the strain hardening is associated with an increase of stress localization in the network. For high strain, breaking bonds dominate the formation of those due to the stress localization and the network yield. This yielding was related to the heterogeneous stress in the material. Moreover, the shear rate does not impact the strain hardening behavior but modified the yielding.

In the non-linear regime, the output signal is no longer sinusoidal and can be interpreted by the Fourier decomposition of this signal (Wilhelm 2002), namely Fourier transform rheology (FT-rheology). Indeed, in the linear regime the output signal is purely the 1st harmonic and the higher harmonics appears at the non-linear regime. Recently, the strain hardening was studied with the Fast Fourier transform (FFT) rheology (Hilliou *et al.* 2009). An increase of the 3rd harmonic with the strain hardening for carrageenan gels was demonstrated (Hilliou *et al.* 2009). In this line, in another study the increase of the ratio between the third and first harmonic elastics modulus (G'_3/G'_1) was demonstrated during the strain hardening of agarose gels (Melito *et al.* 2012).

1.4.2.2.2 Advances on techniques

The studies of the structure of gels, fluids or solids in the non-linear regime increased in the last years. This can be explained by the progress of the techniques and the importance of the behavior of the materials at high deformation. The LAOS, large amplitude oscillatory strain, is based on the study of the non-linear waveforms of the input and the output signals of the rheometer (Hyun *et al.* 2011). The different forms of the non-linear waveforms were described by Klein *et al.* (Klein *et al.* 2007). They described a relation between the waveforms of output signals such as triangle, rectangle and sawtooth with an increases of the high frequency harmonics. The physical sense of the even harmonics, especially the second harmonic, is still unclear. Some authors proposed a link between the absence of the second harmonic with the absence of the wall slip using the FT-rheology (Wilhelm 2002; Klein *et al.* 2007). Others authors proposed a link of the second harmonic and the change in microstructure of the gel (Sagis *et al.* 2001) or the combination of high elasticity and the geometry inertia (Atalik and Keunings 2004).

In LAOS, the Lissajous curves are a principal method to analyze the materials. The deviation of the linearity is observed in the shear stress *vs* shear rate (or strain) curves. The ellipse shape (or circle in the stress *vs* strain) of the curves is characteristic of the linear viscoelastic regime. The deviation and disorder of the shape is provided by the non sinusoidal form of the signals. Pipkin space is used in a strain-frequency space to regroup the Lissajous curves. The Lissajous curves as used to compare the rheological properties, yielding and flow, of the hard and soft spheres (van der Vaart *et al.* 2013). The LAOS protocol was validated for liquids (Ewoldt *et al.* 2008) and gels (Melito *et al.* 2012). For example, the plastic rearrangements during the fluidization of a colloidal gel were studied by LAOS method (Laurati *et al.* 2014)

References

Allain, C., *et al.* (1995). "Aggregation and Sedimentation in Colloidal Suspensions." Physical Review Letters **74**(8): 1478-1481.

Benítez, E. I., *et al.* (2010). "Fractal Dimension and Mechanism of Aggregation of Apple Juice Particles." Food Science and Technology International **16**(2): 179-186.

Berthelot, K., *et al.* (2014). "Hevea brasiliensis REF (Hev b 1) and SRPP (Hev b 3): An overview on rubber particle proteins." Biochimie **106**(0): 1-9.

Berthelot, K., *et al.* (2014). "Rubber particle proteins, HbREF and HbSRPP, show different interactions with model membranes." Biochimica et Biophysica Acta (BBA) - Biomembranes **1838**(1, Part B): 287-299.

Blackley, D. C. (1996). Polymer Latices: Science and Technology. London, Chapman & Hall.

Bonfils, F., *et al.* (2005). "Evolution in the natural rubber native structure and plasticity retention index from the first tapping of clonal trees." Journal of Applied Polymer Science **97**(3): 903-909.

Brenner, T., *et al.* (2009). "Rheology of thermo-reversible fish protein isolate gels." Food Research International **42**(8): 915-924.

Buscall, R., *et al.* (1988). "Scaling behaviour of the rheology of aggregate networks formed from colloidal particles." Journal of the Chemical Society, Faraday Transactions 1: Physical Chemistry in Condensed Phases **84**(12): 4249-4260.

Cao, X. J., *et al.* (2012). "Hydrodynamic and interparticle potential effects on aggregation of colloidal particles." Journal of Colloid and Interface Science **368**(1): 86-96.

Cornish, K., *et al.* (1999). "Rubber particles from four different species, examined by transmission electron microscopy and electron-paramagnetic-resonance spin labeling, are found to consist of a homogeneous rubber core enclosed by a contiguous, monolayer biomembrane." Planta **210**(1): 85-96.

Dai, L. J., *et al.* (2013). "In-depth proteome analysis of the rubber particle of Hevea brasiliensis (para rubber tree)." Plant Molecular Biology **82**(1-2): 155-168.

Dinsmore, A. D., *et al.* (2001). "Three-dimensional confocal microscopy of colloids." Applied Optics **40**(24): 4152-4159.

Dukhin, A. S., *et al.* (2007). "Gravity as a factor of aggregative stability and coagulation." Advances in Colloid and Interface Science **134-35**: 35-71.

Ehabé, E., *et al.* (2005). "Modelling of Mooney viscosity relaxation in natural rubber." Polymer Testing **24**(5): 620-627.

Ewoldt, R. H., *et al.* (2008). "New measures for characterizing nonlinear viscoelasticity in large amplitude oscillatory shear." Journal of Rheology **52**(6): 1427-1458.

Farr, R. S. and R. D. Groot (2009). "Close packing density of polydisperse hard spheres." The Journal of Chemical Physics **131**(24): 244104.

Furukawa, A. and H. Tanaka (2010). "Key Role of Hydrodynamic Interactions in Colloidal Gelation." Physical Review Letters **104**(24): 245702.

Gaboriaud, F., *et al.* (2012). "Unravelling the nanometre-scale stimuli-responsive properties of natural rubber latex particles using atomic force microscopy." Soft Matter **8**(9): 2724-2729.

García, C. P., *et al.* (2013). "Microscopic Analysis of the Interaction of Gold Nanoparticles with Cells of the Innate Immune System." Sci. Rep.

Gibaud, T., *et al.* (2012). "New routes to food gels and glasses." Faraday Discussions **158**(0): 267-284.

Gidrol, X., *et al.* (1994). "Hevein, a lectin-like protein from Hevea brasiliensis (rubber tree) is involved in the coagulation of latex." Journal of Biological Chemistry **269**(12): 9278-9283.

Gisler, T., *et al.* (1999). "Strain Hardening of Fractal Colloidal Gels." Physical Review Letters **82**(5): 1064-1067.

Hagiwara, T., *et al.* (1997). "Fractal Analysis of the Elasticity of BSA and β-Lactoglobulin Gels." Journal of Agricultural and Food Chemistry **45**(10): 3807-3812.

Hagiwara, T., *et al.* (1998). "Fractal analysis of aggregates in heat-induced BSA gels." Food Hydrocolloids **12**(1): 29-36.

Hamley, I. W. (2013). Introduction to soft matter: synthetic and biological self-assembling materials, John Wiley & Sons.

Hasma, H. and A. Subramaniam (1986). "Composition of lipids in latex of Hevea brasiliensis clone RRIM 501 [Malaysia]." Journal of Natural Rubber Research (Malaysia).

Herrmann, H. J., *et al.* (1984). "Backbone and elastic backbone of percolation clusters obtained by the new method of 'burning'." Journal of Physics A: Mathematical and General **17**(5): L261.

Hillebrand, A., *et al.* (2012). "Down-Regulation of Small Rubber Particle Protein Expression Affects Integrity of Rubber Particles and Rubber Content in Taraxacum brevicorniculatum." Plos One **7**(7).

Hilliou, L., *et al.* (2009). "Structural and mechanical characterization of kappa/iota-hybrid carrageenan gels in potassium salt using Fourier Transform rheology." Food Hydrocolloids **23**(8): 2322-2330.

Ho, C. C. (1989). "Changes in electrokinetic properties of natural rubber latex after surface chemical modifications." Colloid and Polymer Science **267**(7): 643-647.

Ho, C. C., *et al.* (1996). "Surface Structure of Natural Rubber Latex Particles from Electrophoretic Mobility Data." Journal of Colloid and Interface Science **178**(2): 442-445.

Holthoff, H., *et al.* (1996). "Coagulation rate measurements of colloidal particles by simultaneous static and dynamic light scattering." Langmuir **12**(23): 5541-5549.

Honig, E. P., *et al.* (1971). "Effect of hydrodynamic interaction on the coagulation rate of hydrophobic colloids." Journal of Colloid and Interface Science **36**(1): 97-109.

Hyun, K., *et al.* (2011). "A review of nonlinear oscillatory shear tests: Analysis and application of large amplitude oscillatory shear (LAOS)." Progress in Polymer Science **36**(12): 1697-1753.

Ikeda, S., *et al.* (1999). "Rheological Study on the Fractal Nature of the Protein Gel Structure." Langmuir **15**(25): 8584-8589.

Intapun, J., *et al.* (2010). "Effect of microorganisms during the initial coagulum maturation of Hevea natural rubber." Journal of Applied Polymer Science **118**(3): 1341-1348.

IRSGReport (2015). IRSG Rubber Industry Report.

Jacob, J.-L., *et al.* (1993). "The composition of natural latex fromHevea brasiliensis." Clinical Reviews in Allergy **11**(3): 325-337.

Kim, C., *et al.* (2008). "Characterization of natural rubber using size-exclusion chromatography with online multi-angle light scattering: Study of the phenomenon behind the abnormal elution profile." Journal of Chromatography A **1213**(2): 181-188.

Klein, C. O., *et al.* (2007). "Separation of the Nonlinear Oscillatory Response into a Superposition of Linear, Strain Hardening, Strain Softening, and Wall Slip Response." Macromolecules **40**(12): 4250-4259.

Kolb, M., *et al.* (1983). "Scaling of Kinetically Growing Clusters." Physical Review Letters **51**(13): 1123-1126.

Kovalchuk, N. M. and V. M. Starov (2012). "Aggregation in colloidal suspensions: Effect of colloidal forces and hydrodynamic interactions." Advances in Colloid and Interface Science **179**: 99-106.

Krieger, I. M. and T. J. Dougherty (1959). "A Mechanism for Non-Newtonian Flow in Suspensions of Rigid Spheres." Transactions of The Society of Rheology (1957-1977) **3**(1): 137-152.

Lattuada, M., *et al.* (2003). "Aggregation kinetics of polymer colloids in reaction limited regime: experiments and simulations." Advances in Colloid and Interface Science **103**(1): 33-56.

Lattuada, M., *et al.* (2003). "Estimation of Fractal Dimension in Colloidal Gels." Langmuir **19**(15): 6312-6316.

Laurati, M., *et al.* (2014). "Plastic rearrangements in colloidal gels investigated by LAOS and LS-Echo." Journal of Rheology **58**(5): 1395-1417.

Liao, J., *et al.* (2003). "Linear aggregation of gold nanoparticles in ethanol." Colloids and Surfaces A: Physicochemical and Engineering Aspects **223**(1–3): 177-183.

Liengprayoon, S., *et al.* (2011). "Glycolipid composition of Hevea brasiliensis latex." Phytochemistry **72**(14-15): 1902-1913.

Lin, M. Y., *et al.* (1989). "Universality in colloid aggregation." Nature **339**(6223): 360-362.

Lin, M. Y., *et al.* (1990). "Universal reaction-limited colloid aggregation." Physical Review A **41**(4): 2005-2020.

Lin, M. Y., *et al.* (1990). "Universal diffusion-limited colloid aggregation." Journal of Physics: Condensed Matter **2**(13): 3093.

Maron, S. H. and P. E. Pierce (1956). "Application of ree-eyring generalized flow theory to suspensions of spherical particles." Journal of Colloid Science **11**(1): 80-95.

Meakin, P. (1983). "Diffusion-controlled cluster formation in 2\char22{}6-dimensional space." Physical Review A **27**(3): 1495-1507.

Meakin, P. (1999). "A Historical Introduction to Computer Models for Fractal Aggregates." Journal of Sol-Gel Science and Technology **15**(2): 97-117.

Melito, H. S., *et al.* (2012). "Validation of a large amplitude oscillatory shear protocol." Journal of Food Engineering **113**(1): 124-135.

Mellema, M., *et al.* (2002). "Effects of structural rearrangements on the rheology of rennet-induced casein particle gels." Advances in Colloid and Interface Science **98**(1): 25-50.

Mendoza, C. I. (2011). "Effective static and high-frequency viscosities of concentrated suspensions of soft particles." The Journal of Chemical Physics **135**(5): 054904.

Mendoza, C. I. and I. Santamaría-Holek (2009). "The rheology of hard sphere suspensions at arbitrary volume fractions: An improved differential viscosity model." The Journal of Chemical Physics **130**(4): 044904.

Moncho-Jordá, A., *et al.* (2001). "The DLCA-RLCA transition arising in 2D-aggregation: simulations and mean field theory." The European Physical Journal E **5**(4): 471-480.

Montes Ruiz-Cabello, F. J., *et al.* (2015). "Interaction Forces and Aggregation Rates of Colloidal Latex Particles in the Presence of Monovalent Counterions." The Journal of Physical Chemistry B.

Mooibroek, H. and K. Cornish (2000). "Alternative sources of natural rubber." Applied Microbiology and Biotechnology **53**(4): 355-365.

Nawamawat, K., *et al.* (2011). "Surface nanostructure of Hevea brasiliensis natural rubber latex particles." Colloids and Surfaces A: Physicochemical and Engineering Aspects **390**(1–3): 157-166.

Ohshima, H. (2010). "Effective Viscosity of a Concentrated Suspension of Uncharged Spherical Soft Particles." Langmuir **26**(9): 6287-6294.

Orakdogen, N., *et al.* (2010). "Evidence of Strain Hardening in DNA Gels." Macromolecules **43**(3): 1530-1538.

Ould Eleya, M. M., *et al.* (2004). "Scaling and fractal analysis of viscoelastic properties of heat-induced protein gels." Food Hydrocolloids **18**(2): 315-323.

Poon, W. C. K. and M. D. Haw (1997). "Mesoscopic structure formation in colloidal aggregation and gelation." Advances in Colloid and Interface Science **73**: 71-126.

Pouzot, M., *et al.* (2006). "Strain hardening and fracture of heat-set fractal globular protein gels." Journal of Colloid and Interface Science **293**(2): 376-383.

Prasad, V., *et al.* (2007). "Confocal microscopy of colloids." Journal of Physics: Condensed Matter **19**(11): 113102.

Quemada, D. (1977). "Rheology of concentrated disperse systems and minimum energy dissipation principle." Rheologica Acta **16**(1): 82-94.

R.Jullien (1987). "Aggregation phenomena and fractal aggregates." Contemp Phys **28**: 477–493.

Rochette, C. N., *et al.* (2013). "Shell Structure of Natural Rubber Particles: Evidence of Chemical Stratification by Electrokinetics and Cryo-TEM." Langmuir **29**(47): 14655-14665.

Sagis, L. M. C., *et al.* (2001). "Constitutive equations for an elastic material with anisotropic rigid particles." Physical Review E **63**(5).

Sainte Beuve J., V. L., Bonfils F. (2006). Caoutchouc naturel - Maitrise de la variabilité.

Sandkühler, P., *et al.* (2005). "Further insights into the universality of colloidal aggregation." Advances in Colloid and Interface Science **113**(2–3): 65-83.

Sansatsadeekul, J., *et al.* (2011). "Characterization of associated proteins and phospholipids in natural rubber latex." Journal of Bioscience and Bioengineering **111**(6): 628-634.

Shaw, D. (1992). Colloid & Surface chemistry.

Shewan, H. M. and J. R. Stokes (2015). "Analytically predicting the viscosity of hard sphere suspensions from the particle size distribution." Journal of Non-Newtonian Fluid Mechanics(0).

Shih, W.-H., *et al.* (1990). "Scaling behavior of the elastic properties of colloidal gels." Physical Review A **42**(8): 4772-4779.

Sittikijyothin, W., *et al.* (2007). "Heat-induced gelation of β-lactoglobulin at varying pH: Effect of tara gum on the rheological and structural properties of the gels." Food Hydrocolloids **21**(7): 1046-1055.

Sorensen, C. M. and A. Chakrabarti (2011). "The sol to gel transition in irreversible particulate systems." Soft Matter **7**(6): 2284-2296.

Southorn, W. A. (1960). "Complex Particles in Hevea Latex." Nature **188**(4745): 165-166.

Storm, C., *et al.* (2005). "Nonlinear elasticity in biological gels." Nature **435**(7039): 191-194.

Tanaka, Y. and L. Tarachiwin (2009). "Recent Advances in Structural Characterization of Natural Rubber." Rubber Chemistry and Technology **82**(3): 283-314.

Tang, S., *et al.* (2000). "Fractal Morphology and Breakage of DLCA and RLCA Aggregates." Journal of Colloid and Interface Science **221**(1): 114-123.

Tarachiwin, L., *et al.* (2005). "Structural Characterization of α-Terminal Group of Natural Rubber. 1. Decomposition of Branch-Points by Lipase and Phosphatase Treatments." Biomacromolecules **6**(4): 1851-1857.

Tomilov, A., *et al.* (2013). "Aggregation in Colloidal Suspensions: Evaluation of the Role of Hydrodynamic Interactions by Means of Numerical Simulations." The Journal of Physical Chemistry B **117**(46): 14509-14517.

Trappe, V. and P. Sandkühler (2004). "Colloidal gels—low-density disordered solid-like states." Current Opinion in Colloid & Interface Science **8**(6): 494-500.

Vader, D., *et al.* (2009). "Strain-Induced Alignment in Collagen Gels." Plos One **4**(6).

van der Vaart, K., *et al.* (2013). "Rheology of concentrated soft and hard-sphere suspensions." Journal of Rheology **57**(4): 1195-1209.

Vaysse, L., *et al.* (2012). Natural rubber in Polymer Science: A Comprehensive Reference. Amsterdam, Elsevier BV.

Vaysse, L., *et al.* (2009). Natural Rubber in Sustainable Solutions for Modern Economies,Coord. Dr Rainer Höfer, The Royal Society of Chemistry. Cambridge, UK**:** 339-367.

Verheul, M., *et al.* (1998). "Power law behavior of structural properties of protein gels." Langmuir **14**(9): 2263-2268.

Weitz, D. A., *et al.* (1985). "Limits of the Fractal Dimension for Irreversible Kinetic Aggregation of Gold Colloids." Physical Review Letters **54**(13): 1416-1419.

Weitz, D. A. and M. Oliveria (1984). "Fractal Structures Formed by Kinetic Aggregation of Aqueous Gold Colloids." Physical Review Letters **52**(16): 1433-1436.

Whitmer, J. K. and E. Luijten (2011). "Influence of Hydrodynamics on Cluster Formation in Colloid−Polymer Mixtures." The Journal of Physical Chemistry B **115**(22): 7294-7300.

Wilhelm, M. (2002). "Fourier-Transform Rheology." Macromolecular Materials and Engineering **287**(2): 83-105.

Wisunthorn, S., *et al.* (2012). "SEC-MALS study of dynamic structuring of natural rubber: Comparative study of two Hevea brasiliensis genotypes." Journal of Applied Polymer Science **124**(2): 1570-1577.

Wititsuwannakul, D. a. W., R. (2001). Biochemistry of Natural Rubber and Structure of Latex. Weiheim, Germany.

Wood, D. F. and K. Cornish (2000). "Microstructure of purified rubber particles." International Journal of Plant Sciences **161**(3): 435-445.

Wu, H. and M. Morbidelli (2001). "A Model Relating Structure of Colloidal Gels to Their Elastic Properties." Langmuir **17**(4): 1030-1036.

Wu, H., *et al.* (2013). "Kinetics of colloidal gelation and scaling of the gelation point." Soft Matter **9**(17): 4437-4443.

Zhong, Q. X., *et al.* (2004). "Cooling effects on a model rennet casein gel system: part I. Rheological characterization." Langmuir **20**(18): 7399-7405.

Chapter 2

Materials & Methods

2.1 Natural rubber latex

2.1.1 Sample preparation

The natural rubber latex (NRL) is a biological suspension, which composition varies with many factors such as agronomic conditions (locality, soil, etc), tree genotype and seasonal conditions (rain, temperature, etc). Moreover, the stability of the native natural rubber latex is poor due to the microorganism development, the presence of divalent cations and other biological compounds. To avoid these problems we used a commercial stabilized product. The commercial product is a pre-vulcanized latex from Dalbe (ref. 4770002, France) with a volume fraction of 0.61. The stability is ensured by the presence of ammonia (pH 10.5). This latex is classified in low ammonia latex (< 0.3 %w/w).

2.1.2 Tris-HCl buffer preparation

A Tris-HCl buffer is used for dilution of the NRL suspension in order to produce a large range of volume fraction and to dialyze the commercial NRL. For this, tris(hydroxymethyl)aminomethane (Tris, $C_4H_{11}NO_3$) was used. The Tris-HCl buffer can be used in a pH range between 7.05 and 9.05 as the p*Ka* value is 8.05. For all sample preparation, in Milli-Q water, a Tris-HCl concentration of 25 mM with a pH of 8.5 and an ionic strength of 7 mM was chosen. The pH was adjusted with a 3 M HCl solution.

2.1.3 pH measurements

The pH determination was carried out by potentiometric method using a pH meter model 3220 Hanna Instruments. The methodology is based on the direct determination of hydrogen ion concentration in the solution.

2.1.4 Dialysis of natural rubber latex

Dialysis was done to eliminate the ammonia. For this, the samples were diluted (1:1) in Tris-HCl buffer (pH 8.5 and I =7 mM). Then, using a dialysis membrane (Spectrapor, cut-off 12-14 kDa, diameter 29 mm) previously rinsed with Milli-Q water, the NRL was extensively dialyzed against the same buffer during 7 days in the dark at room temperature. The buffer solution was replaced twice a day for the first 2 days and then once a day to ensure a complete exchange. After dialysis, the NRL suspension volume fraction was between 0.2 and 0.3, and the pH was 8.5. This dialyzed suspension was stable during 3 weeks at 5˚ C without any visible sign of aggregation.

2.2 Characterization of natural rubber latex

After the dialysis step, we determined the density and the volume fraction of particles and we characterized the latex in terms of particle size distribution and electrophoretic mobility.

2.2.1 Density and volume fraction determination

To determine the density of particles in suspension, we used a pycnometer Hubbard which volume is 50 mL. The density of latex was determined by the mass difference between the sample and Milli-Q water. For this, the mass of the empty pycnometer (m_e) and with the Milli-Q water (m_w) were determined. Then, the mass of the sample (m_s) was determined. Knowing the density of water, the density (ρ) of the sample is obtained using the equation 14.

$$\rho = \frac{m_w - m_e}{m_s - m_e} \qquad \text{Eq. 14}$$

The mass fraction of particles was obtained after determination of the total solid content (TSC). The TSC was obtained by the mass difference after evaporation of the water after 4 hours in an oven at 105˚ C. For this, 1 ± 0.1 g of latex was weighed in a Petri dish. The mass fraction of particles is supposed to be the TSC. The volume fraction of particles (Φ_v) was determined using the mass fraction and the density of particles. The amount of the GDL used was taken into account for determining the volume fraction.

2.2.2 Size distribution

The size distribution of the natural rubber latex is obtained with static light scattering (SLS). For details, see chapter 3. NRL samples were double diluted in a high volume of Tris-HCl buffer 25 mM pH 8.5. For the dialyzed latex samples, we followed the evolution of the size distribution during the 3 weeks of storage at 5° C. The suspension was still stable over 3 weeks without any signs of aggregation measured by SLS.

2.2.3 Electrophoretic mobility

The electrophoretic mobility is used to determine the nature of the global charges of solid particles suspended in water. A Malvern Zetasizer 3000 HS was used to study the electrophoretic mobility of NRL particles. A transparent cuvette filled with suspension is connected between two electrodes charged positively and negatively. A constant electric field (E) of 100 V cm^{-1} is applied across the cuvette. The charged particles move to the direction of the opposite electrode and the viscosity forces tend to oppose this movement. A constant velocity (v_e) is obtained when the equilibrium of these forces is reached. The velocity of migration of particles in direction of the opposite electrode is measured with a HeNe laser at 633nm. From the velocity, the electrophoretic mobility (μ_e) is obtained from equation 15.

$$\mu_e = \frac{v_e}{E} \qquad \text{Eq. 15}$$

The electrophoretic mobility can be related with the zeta potential (ζ) by the theory of electrophoresis developed by Smoluchowki (Equation 16).

$$\mu_e = \frac{\varepsilon_r \varepsilon_0 \zeta}{\eta} \qquad \text{Eq. 16}$$

where ε_r (~ 78 at 25°C) is the relative permittivity of the medium, ε_0 is vacuum permittivity (1 C^2 N^{-1} m^{-2}), η is dynamic viscosity of the medium (1.13x10^{-3} Pa s) and ζ is the zeta potential (mV).

For these measurements, a transparent suspension is necessary to avoid multiple scattering. The natural rubber latex is very opaque and high dilutions against a buffer were done to reach a concentration about 6.0x10^{-6} w/w. The suspension was injected into the cuvette using a syringe (5 mL). In order to have a good measurement, it is imperative to prevent formation of bubbles inside the cuvette. The electrophoretic mobility and the zeta potential were obtained directly from the average of three measurements. Then, the global results were calculated from 8 repetitions. These measurements were performed at 25˚ C for different pH and ionic strengths. The pH was varied from 8.5 to 2.2 using 3 different buffers: Tris-HCl, NaH_2PO_4-HCl and citric acid-sodium citrate (Table 2.1). The ionic strength was varied using NaCl between 1mM and 500 mM at pH 8.5 diluted in a Tris-HCl buffer (Table 2.2).

Table 2.1 – Different buffer (Tris-HCl, NaH_2PO_4-HCl and citric acid-sodium citrate) used to obtain a range of pH between 2.2 and 8.5.

pH	Buffer
8.5	Tris-HCl
7	NaH_2PO_4-HCl
6	citric acid-sodium citrate
5	citric acid-sodium citrate
4.5	citric acid-sodium citrate
4	citric acid-sodium citrate
3.5	citric acid-sodium citrate
3	citric acid-sodium citrate
2.2	citric acid-sodium citrate

Table 2.2 – Quantities of NaCl and Tris used to obtain different ionic strength.

Ionic strength (mM)	NaCl (g)	Tris (mM)	Tris (g)	Volume solution (mL)
500	2.88	25	0.3	100
400	2.29	25	0.3	100
300	1.70	25	0.3	100
250	1.42	25	0.3	100
200	1.11	25	0.3	100
100	0.53	25	0.3	100
50	0.25	25	0.3	100
40	0.189	25	0.3	100
30	0.13	25	0.3	100
25	0.10	25	0.3	100
20	0.07	25	0.3	100
15	0.04	25	0.3	100
10	0.03	25	0.3	100
7	0	25	0.3	100
5	0.021	10	0.12	100
2.5	0.007	5	0.06	100
1	0	5	0.06	100

2.3 Acidification

To avoid local effects and heterogeneity of acidification with a weak acid such as those used in industrial processes, we used glucono-delta-lactone (GDL, ref G2164, Sigma-Aldrich) which allows a progressive acidification of the latex. The GDL hydrolyzes *in situ* (Pocker and Green 1973) in solution and gluconic acid is progressively released in the medium (Figure 2.1).

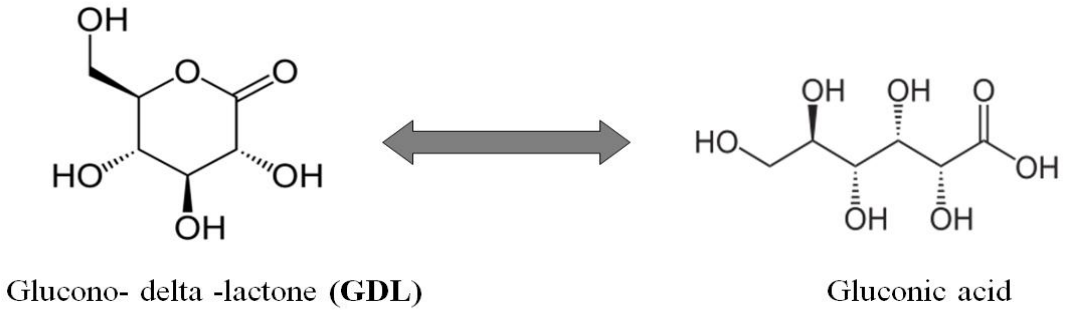

Figure 2.1: GDL hydrolysis into gluconic acid.

Thus, the acidification with GDL is homogenous in the entire volume. The GDL acidification depends on the concentration but it is much faster than the natural acidification in the field. Indeed, in the natural acidification of the field latex, the acidification occurs after 20-24 hours. In fact, the kinetic of GDL acidification resembles the acidification process occurring to prepare off-latex grade TSR5 (acidification at pH 4.8). The kinetics of GDL diluted in Tris-HCl buffer 25mM pH 8.5 solution with different amounts of GDL is plotted in Figure 2.2. Clearly, kinetics depends on the GDL amount and a constant final pH around 4 is obtained for concentrations of GDL higher than 1 % (Inset Figure 2.2).

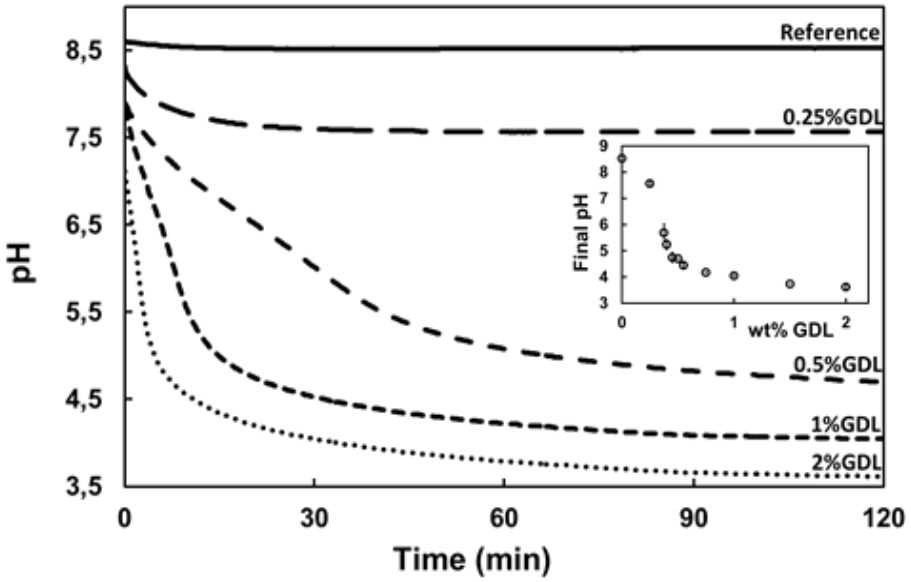

Figure 2.2: pH as function of time for different kinetics of acidification in buffer solution using different amounts of GDL. Inset: final pH as function of amount of GDL.

GDL is directly added on 30 mL of prepared diluted NRL. The quantities of GDL will depend on the particle volume fractions. To obtain the same kinetic of acidification for all volume fractions, we varied the GDL amount for each volume fraction of NRL particles used. Figure 2.3 shows the batches of acidification for two volume fractions, 0.0025 and 0.1 with different values of GDL (between 0.25 and 2 %v/v). Clearly, kinetics depends on volume fraction and amount of GDL.

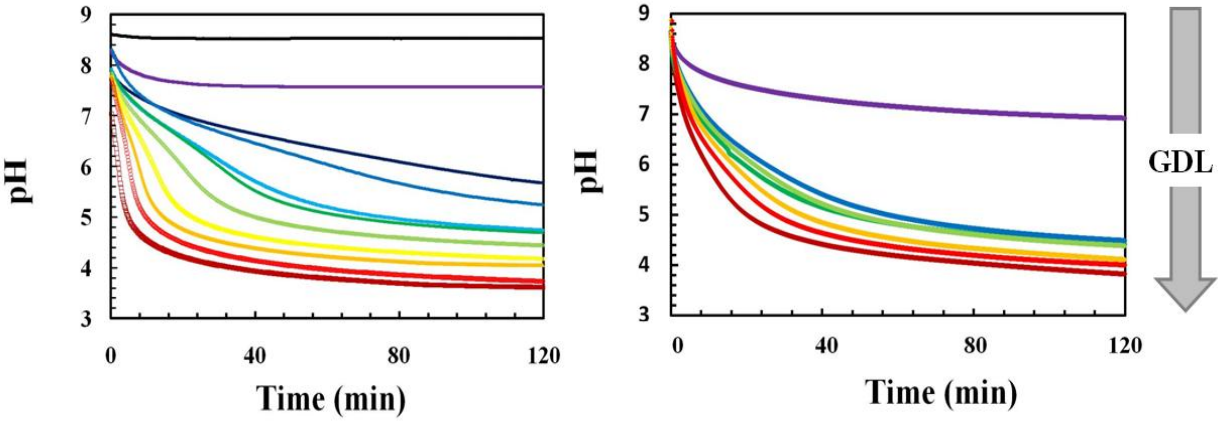

Figure 2.3: pH as function of time for several kinetics of acidification in buffer solution using between 0.25 and 2 %v/v of GDL for Φ_v =0.0025 (left) and Φ_v =0.1 (right). The amount of GDL used increases from top to bottom in both curves.

The selected kinetics of acidification are showed in Figure 2.4. Times to reach pH 6 and pH 5 were about 17 ± 2 minutes and 33 ± 5 minutes respectively with a final pH of 4 ± 0.13 after 4 hours. For all samples with $\Phi_v < 0.1$, the amount of added GDL is fixed to 1 %. For $\Phi_v \geq 0.1$, the amount of GDL increases with the volume fraction (inset Figure 2.4). In the cases where the suspensions are obtained without dialysis (directly from the bottle), the amount of GDL to obtain the same kinetics was increased due to the presence of the ammonia (high pH). The concentrations of GDL used are given in Table 2.3.

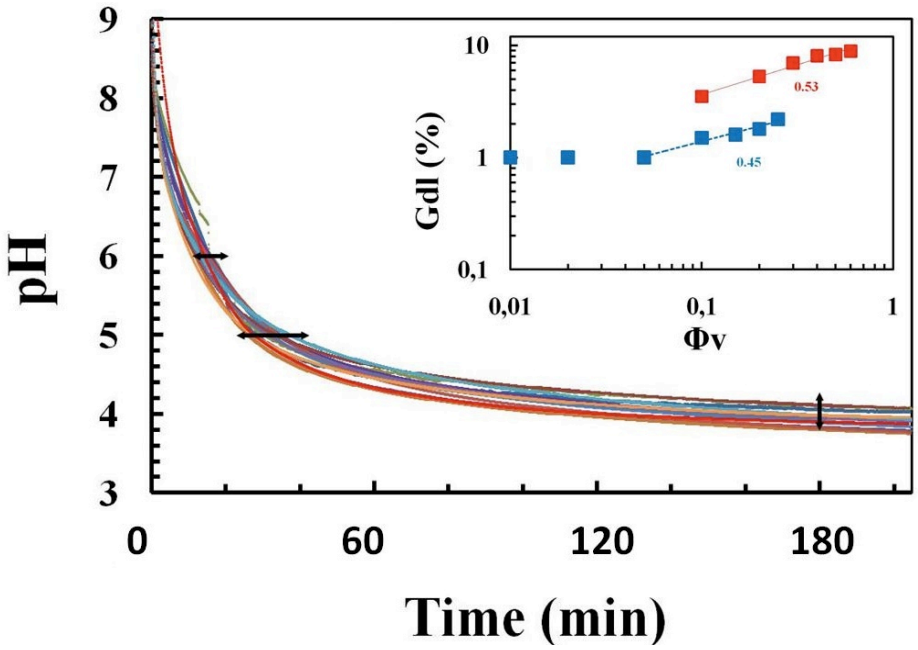

Figure 2.4: pH as function of time during the acidification of natural rubber latex in a large range of volume fraction. Inset: GDL amount as function of volume fraction for the dialyzed (blue) and non-dialyzed (red) samples.

Table 2.3 – Concentration of GDL as a function of particles volume fraction.

Sample	Latex (%v/v)	GDL (%)
Dialyzed	1	1
Dialyzed	2	1
Dialyzed	5	1
Dialyzed	10	1.5
Dialyzed	15	1.6
Dialyzed	20	1.8
Dialyzed	25	2.2
Non-dialyzed	10	3.5
Non-dialyzed	15	4.5
Non-dialyzed	20	5.3
Non-dialyzed	30	7
Non-dialyzed	40	8.1
Non-dialyzed	50	8.3
Non-dialyzed	60	8.9

2.4 Aggregation monitoring

To determine the onset of acid-induced aggregation, we used different light scattering techniques. NRL is particularly difficult to characterize because of the high level of opacity of the suspension observed at very low volume fraction. Moreover, the particle diameter is

relatively important, approaching (or exceeding) one micrometer. As a result, dynamic static light scattering (DLS), which is usually used to analyze colloidal suspensions, is not appropriate for our system.

To study the onset of aggregation of NRL particles in a large range of volume fractions we used a combination of static light scattering (SLS), turbidity and diffusion wave spectroscopy (DWS). The procedure used for the DWS measurements is described in chapter 3.

2.4.1 Static light scattering (SLS)

In static light scattering, diffusion is treated as the result of statistical fluctuations of the position of the particle. The intensity of the scattered light is a function of the wavelength λ, the scattering angle (θ), the particle diameter (d) and the relative index of refraction (n_{ir}) of the particle and the medium. Particle size, assuming a spherical shape, is obtained using the Mie theory.

We used a Malvern Mastersizer 2000 (Malvern Instruments, UK), equipped with a Hydro 2000S wet sample dispersion unit, to determine the size distribution of the dialyzed NRL suspension. It is equipped with a red and blue laser sources at 633 and 444 nm respectively. This technique was used to determine the size distribution of natural rubber latex and the onset of aggregation during acidification.

During an acidification, monitored with a pHmeter, small aliquots (2 drops using a plastic pipette of 3 mL) of latex were taken at different times to determine the onset of aggregation. These aliquots, collected at different pH (and times), were diluted in 50 mL buffer. Then, some drops were introduced in the SLS system filled with Tris-HCl buffer 25 mM pH 8.5. The exact quantity introduced, was adjusted to reach an obscuration level between 2 % and 4 % in order to avoid multiple scattering. The refractive index (n_i) of the NR particles is 1.52, the absorbance value of particles was taken as 0.001 and the refractive index of water is 1.33.The mean particle diameters obtained for each aliquot were normalized by the mean particle diameter obtained for the initial sample before acidification (pH 8.5). For more details, see chapter 3.

2.4.2 Turbidity

Turbidity is the phenomenon by which a light beam passing through a liquid medium is attenuated due to scattering by particles. The scattering of incident light beam depends on the shape and size of particles. The backscattering detector is used in the case of the natural rubber latex due to the level of opacity.

For each diluted suspension, turbidity was monitored *in situ* during 2 hours of acidification with a McVan Instruments® Analite NEP 160 portable probe. The measurement is directly expressed in NTU (Nephelometric Turbidity Unit). For this, 150 mL of prepared NRL suspensions was stirred with 1 % of GDL amount a magnetic stirrer during 2 hours. Turbidity

was used for NRL suspensions with volume fractions (Φ_v) between $3.5x10^{-5}$ and $1.2x10^{-3}$. In this Φ_v range, a calibration curve showed a linear dependence of turbidity on particle concentration.

2.5 Rheology experiments

2.5.1 Introduction

The viscoelastic properties of natural rubber latex gels were characterized by rheology. For this, we used different Couette geometries in different stress-controlled rheometers. The different Couette geometries were used to prove the absence of wall slip during measurements. Gelation of natural rubber latex was performed *in situ* in the rheometer and then the gels were characterized by a frequency and stress sweep in an oscillatory mode. Then, the impact of the shear on the gelation and on the structure of the gel formed was followed. To analyze the displacement fields inside the gel during the oscillations, a classic rheometer coupled with an ultrasonic speckle velocity (USV) was used. The viscosity of the natural rubber latex before gelation was determined in function of volume fraction.

This section is divided into 6 parts: a theoretical background, a description of the equipments used, an oscillatory procedure used, a gelation under shear procedure, a rheo-ultrasound technique used to analyze the displacement fields inside the gel and the viscosity measurements (rotational mode).

2.5.2 Theoretical background

Rotational rheometers are classified in two categories: strain-controlled and stress controlled. They can be equipped with different measurement devices like concentric cylinders (Couette), cone-plate, parallel plates and rectangular torsion (Mezger 2006). The choice of the geometry depends on the viscosity and the nature of the material; liquid or solid (Figure 2.5).

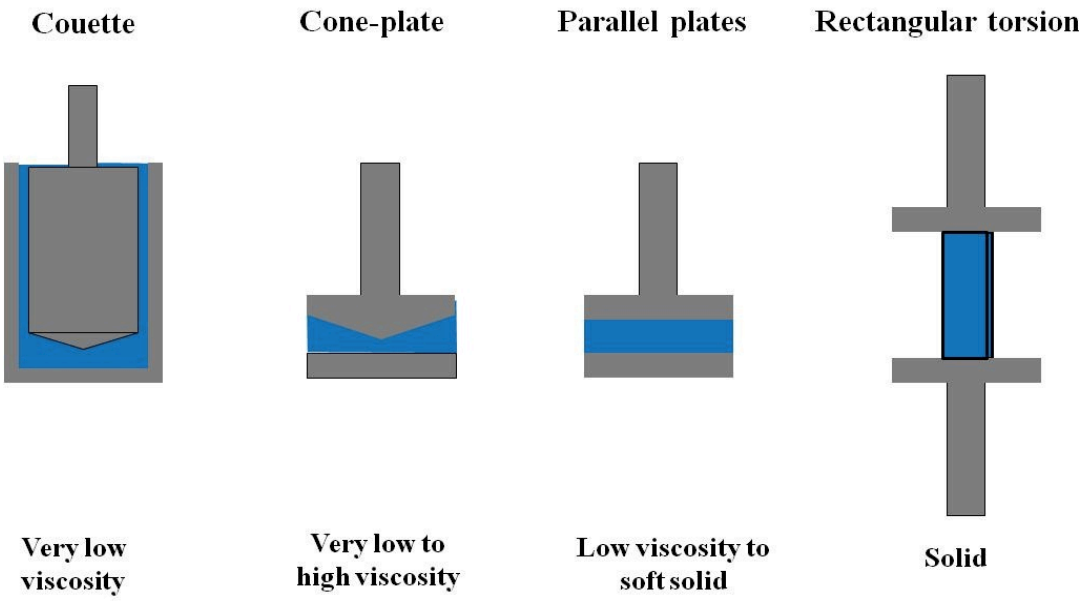

Figure 2.5: Rheological measurement devices for different kinds of materials and viscosity levels. From left to the right: Couette for very low viscosity, cone-plate for very low to high viscosity, parallel plates for low viscosity to soft solid and rectangular torsion for solid.

A Couette system consists of an external cylinder (cup) and an internal cylinder (mobile) with radii R_e and R_i respectively (Figure 2.6). Another important parameter is the effective immersed length of the mobile (H_e). The temperature of the sample can be easily controlled due to the large contact area.

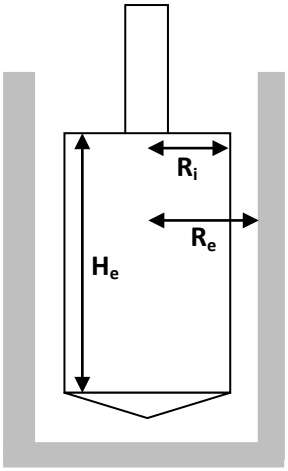

Figure 2.6: Illustration of a Couette cup and mobile with their respective dimensions.

The gap between the cup and the mobile should be small enough so that the sample confined in the gap experiences a constant shear rate. When the mobile is rotating at angular frequency (ω), the shear rate ($\dot{\gamma}$) is given by the equation 18.

$$\dot{\gamma} = \omega \frac{{R_e}^2}{{R_e}^2 - {R_i}^2} \quad \text{Eq. 17}$$

If the torque measured on the mobile is T, the shear stress σ in the sample is given by the equation 18.

$$\sigma = \frac{T}{2\pi {R_e}^2 H_e} \quad \text{Eq. 18}$$

2.5.3 Equipments used

The rheological properties of the natural rubber latex gels were studied with three different stress-controlled rheometers: an AR2000ex, an ARG2 (TA instruments) and an MCR702 (Anton Paar). In all cases, a Couette geometry was chosen due to the low viscosity of natural rubber latex.

A difficulty which can be observed during rheological measurements is the wall slip, especially with smooth surface mobiles. The contact of the mobile surfaces with the material can generate a slip at the walls. This phenomenon occurs depending on the viscosity of the material and the speed of rotation of the mobile. A thin layer of fluid near the surface is formed which causes measurement errors and wrong interpretations of results. To avoid these wall-slip problems, a sanded, serrated (stripe of 0.5 mm) and plastic geometries (cup and mobile) were tested for our experiments. Figure 2.7 shows the illustrations of sanded and serrated mobile.

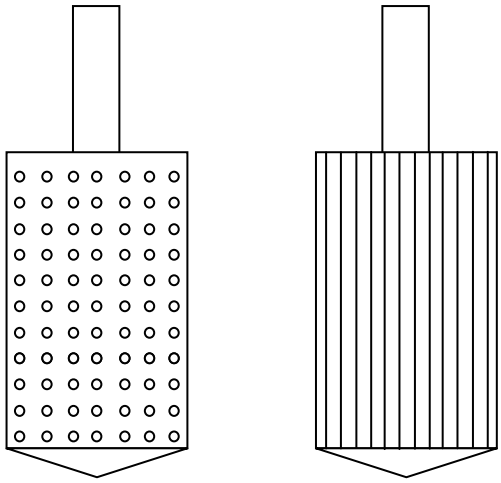

Figure 2.7: Illustration of a sanded (left) and serrated (right) Couette mobiles.

For the different Couette devices used on the different rheometers, the surface, the material, the dimensions and the inertia varied as indicate in Table 2.4.

Table 2.4 – Characteristics of the different Couette devices used.

Surface	Material	R_e (mm)	R_i (mm)	H_e (mm)	Rheometer
Smoothed	Aluminum	15	14	42	AR2000ex
Serrated	Aluminum	15	14	42	AR2000ex
Sanded	Aluminum	11	10	30	MCR702
Plastic*	Transparent PMMA	25	23	60	ARG2

* The plastic mobile is sanded and the cup is smoothed.

2.5.4 Oscillatory measurements procedure

The gelation of the natural rubber latex was performed *in situ* in the rheometer using the different Couette geometries as described before. This gelation step was followed during 4 hours, in the following it is called the time sweep step (Figure 2.8a). Then, the gel formed after this step was submitted to two different mechanical characterizations. The first was a frequency sweep step (Figure 2.8b) while the second was a stress (or strain) sweep step until to the fracture of the gel (Figure 2.8c).

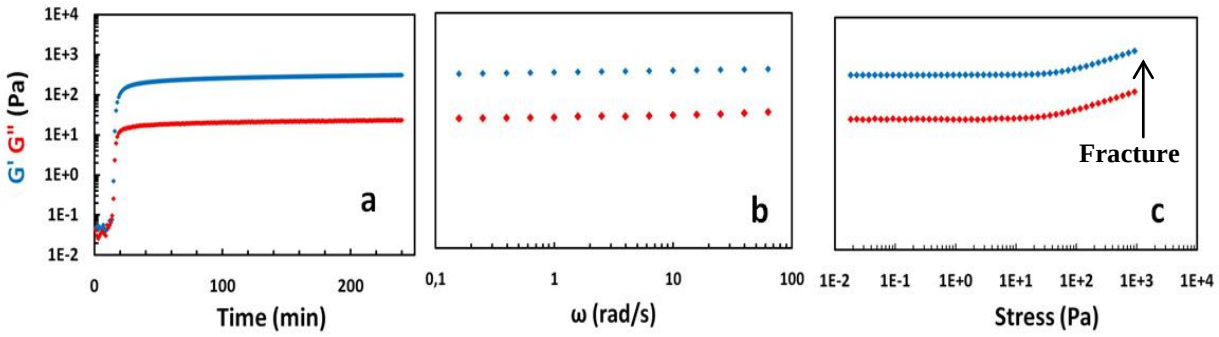

Figure 2.8: Illustration of *G'* and *G"* in function of time (a), and then successively in function of frequency (b) and in function of stress (c) for a natural rubber latex gels Φ_v =0.1.

2.5.4.1 Time sweep measurements

In the time sweep step, the response of the material is monitored at a constant frequency, stress (or strain) and temperature. During this step, the gelation is made *in situ* in the Couette geometry at low values of frequency and strain (or stress) in order to not disrupt the system. The 30 mL of NRL suspensions and corresponding amount of GDL were weighted and then magnetically mixed during 40 s in order to obtain a good dispersion of the GDL. Then, the sample was put into the rheometer. The time between the addition of the GDL and the beginning of the measurement was taken into account. The measurements were performed at 1 Hz, 0.5 % of strain during 4 hours at 20° C. Initially, the values of *G'* and *G"* are very low (liquid state, before gelation), then they increase dramatically and reach a plateau value, G'_0. In this study, the plateau value is measured after 4 hours, and defined the elastic modulus of natural rubber latex gel.

The gelation time is generally measured as the cross-over of *G"* and *G'*. However in the case of natural rubber latex, in some measurements the cross-over of *G'* and *G''* was not observed and the initially *G'* measured was greater than the *G"*. This can be explained by the low values of *G'* and *G"* measured in the early stages of gelation. At the beginning of measurements, the latex is liquid with a very low viscosity and the rheometer is not able to measure correctly. Indeed, the input and output signals from rheometer are very noisy and not sinusoidal. The values measured before the gelation point are not stable and vary from a measurement to another. Thereby, the gelation time is defined as the time at maximum values of the first derivate of *G'* in function of time. However, the values obtained by the two methods are equivalent when comparison can be done (annex I). Finally, the total gelation time is determined by the time obtained by rheological measurement added by the time taken after the addition of the GDL (~40 s).

2.5.4.2 Frequency sweep measurements

After 4 hours of time sweep, *G'* and *G"* of gels were measured as a function of frequency. In the frequency sweep step, the response of the material to the increased frequency is monitored at constant stress (or strain) and temperature. Measurements were performed between 0.01 Hz and 10 Hz at 0.5 % strain at 20° C.

2.5.4.3 Stress sweep measurements

The evolution of *G'* and *G"* in function of stress was observed from 0.02 Pa up to the gel fracture. The stress is applied instead of the strain because for high values, the sinusoidal form of the signals performed from the rheometer is better.

The NRL gels exhibited a strain hardening behavior which is characterized by the increases of *G'* and *G"* with the progressive increase of strain (or stress). To study the reversibility of the strain hardening behavior, the stress was increased and decreased successively. The maximum values for each step were progressively increased.

2.5.5 Influence of the strain on the gelation

In the conditions of gelation taken as a reference, done at very low strain (0.5 %), the effect caused by the shear forces was negligible, as illustrated by the fact that the mechanical properties of the final gel were identical to the one measured on gel formed at rest. In the case of the gelation under higher shear, the shear forces can impact the system and then the formation of the gel. Therefore, we studied the rheological properties of gel formed under variable oscillatory strain values (0.5 % to 150 %). For this, different constant values of the initial strain were applied at the beginning of the experiment and during all the gelation process during the time sweep step. After the formation of the gel, it was characterized by a stress sweep step as described in the previous section.

2.5.6 Rheo-ultrasound

The results from this section are obtained from collaboration with the Dr. Manneville group, ENS Lyon. The Rheo-Ultrasound technic was used to analyze the displacement fields inside the gel during the oscillatory measurements. For this, a classic stress-controlled rheometer, ARG2 TA Instruments, is coupled with an ultrasonic speckle velocity (USV) (Manneville *et al.* 2004). The USV is based on the interactions between the particles of the sample and the ultrasonic pulses. The speckles, spots in an image, are produced by the backscattering signal obtained from successive pulses and are obtained as a function of time.

A transparent PMMA Couette geometry (R_e =25 mm, R_i =23 mm, H_e =60 mm) was used inside a water box to ensure good performances (Figure 2.9). An ultrasonic 2D-scanner is used during the oscillatory measurements. The NRL gel was formed *in situ* as explained previously in the time sweep step during 30 minutes. Polystyrene particles (Dynoseed TS20µm) were used as an ultrasonic contrast agent without any impact in rheological properties. The addition of these particles is needed because the NRL particles do not have good acoustic properties. It is added 1.5 %v/v of polystyrene particles to 35 mL of latex before the addition of the GDL, then the system was mixed magnetically during 40s. To avoid the sedimentation of the particles we used a larger amount of GDL (5 %) such that the system form a gel before sedimentation could occur.

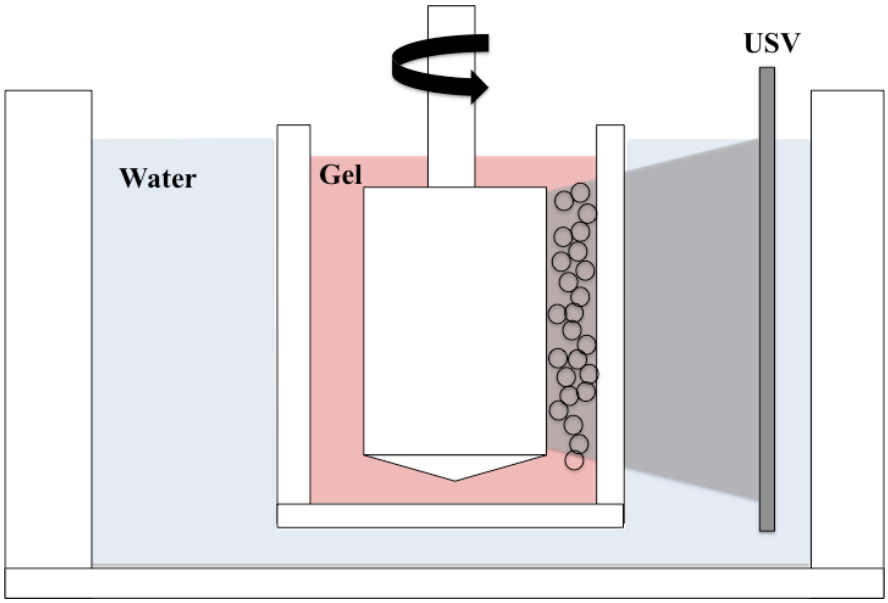

Figure 2.9: Illustration of Rheo-ultrasound equipment.

After the formation of the gel, the strain was increased step by step. For each step, the oscillatory strain was first kept constant for 5 minutes. The ultrasonic measurements were performed with 20 sequences of 3000 pulses at 350 Hz simultaneously with the oscillatory measurements.

The displacements occurring inside the gel during oscillations were obtained from the speckles in function of time. The velocity profiles (v) were obtained from USV using equation 19.

$$v = \sum_{f=1}^{8} v_f \sin\left(2\pi f t - \varphi_f\right) \qquad \text{Eq. 19}$$

where $v_f > 0$ is the x velocity (mm s^{-1}), f is the frequency (Hz), t is the time (s) and φ_f is the phase shift ($\pi > \varphi_f > -\pi$).

The harmonics were obtained from Fourier decomposition (Fast Fourier Transformer- FFT) of the local velocity versus the time. Matlab® was used to analyze all results.

2.6 Viscosity determination

In the case of viscosity measurements on NRL suspensions, a shear rate was applied and varied between 100 and 10^{-3} s^{-1}. The values of viscosity are extracted on the second Newtonian plateau (Figure 2.10). The values of the shear rate for each step (Newtonian plateau and transition regime) depend on the nature of particles and their size. A power law between the viscosity and the shear rate in this transition regime as described in literature.

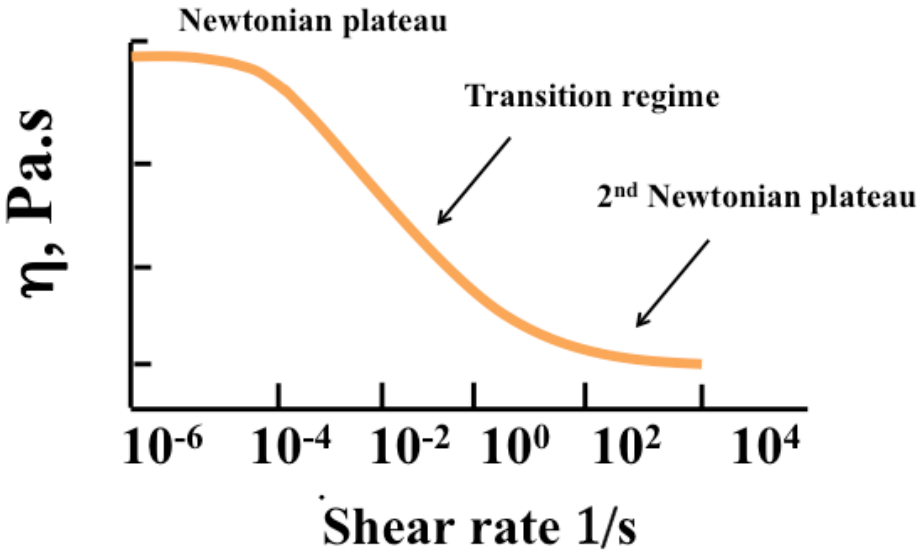

Figure 2.10: Illustration of flow curves, viscosity =f (shear rate), with three different regimes.

2.7 Confocal laser scanning microscopy

The confocal laser scanning microscope uses a laser light source for promoting excitement of molecules. Some molecules when excited by high energy light absorb energy, change their energy state and emit photons at a lower energy in form of light. This phenomenon is called fluorescence. The color of the light emitted depends on the material and on the incident wavelength. The confocal laser scanning microscope through a serial set of lenses is capable of focusing a cone of laser light at a pre-particular depth in the specimen to be studied. Changing the focus point, the whole plan under study can be excited point by point. Thus, only light in the focus points is recorded with the help of a computer coupled to photomultiplier tubes and which enables to construct two-dimensional images (Prasad *et al.* 2007; Eric and Denis 2014).

The NRL particles and the gel formed were observed by confocal microscopy. To do so, we used Nile Red (ref N3013-100MG, Sigma-Aldrich), a lipophilic fluorescent dye specific to the membrane surrounding biological particles.

Suspensions and gels were observed in inverse confocal laser microscope (TCS SP8, Leica, Wetzlar, Germany) employing Argon laser (wavelength 488 nm for excitation) with a 63xoil objective. The sample preparation procedure was as follows:

(1) 1 % of Nile Red was dissolved in Ethanol during 4 hours under magnetically mixed.
(2) 300 µL of the dye was added in 5 mL of latex suspensions* and magnetically mixed during 24 hours.
(3) A drop of sample is placed with a plastic disposable pipette between a microscope slide and a cover, previously mounted (~ 4 µm between slide and cover slip). The sample spreaded between the slide and the coverslip by capillarity.

* the volume fraction of latex suspensions used was varied between 0.025 and 0.1.

For the gel samples, 1 % of GDL was added before step 3.

References

Eric, R. W. and S. Denis (2014). Confocal Microscopy. Encyclopedia of Biomaterials and Biomedical Engineering, Second Edition, Taylor & Francis. **null:** 705-714.

Manneville, S., *et al.* (2004). "High-frequency ultrasonic speckle velocimetry in sheared complex fluids." European Physical Journal-Applied Physics **28**(3): 361-373.

Mezger, T. G. (2006). The rheology handbook : for users of rotational and oscillatory rheometers. Hannover, Vincentz Network.

Pocker, Y. and E. Green (1973). "Hydrolysis of D-glucono-delta-lactone. I. General acid-base catalysis, solvent deuterium isotope effects, and transition state characterization." Journal of the American Chemical Society **95**(1): 113-119.

Prasad, V., *et al.* (2007). "Confocal microscopy of colloids." Journal of Physics: Condensed Matter **19**(11): 113102.

Chapter 3

Acid-induced aggregation and gelation of natural rubber latex particles

Coagulation of natural rubber latex suspensions into an elastic gel is the first step of their processing into rubber. We studied this transition under controlled acidification conditions with the aim of identifying the main parameters controlling gel formation. The onset of aggregation and the percolation events observed during continuous acidification were monitored on a large range of volume fractions by a combination of light-scattering techniques adapted to the different degrees of suspension opacity (namely, diffusing wave spectroscopy, static light scattering and turbidimetry) and by rheology. We consequently established the state diagram of NRL particles in the pH–Φ_v space during acidification. Within this diagram, we identified three states: a suspension, a two-phase macroscopically separated system in between a gel and a suspension, and a gel. The rheological properties of the gels were characterized as a function of the volume fraction Φ_v. The elastic modulus scale with $\Phi_v^{3.35}$, it shows remarkable consistency independently of the acidification kinetics and final pH.

This chapter is an article already published in Colloids and Interface A: Physicochemical and Engineering Aspects under the following reference:

De Oliveira Reis G., Menut P., Bonfils F., Vaysse L., Hemar Y., Sanchez C., Acid-induced aggregation and gelation of natural rubber latex particles, Colloids and Surfaces A: Physicochemical and Engineering Aspects, Vol. 482, 2015, Pg. 9-17.

3.1 Introduction

Natural rubber latex (NRL) is the cytoplasm of laticiferous cells from Hevea brasiliensis trees (Jacob *et al.* 1993). It is a complex colloidal suspension containing 30 to 45 %vol of rubber particles and 10 to 20 %vol of lutoids (Dauzac *et al.* 1982). Both are suspended in an aqueous phase, or serum, containing a large number of biochemical compounds including minerals, soluble carbohydrates, and proteins (Jacob *et al.* 1993). Rubber particles mostly consist of a poly(cis-1,4-isoprene) core surrounded by a complex membrane made of phospholipids (Cornish *et al.* 1999; Sansatsadeekul *et al.* 2011) and proteins (Dennis and Light 1989). The organization of proteins and phospholipids on the membrane of these particles is still unclear. Some authors have proposed that it is organized in patches (Nawamawat *et al.* 2011) while others assumed a structural organization in stratified layers (Rochette *et al.* 2013), with a thickness in the range of 10 to 20 nm (Singh *et al.* 2003; Gaboriaud *et al.* 2012).

After tapping, different biochemical reactions in the NRL suspension result in its coagulation (Hanower *et al.* 1976; Brzozowska-Hanower *et al.* 1978; Gidrol *et al.* 1994; Wititsuwannakul *et al.* 2008). Coagulation mostly occurs naturally in the cup due to bacterial-induced acidification and in some cases by manual addition of an acid. Coagulation can be avoided by adding ammonia to increase the pH to >10, which is a method used for the production of concentrated latex. In such commercial suspensions, particles are stabilized by the presence of both proteins and fatty acids resulting from the hydrolysis of phospholipids at a high pH (Ho *et al.* 1996), as well as by the addition of stabilizers. These different compounds, generated *in situ* or added, ensure a repulsion range which has been experimentally estimated to be around 50 nm in a 1 mM NaCl solution. This distance strongly depends on the ionic strength, but remains rather short in comparison to the particle size (Gaboriaud *et al.* 2012).

In colloidal systems undergoing aggregation, particles initially form clusters characterized by a fractal structure. As their fractal dimension is less than the spatial dimension, the growth of these clusters induces an increase in their effective volume fraction, till they reach the close packing stage (Sorensen and Chakrabarti 2011), defined as the gel point. Further aggregation or cluster interpenetration might continue, and as a final result particles will form a percolating, three-dimensional network. Experimentally, attraction between particles can be induced by the addition of a depleting, non-adsorbing polymer, or by a change in the physical-chemical composition of the solvent, such as a change in ionic strength or pH. It has been shown that the exact conditions required to observe particle gelation or clustering depends on three parameters: the particle volume fraction, Φ_v, inter-particle attraction, U, expressed relatively to the thermal energy k_BT, and the range of attraction, ξ (Lu *et al.* 2006).

Although the very specific structure, composition and properties of NRL particles have yet to be fully elucidated, it is believed that these features are very important in the mesoscopic organization of the different rubber components in the final product used by tire manufacturers (Toki *et al.* 2008; Carretero-Gonzalez *et al.* 2010; Wisunthorn *et al.* 2012). While many studies have been carried out on the structure, composition and properties of raw natural rubber, very little is known about the first steps involved in product manufacture,

especially during the acidification step. A better understanding of this step would help to control the structure of the gel and therefore to improve the quality of raw natural rubber products.

This paper is organized as follows. First, we characterized particle properties in terms of size distribution and electrophoretic mobility. Second, we established the suspension state diagram pH-Φ_v by varying systematically the pH (between 8.5 and 4) and the particle volume fractions ($1.0\text{x}10^{-4} < \Phi_v < 2.0\text{x}10^{-1}$). Three states were observed: a stable suspension, a macroscopic phase separation between gel and a suspension, and a gel. We followed the time-dependence behavior of the system over 5 weeks. Third, we studied the case were aggregation and then gelation of the entire suspension occurs through a continuous, *in situ* acidification. This was obtained through hydrolysis of an added compound, namely glucono-δ-lactone, which decreased the pH to 4 in less than 2 hours. We characterized the onset of aggregation using three different optical techniques adapted to the various levels of opacity and rheology to complete the state diagram. Finally, in section four we studied the rheological properties of the gels.

3.2 Materials & Methods

3.2.1 Materials and Sample Preparation

Natural rubber latex (NRL) composition depends on many parameters, such as agronomic conditions, tree genotype and seasonal variations. Its characterization is additionally complicated by the fact that the raw, native product is highly unstable. To avoid those difficulties, a commercial product from Dalbe, France (ref. 4770002), which contained pre-vulcanized particles of NRL stabilized with ammonia, was used. The pH of the product was around 10.5, and its dry mass around 59 %wt. The suspensions contained a large amount of ammonia and some preservatives. Therefore, before use, samples were first diluted with an equivalent amount of Tris-HCl buffer (pH 8.5, ionic strength =7 mM), and then extensively dialyzed against the same buffer using a dialysis tube (SpectraPor, cut-off 12-14 kDa, diameter 29 mm). Dialysis was conducted for 7 days, at ambient temperature in the dark, replacing the buffer solution daily. After extensive dialysis, the suspension volume fractions Φ_v ranged typically between 0.25 and 0.30. Dialyzed suspensions were kept at 4°C and used within three weeks. Suspensions with various concentrations were then prepared by dilution with the appropriate amount of Tris-HCl buffer.

When suspensions with a higher volume fraction were required, the commercial suspension was directly diluted with the buffer to reach the required volume fraction, without dialysis. We show later in this paper that this did not affect the studied properties.

3.2.2 Electrophoretic Mobility

Electrophoretic mobility measurements were carried out using a Malvern Zetasizer 3000 HS. The electric field was held constant at 100 V/cm. The electrophoretic mobility of latex particles was measured at 25° C for different pH and ionic strengths conditions, at a concentration of 6.0×10^{-6} w/w. The pH was controlled using either Tris, phosphate acid or citric acid buffer, and adjusted using HCl, or sodium citrate for the latter buffer. For measurements at various ionic strengths (1 mM to 500 mM NaCl), a pH 8.5 Tris buffer was chosen. The electrophoretic mobility values were the average of 8 measurements on separate samples.

3.2.3 Particle sizing

A Malvern Mastersizer 2000 (Malvern Instruments, UK), equipped with a Hydro 2000S dispersion unit filled with the Tris-HCl buffer solution was used to characterize particle size by SLS. The refractive index of the particles was assumed to be 1.52 (Wales 1962; Nwadinigwe 1988), and the absorbance 0.001, a refractive index of 1.33 was used for the Tris-HCl buffer. Particle size values were inferred from the Mie theory, assuming a spherical shape. The particles concentration was adjusted to reach obscuration levels between 2 and 4 %, in order to avoid multiple scattering which occurs at high concentration.

3.2.4 Acidification procedure

In water, glucono-δ-lactone (GDL) (ref G2164, Sigma-Aldrich) progressively hydrolyzes into gluconic acid, which decreases the pH of the medium. This offers a convenient way of controlling the acidification kinetics of NRL suspensions, avoiding local effects usually encountered when high acid concentrations are used. In addition, such an acidification process closely resembles the bacterial acidification that occurs in the natural coagulation occurring after tapping.

Monitoring the pH of the NRL suspensions clearly showed their dependence on the GDL concentration, which also affected the final pH value. For a given concentration of GDL, no significant variation in acidification kinetics was observed with the volume fraction $\Phi_v \leq 1.0\text{x}10^{-1}$. Therefore, 1 %wt GDL as a standard condition was used to ensure a final pH close to 4 in less than 2 hours. For $\Phi_v > 1.0\text{x}10^{-1}$, a slight dependence of the acidification kinetics on ϕ_v was observed; as a result, acidification kinetics was recorded in each case for further result analysis. In the specific case detailed later where we used non-dialyzed suspension (for $\Phi_v > 3.0\text{x}10^{-1}$) a stronger dependence of the kinetics of acidification on the particle concentration was observed. In those cases, the amount of GDL was varied to reproduce standard acidification conditions.

3.2.5 Aggregation monitoring

Aggregation mechanisms were monitored during acidification using light-scattering techniques. Dynamic light scattering is a technique widely used to characterize such processes, but cannot be applied either on a highly opaque suspension or for the characterization of large particles or aggregates which are less sensitive to Brownian motion. As a result, we combined three other techniques to monitor particle aggregation in a large range of volume fractions. The diversity of the three methods precluded a direct comparison between the results obtained here, and they were found to be complementary and consistent with each other.

3.2.6 Diffusive wave spectroscopy (DWS)

For moderately diluted suspensions, i.e. for $2.8\text{x}10^{-3} \leq \Phi_v \leq 2.8\text{x}10^{-2}$, the use of DWS enables the quantitative determination of size changes of the diffusing objects in suspensions. Transmission DWS experiments were performed in a cross-correlation mode in an experimental set-up fully described elsewhere (Hemar and Pinder 2006). Samples were measured in plastic glass cuvettes of 10 mm path length (L). The cuvettes were held in a TLC 50/E Peltier temperature controlled holder (Qantum Northwest Inc., Seattle, WA, USA). The beam of a 35 mW HeNe laser (HRP350-EC, Thorlabs Inc., New Jersey, USA), with a wavelength of $\lambda = 632$ nm was expanded to approximately 8 mm at the surface of the cuvette, using a beam expander (BE03M-A, Thorlabs Inc., New Jersey, USA). The scattered light was collected by single-mode optical fibers (P1-3224-PC-5, Thorlabs Inc., Germany), fitted with a GRIN lens (F230FC-BFC, Thorlabs Inc., Germany). A polarizer (LPVISE100-A, Thorlabs Inc., Germany) was installed in front of the lenses and set in cross polarization to the laser to ensure collection of scattered light only. The optical fiber was linked to a bifurcated Y fiber configuration (Fiber Optic Network Technology Co, Surrey, BC, Canada), which was attached to two photomultiplier modules (HC 120-08, Hamamatsu Photonics, Japan). The correlation function was measured using a correlator (Flex99OEM-12, correlator.com, Bridgewater, NJ, USA).

In DWS, in transmission geometry, the autocorrelation function $g_{(1)}(t)$ is given by (Weitz *et al.* 1993):

$$g_{(1)}(t) = \frac{\frac{L/l^*+4/3}{z_0/l^*+2/3}\left\{\sinh\left[\frac{z_0}{l^*}\sqrt{\frac{6t}{\tau}}\right]+\frac{2}{3}\sqrt{\frac{6t}{\tau}}\cosh\left[\frac{z_0}{l^*}\sqrt{\frac{6t}{\tau}}\right]\right\}}{(1+8t/3\tau)\,sinh\left[\frac{L}{l^*}\sqrt{\frac{6t}{\tau}}\right]+\frac{4}{3}\sqrt{\frac{6t}{\tau}}cosh\left[\frac{L}{l^*}\sqrt{\frac{6t}{\tau}}\right]} \qquad \text{Eq. 20}$$

where l^* is the scattering mean free path, τ is the relaxation time, z_0 is the penetration depth (generally assumed as equal to l^*) and L is the sample thickness (10 mm), here corresponding

to the depth of the cuvette. The mean free path l^* was obtained by determining the transmitted intensity of a model solution of monodisperse polystyrene latex beads at 25°C.

In the case of particles moving under Brownian motion, the relaxation time τ is given below:

$$\tau = (Dk_0^2)^{-1} \quad \text{Eq. 21}$$

Where $k_0 = 2\pi/\lambda$ is the incident wave vector and D the diffusion coefficient is given by the Stokes-Einstein equation:

$$D = \frac{k_b T}{6\pi\eta R_h} \quad \text{Eq. 22}$$

Where k_B = 1.38x10^{-23} J.K^{-1} is the Boltzmann constant, T is the temperature, R_h is the hydrodynamic radius, and η is the Newtonian viscosity of the continuous phase. Thus, it is possible to determine the evolution of R_h, by fitting the autocorrelation function $g_{(1)}(t)$ using equation 20.

3.2.7 Static light scattering (SLS)

For suspensions whose volume fraction was 2.0x10^{-3} ≤ Φ_v, opacity was such that it was not possible to measure the particle size *in situ*. Therefore, we collected small aliquots of the suspension at different times during acidification, and "quenched" the aggregation process by dilution in a large amount of pH 8.5 buffer. The resulting stable particles, or aggregates, were then characterized as described in the particle sizing section.

3.2.8 Turbidity

For each diluted suspension, turbidity was monitored *in situ* during acidification with a McVan Instruments® Analite NEP 160 portable probe operating in retro-diffusion. The measurement was directly expressed in NTU (Nephelometric Turbidity Unit). Turbidity was used for 3.5x10^{-5} ≤ Φ_v ≤ 1.2x10^{-3}, for which a calibration showed a linear dependence of turbidity on particle concentration.

3.2.9 Rheological characterization

An AR2000ex stress-controlled rheometer (TA instrument), equipped with a Couette geometry (inner radius 14 mm, outer radius 15 mm) was used. The temperature of the sample was kept constant at 20° C by a Peltier thermal regulation system. Samples of NRL were first equilibrated for one hour at room temperature. The required amount of GDL was then added to the sample under magnetic stirring for 40 seconds in order to ensure good dispersion of GDL, before loading onto the rheometer. Sample gelation was monitored for 4 hours in an

oscillatory regime with a frequency of 1 Hz and a strain of 0.5 %. The results showed no measurable impact of the oscillations on the gelation process. Then, the gel was characterized with a frequency sweep from 0.01 to 10 Hz at a constant strain of 0.5 %.

3.3 Results and Discussion

3.3.1 Particle characterization

This section focuses on the intrinsic characterization of the latex particles. First their size and electrophoretic mobility are characterized in comparison with the results previously reported in the literature. Then the softness of the latex particle membrane is characterized using the analysis of electrophoretic mobility at different ionic strengths.

3.3.1.1 Particle density, electrophoretic mobility and size distribution

Particle size determined by SLS exhibited a unimodal distribution centered around 0.9 µm, and a volume based average diameter of approximately 1 µm (Figure 3.1a). From the volume weighted ($D_{4,3}$ =2.6 µm) and surface weighted ($D_{3,2}$ =0.82 µm) mean particle size, we estimated the random close packing of the suspension at Φ_{rcp} =0.715 (Farr and Groot 2009; Shewan and Stokes 2015) .The electrophoretic mobility of the rubber particles as a function of pH (Figure 3.1b) showed that the membrane of particles was negatively charged under storage conditions (pH 8.5, ionic strength =7 mM), and that this membrane charge decreased continuously with the pH decrease, as observed in previous studies (Bowler 1953; Sansatsadeekul *et al.* 2011). The isoelectric pH (pH_i), corresponding to zero mobility, was 3.18. This value was lower than what has been found previously for fresh *Hevea brasiliensis* latex (Bowler 1953; Ho and Ng 1979; Ho *et al.* 1996) (between 3.8 and 4.7) however it is known to depend on different parameters such as the membrane composition, the clonal origin, the storage time or the chemical treatments (Bowler 1953; Ho 1989; Ho *et al.* 1996) of the rubber suspensions.

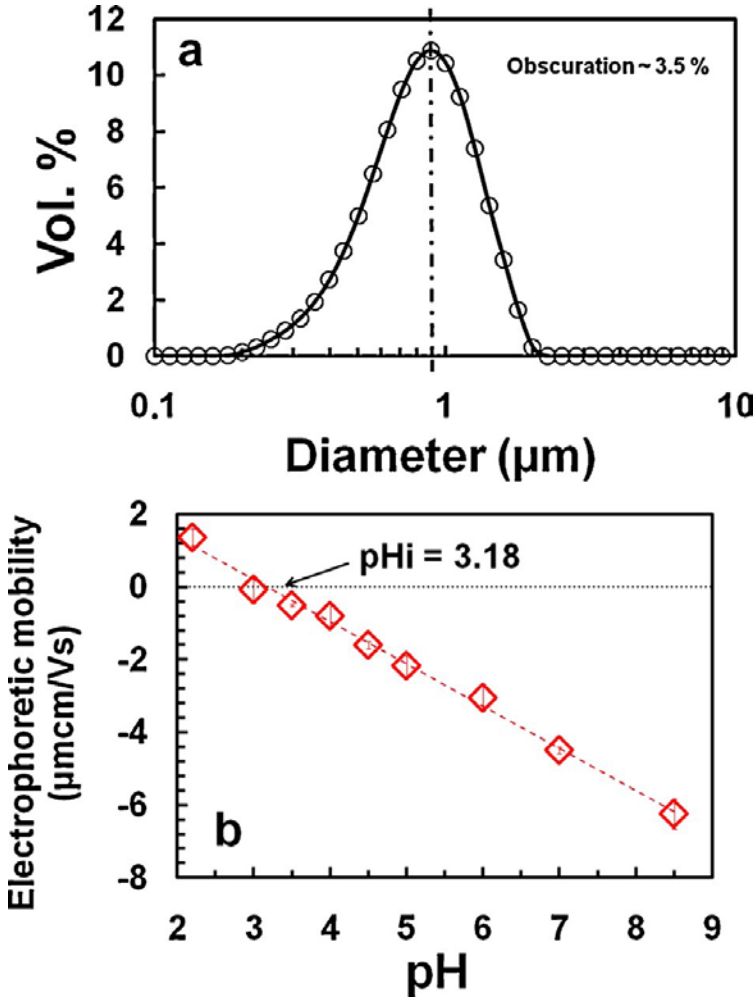

Figure 3.1: (a) Volume particle size distribution of the dialyzed NRL suspension. (b) The electrophoretic mobility of the dialyzed NRL particles as a function of the pH (ionic strength =7m).

3.3.1.2 Particle surface membrane characterization

The electrophoretic mobility of NRL particles was measured at pH 8.5 for different ionic strengths varying from 1 to 500 mM (Figure 3.2). Electrophoretic mobility decreased as the ionic strength increased, indicating that the negative charges localized on the particle surface membrane were increasingly screened. At 150 mM NaCl an electrophoretic mobility value of -2.4 µm.cm.V^{-1}.s^{-1} was obtained, which was in the range of -2.2 to -3.0 µm.cm.V^{-1}.s^{-1} reported for different natural rubber latex particles (Bowler 1953; Ho and Ng 1979; Ho 1989) with the same amount of added NaCl.

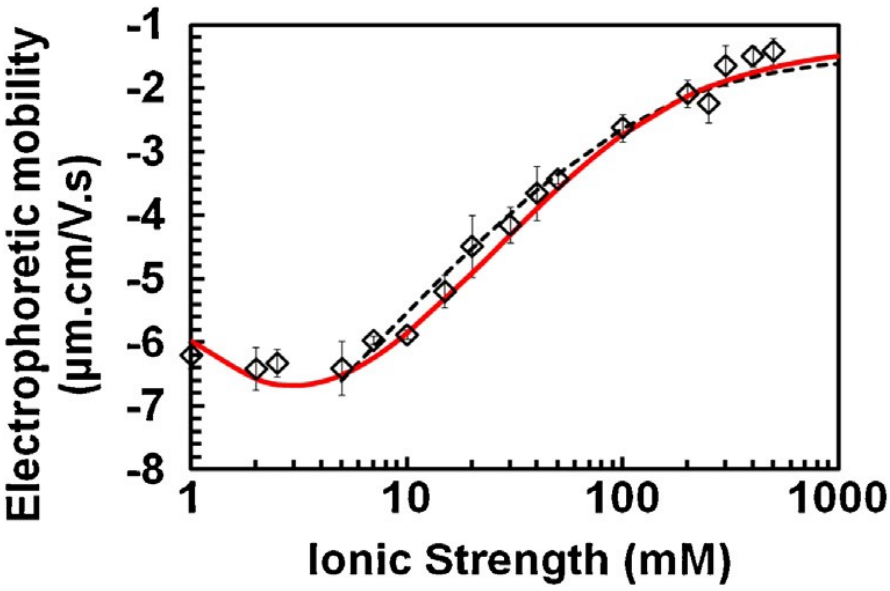

Figure 3.2: Electrophoretic mobility at pH 8.5 as a function of the ionic strength. The black dashed curve and continuous red curves represent fits using Oshima and Duval formalism, see text for more details.

Hard particles exhibit a mobility that goes to zero for sufficiently large ionic strengths as a result of membrane charge screening by ions in the medium. Here we instead observed that a plateau value of around -1.5 µm.cm.V^{-1}.s^{-1} was reached at the higher ionic strength used. The presence of such a plateau value is the characteristic electro-osmotic signature of a charged, soft interphase in the periphery of the particles (Duval and Gaboriaud 2010). Since the soft characteristic of latex particles surface was experimentally demonstrated, the membrane was not characterized by a zeta potential (ζ) as it would be for hard particles. Instead we applied the soft particle electro-kinetic theory from Ohshima (Ohshima 1995). According to this theory, a soft particle experiences a finite degree of penetration of the hydrodynamic flow within the porous, permeable complex interphase. This degree of penetration depends on the membrane layer thickness, charge density and distribution of charges and friction between adsorbed polymer chains and solvent (Ohshima 1995). The analytical expression for the electrophoretic mobility μ of a soft particle of core radius denoted as a and soft membrane layer thickness d is given by (Ohshima 1995; Ohshima 2009; Duval and Gaboriaud 2010):

$$\boldsymbol{\mu} = \frac{\varepsilon_r \varepsilon_0}{\eta} \frac{{\psi_0}/{K_M} + {\psi_D}/{\lambda}}{{1}/{K_M} + {1}/{\psi}} + \frac{eZN}{\eta \lambda^2} \qquad \text{Eq. 23}$$

where ε_r and ε_0 are, respectively, the dielectric permittivity of the medium and of vacuum, η is the dynamic viscosity, K_M is the reciprocal Debye thickness of that layer as corrected for Donnan potential, ψ_D the Donnan potential and ψ_o represents the membrane potential, e the elementary electron charge, Z the ion valence and N the homogeneous membrane charge density. The parameter λ characterizes the degree of friction exerted on the liquid flow in the membrane layer. The Brinkman screening length $1/\lambda$ relates to the drag of the polymer segments and typically reflects the extent of hydrodynamic flow penetration within the soft

interphase (Duval and Gaboriaud 2010; Louie *et al.* 2012). It is representative of the permeability or "softness" of the membrane layer.

Fitting equation 23 to the experimental data determined the two key adjustable parameters, $1/\lambda$ and *ZN* the volume charge density in the surface membrane layer. The fitting exercise (Figure 3.2) resulted in values of 0.9 nm and -0.2 M for $1/\lambda$ and *ZN*, respectively. These results were in very good agreement with Ohshima and co-workers' results on *Hevea brasiliensis* latex particles (Ho *et al.* 1996). These authors applied the soft particle theory at pH 8-9 for 3-month-old or 4-year-old lattices and found $1/\lambda$ values of 0.7 or 0.9 nm, respectively, and a *ZN* value of -0.2 M. We can infer from these results that latex particles are highly charged at pH 8.5, explaining their high colloidal stability.

The Ohshima theory correctly described our experimental data down to about 5 mM ionic strength (black dashed curve in Figure 3.2). Below 5 mM ionic strength, the theory failed to fit the measured electrophoretic mobility, as the experimental data leveled off and even seemed to increase again (more negative electrophoretic mobility) at the lowest ionic strength used (1 mM). These effects may have been due to polarization/relaxation effects, not included in the Ohshima theory (Duval and Gaboriaud 2010; Louie *et al.* 2012). Such effects can be integrated using the formalism developed by Duval *et al.* (Duval and Ohshima 2006), which indeed allowed a better description of the data at low ionic strength (continuous red curve in Figure 3.2). Using the Duval *et al.* (Duval and Ohshima 2006) approach, values of 0.85 nm,-0.22 M and 2 nm were found for $1/\lambda$, *ZN* and d (the soft membrane layer thickness), respectively. These values are consistent with the study of *Rochette et al.* (Rochette *et al.* 2013), giving a surface layer thickness of 3-4 nm for NRL particles of small diameter (less than 100nm in average).

3.3.2 State diagram of natural rubber latex

In this section we establish the state diagram of the system. For a given volume fraction (ranging from $1.0\text{x}10^{-4}$ to $2.0\text{x}10^{-1}$), various pH were imposed either by the addition of a citric acid/sodium citrate buffer or through a rapid acidification with GDL. In the last case, the amount of GDL was adjusted to reach the desired pH (from 8 to 4) in less than 2 hours. The visual appearance of the different suspensions and the evolution of the particle average sizes measured by SLS were monitored for 5 weeks at 20° C.

Three different behaviors were observed. At high pH, the suspension remained stable over time (during the five weeks of measurement) without any sign of aggregation (no size increase measured by SLS). For lower pH, we instead observed particle aggregation, and this could lead to two different behaviors depending of the conditions. In some cases, mostly for the lower pHs, gelation took place in the entire volume of the sample. In some other cases, a gel only formed in the upper part of the vial, with a suspension remaining below the gel. We term this behavior a "macroscopic" phase separation, a phenomenon that can be attribute to the effect of gravitational forces, (Allain *et al.* 1995; Kim *et al.* 2013). As the particles density is lower than one, gravitational forces result here in an upwards migration of the particles. On

individual particles (before aggregation), this force is limited and Brownian motion is sufficient to prevent particles creaming. But once particles aggregate in clusters of larger size, this force increases and, if percolation does not occur rapidly, will eventually result in the creaming of growing clusters, which accumulate in the upper part of the vial where they form a gel.

Those three states have been identified for different conditions of pH and volume fraction, after 4 hours, as indicate in Figure 3.3a. While stable suspensions (empty symbols) were obtained for the higher pH and/or lower volume fractions, the complete gelation (full symbols) was only observed at low pH and volume fractions above 10^{-2}.

The impact of time was assessed after 1, 2 and 5 weeks (Figure 3.3b to 3.3d). Time has no visible effect on suspensions that was already either completely gelled or macroscopically phase separated. However, some suspensions stable on small time scales showed evidence of a macroscopic phase separation if observed for longer times. This is illustrated on the state diagram by the increase in size of this region (half-filled symbols), with a upper limit moving with time towards higher pH.

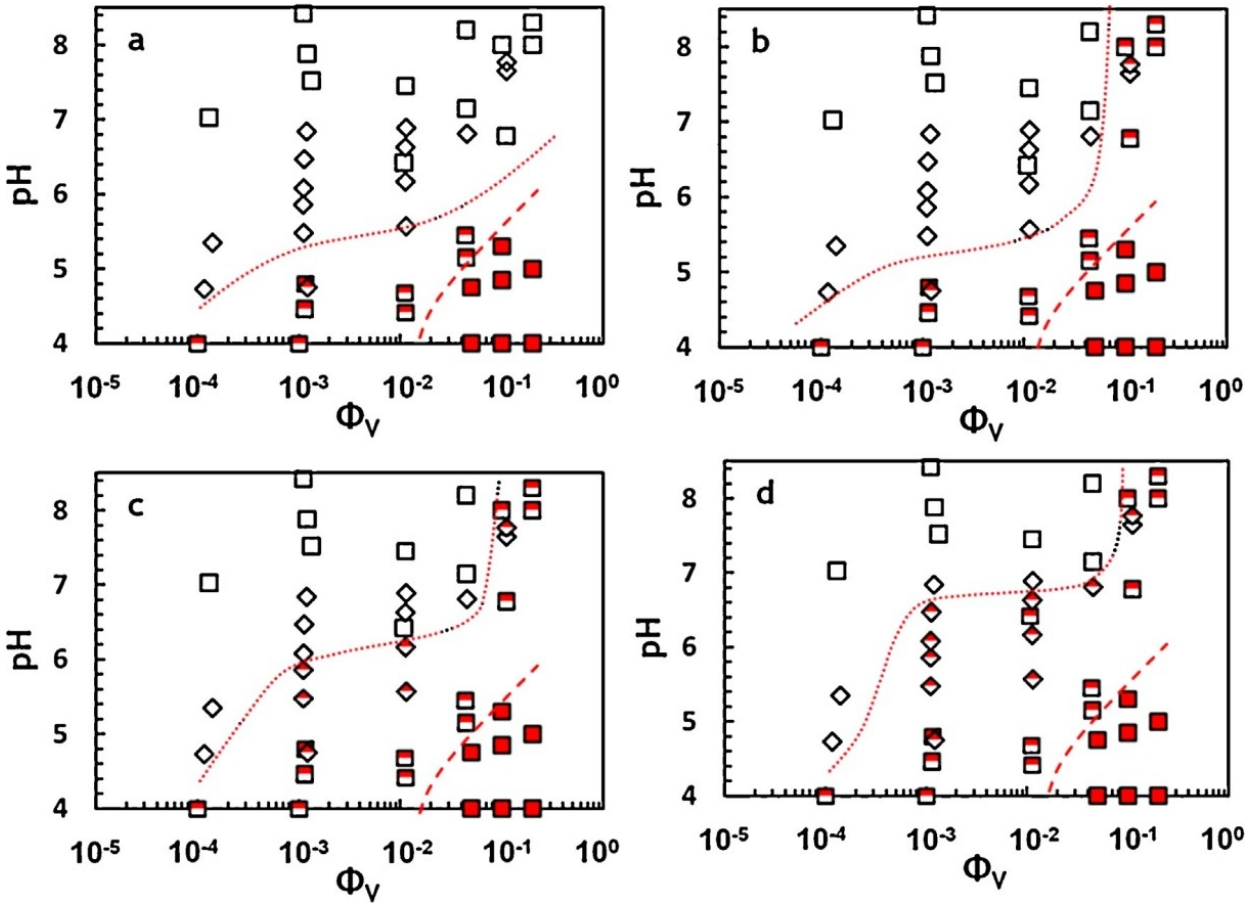

Figure 3.3: State diagram of natural rubber latex in pH- Φ_v space: (a) after 4 hours, (b) after 1 week, (c) after 2 weeks and (d) after 5 weeks. Square: GDL acidification and diamonds: buffer acidification. Stable suspension: empty symbols, macroscopic phase separation: half-filled symbols and gel: filled symbols. Dashed and dotted lines which represent the limits between two states are only guides for the eyes.

3.3.3 Structure formation during continuous acidification

The state diagram being established, we studied the temporal evolution of the system during a continuous acidification, which represents the real conditions of preparation of latex coagulum. In-situ hydrolysis of GDL resulted in a homogeneous continuous and rapid (t < 2h) acidification from pH 8.5 to pH 4. The initially stable suspension evolves from a repulsive system (at pH 8.5) to an attractive one (at pH 4). Accordingly, particles initially present as individual objects first aggregate and then, depending on the volume fraction, form a gel network or macroscopically phase-separate. We first characterized the onset of aggregation and of gelation, and then compared these with the state diagram previously established.

3.3.3.1 Onset of aggregation

Accurate determination of the onset of aggregation is a difficult task, particularly because NRL suspensions are opaque even at very low volume fractions and thus greatly scatter light. A combination of different methods was used to monitor the onset of particle aggregation for $3.5x10^{-5} < \Phi_v < 4.3x10^{-1}$. At low volume fractions turbidity was used to determine the onset of aggregation. For intermediate volume fractions, diffusing wave spectroscopy (DWS), which is based on the analysis of multiple light scattering, was used. This technique allowed quantitative determination of the evolution of the hydrodynamic radius of the diffusing objects in the suspensions. Finally, for higher volume fractions, it was no longer possible to directly use these techniques to measure particle size *in situ*. To remedy this drawback, sample aliquots were collected from concentrated samples at various times during acidification and the aggregation was quenched by dilution of the sample aliquot in a large amount of buffer at pH 8.5. Size distribution and volume mean diameter ($D_{4.3}$) were here analyzed using SLS. In the following sections, first the results obtained by each method are described independently. Diameters presented here were normalized by their initial value (determined at pH 8.5, before acidification begins) for comparison, as the absolute values could slightly vary depending on the measurement method used. In addition, it is important to note that the measured diameters are only used qualitatively to determine the onset of aggregation, identified as an increase in the measured particle size. We stress the fact that since different techniques are used to characterize aggregation of the system, and that the pH and concentrations also varied depending on the measuring technique used, the particle size cannot be directly compared. Therefore we will limit our analysis in this section to the identification of the onset of aggregation, and the experimental results will be combined to infer an overall view of the effect of Φ_v on the pH of the onset of aggregation.

3.3.3.1.1 Diffusing wave spectroscopy (DWS)

DWS offers a convenient way of monitoring *in situ* the particle size evolutions during the acidification process, for $2.8x10^{-3} < \Phi_v < 2.8x10^{-2}$. This was done through measurements in the shift of the correlation function towards longer lag times. An example of the measured correlation function $g_{(1)}(t)$ and the theoretical fit using eqs. (1-3) can be observed in the inset

to Figure 3.4a. Depending on the amount of GDL added to the suspension, acidification proceeded at different rates. Accordingly, the time at which aggregation was observed, associated with the onset of normalized diameter increase, varied from a few minutes to about one hour for suspension of Φ_v =1.1x10^{-2} (Figure 3.4a). However, replotting this same normalized diameter evolution as a function of the pH (which continuously decrease during acidification), showed that the onset of aggregation occurred at the same pH (pH 5 for this volume fraction), independently of the GDL concentration used (from 0.5 to 2 %), and therefore of the acidification kinetics (Figure 3.4b). This result clearly demonstrates that the parameter that controls the onset of aggregation is the pH, at least for time scales that do not exceed few hours. Even if the normalized diameter values have to be taken with caution as already explained, we could already see from this figure that the acidification kinetics influenced also the aggregation rate, a point that will be discussed later (see Figure 3.4a and 3.4b, and note that the time scale in Figure 3.4a is logarithmic).

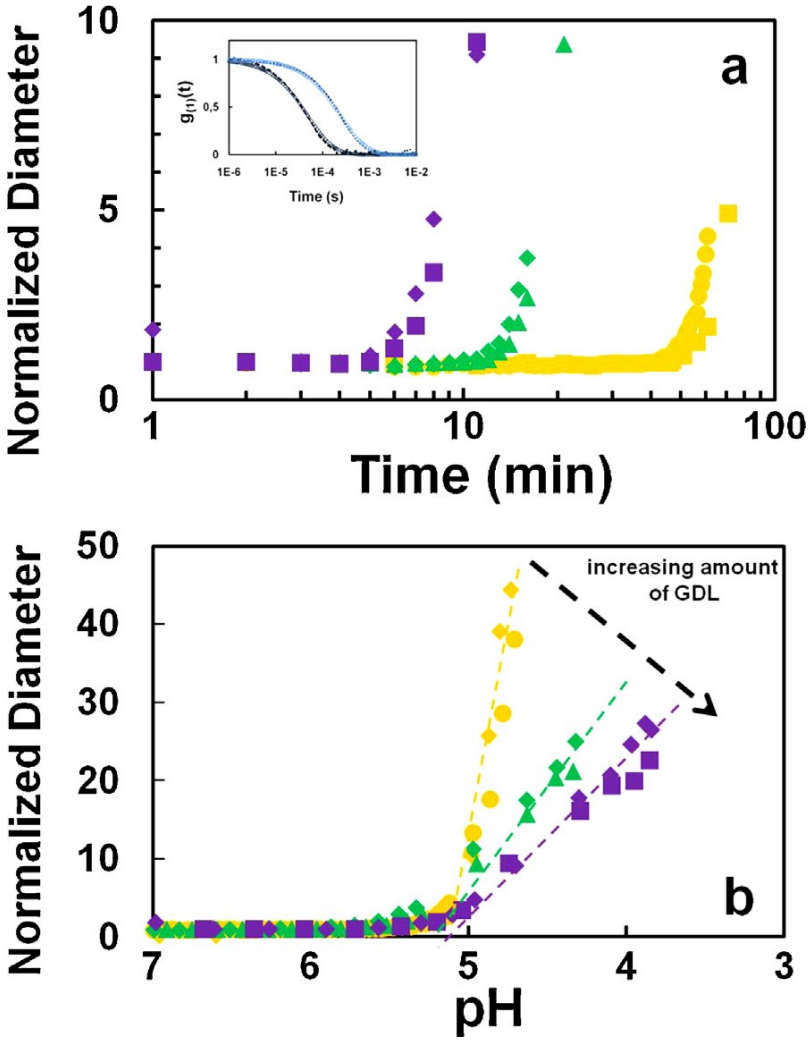

Figure 3.4: Aggregation kinetics of NRL particles upon acidification (Φ_v =1.1x10^{-2}), as measured by DWS. (a) Particle size as a function of the acidification time for different amounts of added GDL concentrations: 0.5 wt% (yellow), 1 wt% (green) and 2 wt%.(purple). Repeat experiments are presented for each GDL concentration with different symbols. Inset in (a) show measured correlations functions (symbols) and theoretical fits (solid lines) after 1 minute (square) or 18 minutes (circles) of acidification by addition of 1 wt% GDL. (b) Same particle size evolution, but plotted this time as a function of pH.

3.3.3.1.2 Static light scattering (SLS)

At high volume fractions ($2.2x10^{-3} \leq \Phi_v \leq 4.3x10^{-1}$) particle size aggregation was characterized by static light scattering. To do so, we observed that the aggregation could be stopped either with a buffer with the same pH as in the solution at the time of sampling (dilution effect), or with a buffer at pH 8.5 (dilution and pH effect), without any noticeable effect on the particle sizes. This suggests that particle aggregates do not breakup under a strong pH increase, an evidence of the irreversible, strong intra-particle bonds formed during aggregation. This could be potentiality associated with interpenetration of the proteins and phospholipids that constitute the soft particle membrane. We used, for simplicity, a pH 8.5 buffer for the results presented here. An example of the change in particle size distributions for quenches realized at different acidification time is reported in Figure 3.5a, for NRL dispersions of $\Phi_v = 2.2x10^{-2}$. The size distribution of the sample remained initially constant and, when the pH decreased sufficiently, a shift towards a larger size (up to 100 µm) was observed. The pH at the onset of aggregation was independent of the GDL concentration, as observed by DWS at lower volume fractions, but it decreased with the volume fraction (Figure 3.5b).

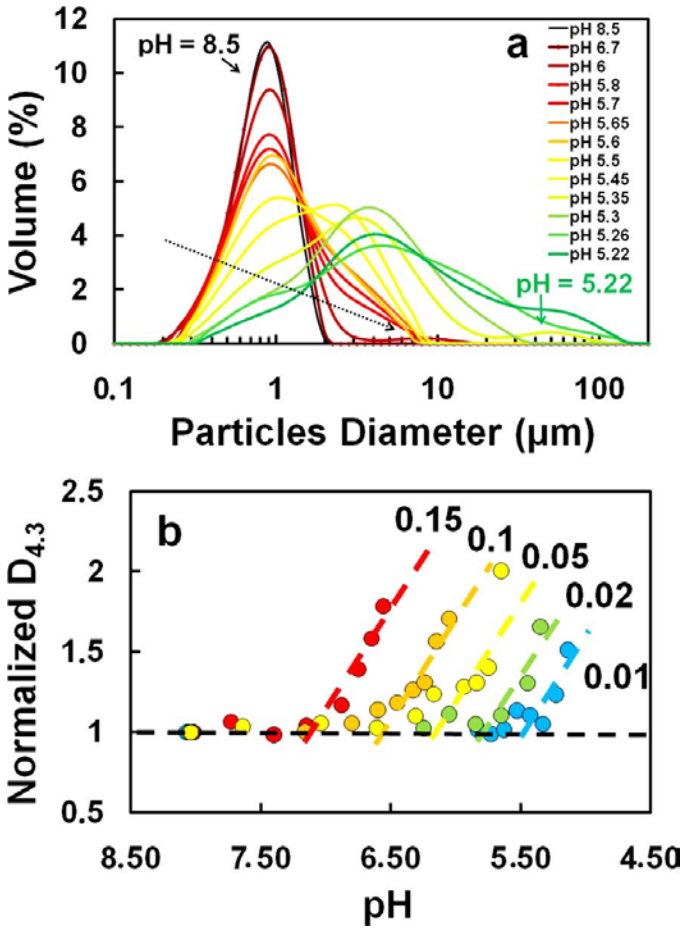

Figure 3.5: (a) Particle size distribution measured by static light scattering for an NRL suspension ($\Phi_v = 2.2x10^{-2}$) upon acidification with 1 % GDL.(b) Normalized size evolution with pH for NRL dispersions with Φ_v ranging from 0.01 to 0.15.

3.3.3.1.3 Turbidity measurements

Suspension turbidity depends on the particle number concentration, size and refractive indices (Gregory 2009), and was therefore used here to capture the onset of aggregation. Turbidity measurements were performed on very diluted suspensions, with $3.0\text{x}10^{-4} < \Phi_v < 1.0\text{x}10^{-3}$. Upon acidification, turbidity was initially constant and then suddenly decreased at a given pH value, identified as the onset of aggregation.

By combining all the results obtained by the three techniques, namely, DWS, SLS and turbidimetry, it was possible to plot the pH of the onset of aggregation as a function of Φ_v, as observed during acidification. These results are coherent but more precise than the observation conducted on short time length to establish the state diagram, as illustrate in Figure 3.6. Clearly, the pH at which aggregation occurs in those conditions (short timescales) depends on the particle volume fraction, and was always higher than the point of zero mobility (pH_i) of the NRL particles. This could be linked to the complex structure of the particles surface, discussed previously: the presence of a soft, permeable, and likely heterogeneously charged layer at the surface of the NRL particles makes the description of this system more complex when compared to solid particles with a homogeneous charge distribution.

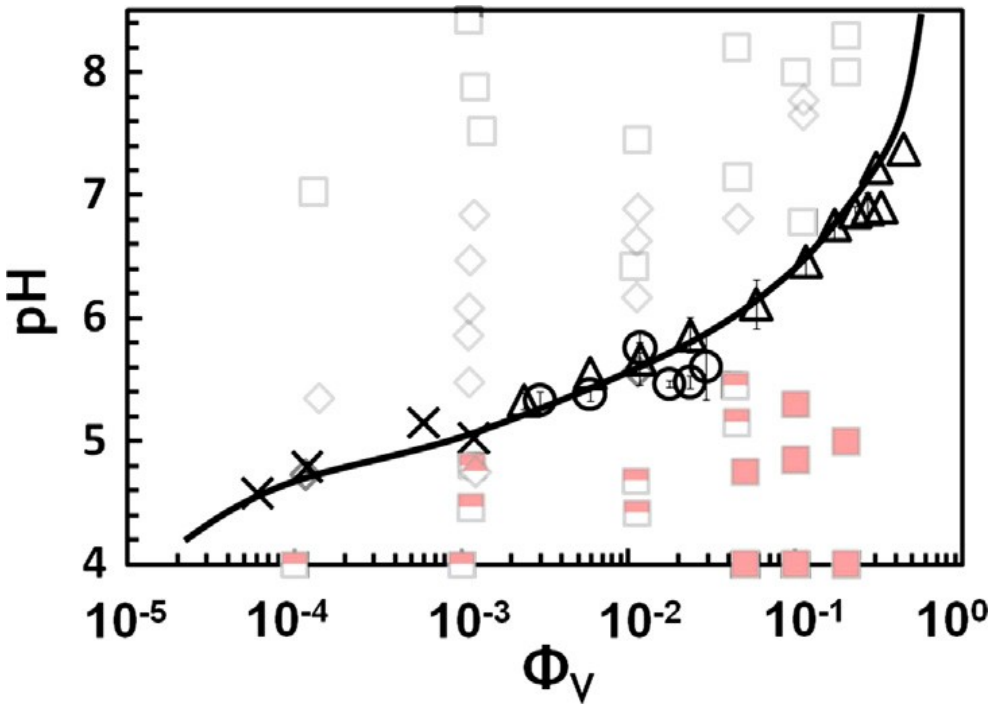

Figure 3.6: pH at the onset of aggregation as measured during acidification, plotted as a function of particle volume fraction. Measure obtained *in situ* by turbidity (cross) and DWS (circles) and after quenching by SLS (triangles). The solid line is a guide for the eyes, the state diagram presented in Figure 3.3a is reproduced in grey for comparison.

3.3.3.2 Gelation

During the acidification procedure (final pH close to 4 in less than 2 hours), the aggregation began, depending on the volume fraction, once the pH value was lower than the pH value represented by a solid line in Figure 3.6. The aggregation proceeded until the complete gelation of the system. Such gels presented a homogeneous appearance, and stuck to the bottom of the vial after upturning it. This procedure allowed the preparation of gels with a volume fraction $\Phi_v \geq 1.0\text{x}10^{-2}$. For lower NRL particle volume fractions, a macroscopic phase separation was observed as described in Section 3.2. A (very) thin layer of gel formed in the upper part of the vial, while a liquid suspension remained beneath it.

For $\Phi_v > 1\text{x}10^{-2}$, gelation was monitored by rheology. To avoid shear-induced aggregation (Dawson 1949), we selected experimental conditions that did not show any measurable effect either on the gelation kinetics or on the final gel properties. At the early stage of acidification, the suspension was liquid-like, and the oscillatory torque was very low, if measurable. After some time, both the elastic modulus *G'* and the viscous modulus *G"* suddenly increased and reached a plateau value (G_0' *or* G_0''), with G_0' being approximately one order of magnitude higher than G_0'' (Figure 3.7a). This indicates the formation of a percolating network of NRL particles. At high Φ_v, gelation occurs very rapidly, while it is delayed to longer times (and lower pH) when the volume fraction is lower.

To estimate the gelation time in NRL suspensions during acidification, we corrected the absolute value experimentally measured by the time required during acidification to reach the pH of onset of aggregation. The first value ($t_{gel\text{-}rh}$), was determined in rheology as the maximum of the first derivative of *G'*, identified by arrows in Fig 3.7a. The second value, the time where the pH of onset of aggregation is reached (t_{pHagg}), was obtained from our aggregation measurements presented in section 3.1, under the same physico-chemical conditions. The experimental gelation time is $t_{gel\text{-}exp} = t_{gel\text{-}rh} - t_{pHagg}$. Plotting this time as a function of particle volume fraction showed a two-step evolution (Figure 3.7b). For volume fractions lower than 0.1, the gelation time only slightly decreased with volume fraction. Considering the irreversible character of the interparticle bonding, one could deduce that aggregation should occur in the diffusion limited cluster aggregation (DLCA) regime. However, comparison with predictions of the gelation time in the DLCA regime (Allain *et al.* 1995) demonstrate that here gelation times are significantly higher. Clearly, pure DLCA behavior did not describe the gelation rate of NRL observed during continuous acidification. We suggest in the following that this behavior could result from three possible causes.

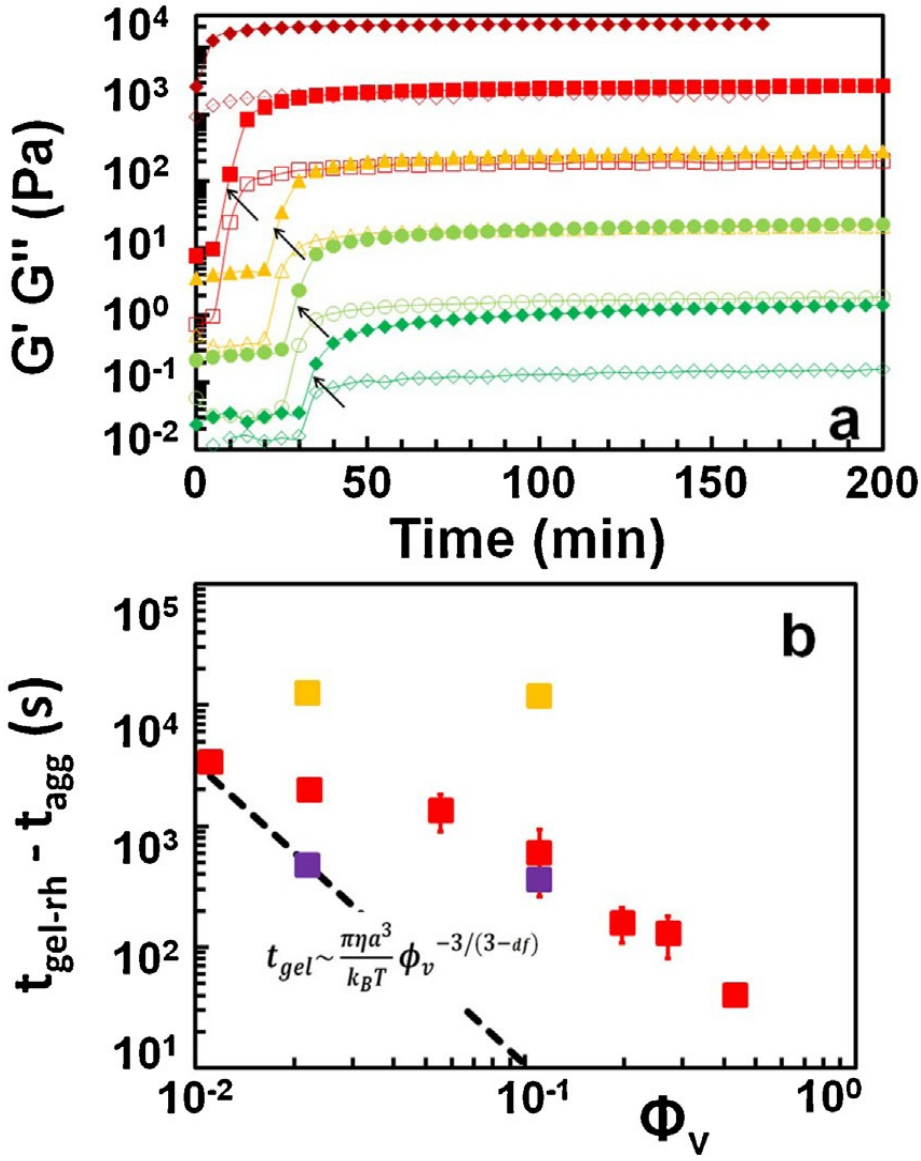

Figure 3.7: (a) Evolution of the elastic (*G'*, full symbols), and viscous modulus (*G"*, open symbols) during acidification, for (from top to bottom) Φ_v = 4.3x10^{-1}, 2x10^{-1}, 1.1x10^{-1}, 5x10^{-2} and 2.5x10^{-2}. (b) Evolution of the experimental gelation time ($t_{gel-exp}$) as a function of volume fraction: Red: standard kinetics. Yellow: 0.4 % GDL, Purples: 2 % GDL. Dashed line: theoretical gelation time (t_{gel}) (Allain *et al.* 1995) for DLCA where the particle radius, a =0.5 µm, the viscosity, η =1x10^{-3} Pa.s and Df =1.8.

Firstly, NRL particles are characterized by a large diameter (around 1 µm) and a density lower than the continuous medium, and thus might be considered at the limit at which gravitational forces affect aggregation rates. The gravity effect on pair interaction forces, collision frequency and the population balance equation have been reviewed by *Dukhin et al.* (Dukhin *et al.* 2007). Experimental results and theories suggest that gravity could either promote stability or speed up aggregation, the latter being especially favored under conditions of low electrostatic repulsion, which as expected during acidification (Dukhin *et al.* 2007). This effect should be stronger at low volume fractions, for which cluster growth before reaching close packing is greater than for high volume fractions.

Secondly, some recent results from numerical simulations showed that hydrodynamic forces could also strongly impact aggregation rates. Because of the incompressible nature of the liquid surrounding the particles, clusters are characterized by a more elongated shape than in the case of a pure Brownian diffusion process, and this lowers the colloid volume fraction threshold for percolation (Furukawa and Tanaka 2010; Whitmer and Luijten 2011; Cao *et al.* 2012). The effect of hydrodynamic interactions depends on the stage of aggregation (initial nucleation or cluster coalescence) and on the volume fraction (Tomilov *et al.* 2013), and therefore could help explain the two-step dependency that we experimentally observed.

Finally, the influence of the charge distribution on the particle surface, which continuously evolves during acidification, is certainly a parameter that should be taken into account. The dependence of aggregation rates on the acidification kinetics can be clearly seen in Figure 3.4, and could explain why the use of a low GDL concentration resulted in long gelation kinetics (yellow squares in Figure 3.7b). Some authors have also suggested that the particle membrane consists of patches made of different protein and phospholipids composition (Nawamawat *et al.* 2011). During the pH decrease, some positive and negative charges may therefore be simultaneously present on the particle membrane, generating some attraction which could affect the aggregation process, in comparison with a purely Brownian diffusion mechanism.

Although the pH of gelation was not determined *in situ* during the rheological measurements, determination of the gelation time by rheology, $t_{gel\text{-}rh}$, (Figure 3.7b) combined with the determination of the acidification kinetics for each Φ_v and at different GDL concentrations allowed us to estimate precisely the pH at which gelation did occur in the rheometer. These results are reported in Figure 3.8. We observed that the gelation pH was similar for the different kinetics, and that the measured values are coherent with the state diagram presented previously in Figure 3.2.

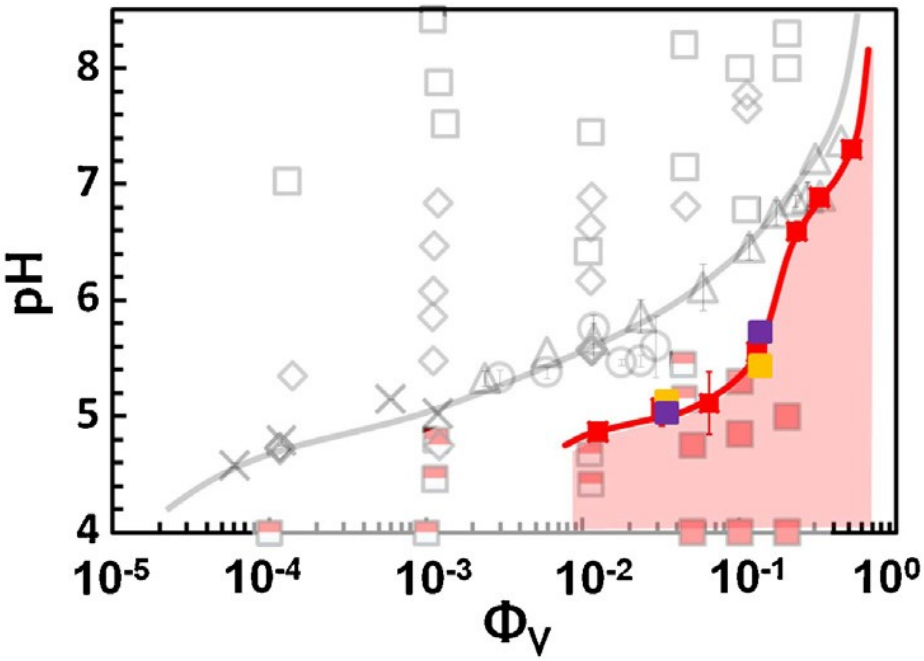

Figure 3.8: pH at gelation as determined by rheology. Red squares: standard kinetics. Yellow: 0.4 % GDL, Purples: 2 % GDL. The red curve is a guide for the eyes. The state diagram presented in Figure 3.3a and completed in Figure 3.6 is reproduced in grey for comparison.

3.3.4 Rheological properties of the gels at pH 4

A frequency sweep performed on the gel at the plateau showed a flat profile for both *G'* and *G"*, except for the weakest gel, as observed for $\Phi_v = 2.5 \times 10^{-2}$ (Figure 3.9a). This last behavior was reminiscent of that observed for gels in which the frequency-dependant viscosity of the liquid trapped in the gel dominates the frequency-independent rheological behavior of the particle network at very high frequency (Trappe and Weitz 2000).

The plot of the plateau value of G'_0 as a function of Φ_v, determined from Figure 3.7a at 1 Hz, shows a power law relationship with an exponent A =3.35 over more than five decades (Figure 3.9b). This is characteristic of fractal gels (Buscall *et al.* 1988). Interestingly it is worth noting that whatever we used dialyzed or non-dialyzed (for $\Phi_v > 0.30$) NRL suspensions, fast or low acidification kinetics, and different final pH, the rheological results are all aligned on the same line. Properties of NRL gel, for a given volume fraction, are very stable and rather independent of the conditions in which they were formed, at least in the range of conditions investigated here.

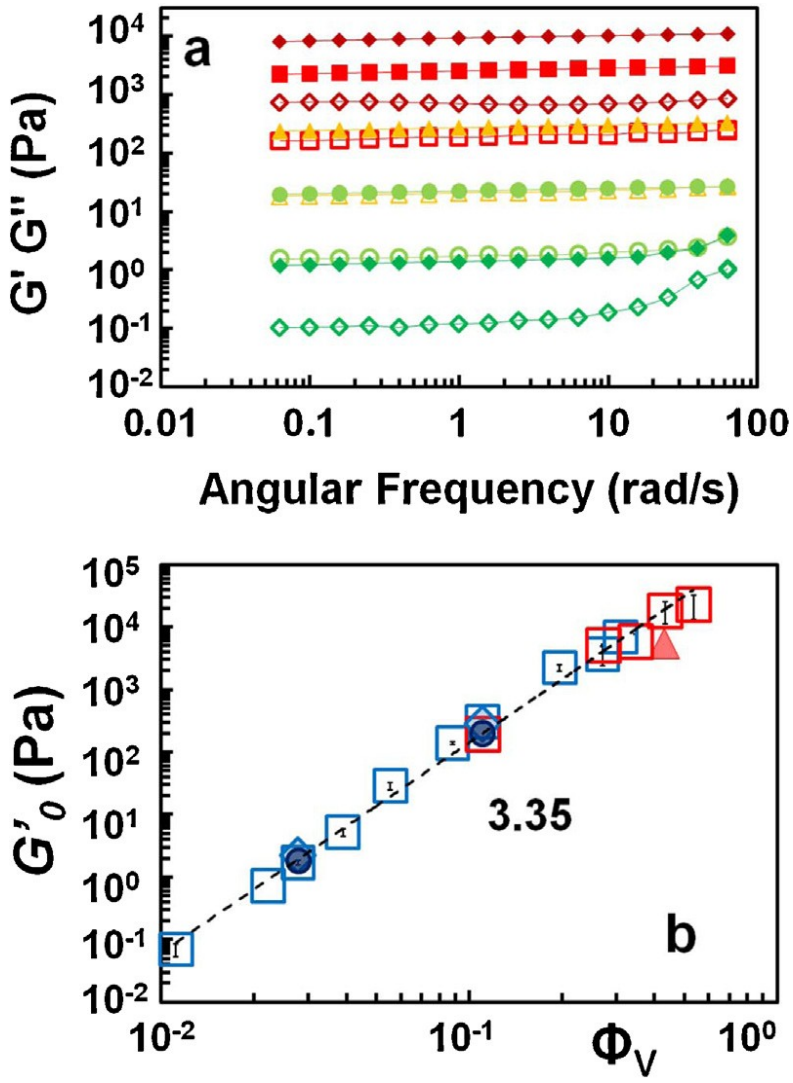

Figure 3.9: (a) Frequency sweep: elastic (*G'*, full symbols) and viscous (*G"*, open symbols) moduli dependence on the angular frequency for (from top to bottom) Φ_v = 4.3x10^{-1}, 2.0x10^{-1}, 1.1x10^{-1}, 5x10^{-2} and 2.5x10^{-2}. (b) Plateau value of the elastic modulus (G'_0) as a function of NRL volume fraction. Squares = standard acidification procedures with a final pH 4 (Blue: dialyzed NRL suspensions, red: non-dialyzed NRL suspensions). Circles: final pH 3. Diamonds: final pH 4.5. Triangles: final pH 5.5.

3.4 Conclusions

In this work, the acid-induced aggregation and gelation of NRL particles was investigated. Three different states (stable suspension, gel, and macroscopic phase separation between a gel and a suspension) were observed depending on pH, ϕ_v and time. The onset of rapid aggregation was measured over four orders of magnitude in volume fraction, by a combination of three different techniques. Independently of the acidification kinetics, the pH at which aggregation was initiated increased rapidly with the particle volume fraction, and is always higher than the point of zero mobility (pH_i) determined by electrophoretic mobility measurement. Once aggregation began, particle-particle adhesion seemed to be irreversible.

Even quenching newly formed clusters in a buffer at pH 8.5 did not show any measurable effect on the aggregate size.

For volume fractions higher than 10^{-2}, acidification to a pH close to 4 resulted in the complete gelation of the system. Gelation kinetics did not follow the classical prediction based on Brownian motion. This suggests that other effects, such as gravity, hydrodynamic interactions, variation in the charge density or the simultaneous presence of opposite charges, could affect the aggregation kinetic. Further studies are needed to understand these different effects.

NRL gels showed remarkable mechanical properties: their elastic modulus only depended on the volume fraction, independently of the aggregation kinetics or of the final pH. A scaling relationship for the plateau elastic modulus as a function of the volume fraction with a power law exponent of 3.35 was found. This mechanical behavior is characteristic of a fractal gel. First results showed that such gels exhibit a strong strain hardening phenomenon. Further rheological characterizations are needed to understand the structure-function relationship of this natural exceptional.

Acknowledgment

The authors thank Jérôme Duval (INPL/CNRS) for help in the electrophoretic mobility analysis. Laurie Ferrandez, Jeanne de Préval, Weam Banjar, and Lucas Martinez helped with some of the experimental work presented here. We thank Luca Cipelletti, Michel Cloitre and Emanuela Zaccarelli for useful discussions. This work was carried out with support from CNPq, National Council for Scientific and Technological Development – Brazil.

References

Allain, C., *et al.* (1995). "Aggregation and Sedimentation in Colloidal Suspension." Physical Review Letters **74**(8): 1478-1481.

Bowler, W. W. (1953). "Electrophoretic Mobility Study of Fresh Hevea Latex." Industrial and Engineering Chemistry **45**(8): 1790.

Brzozowska-Hanower, J., *et al.* (1978). "Étude du mécanisme de la coagulation du latex d'Heves brasiliensis (Ihnth) Müll. Arg. II. Systèmes enzymatiques impliqués dans le Processus I . Phénol oxydases." Physiologie Végétale **13**(2).

Buscall, R., *et al.* (1988). "Scaling behavior of the rheology of aggregate networks formed from colloidal particles." Journal of the Chemical Society-Faraday Transactions I **84**: 4249-4260.

Cao, X. J., *et al.* (2012). "Hydrodynamic and interparticle potential effects on aggregation of colloidal particles." Journal of Colloid and Interface Science **368**(1): 86-96.

Carretero-Gonzalez, J., *et al.* (2010). "Molecular dynamics of natural rubber as revealed by dielectric spectroscopy: The role of natural cross-linking." Soft Matter **6**(15): 3636-3642.

Cornish, K., *et al.* (1999). "Rubber particles from four different species, examined by transmission electron microscopy and electron-paramagnetic-resonance spin labeling, are found to consist of a homogeneous rubber core enclosed by a contiguous, monolayer biomembrane." Planta **210**(1): 85-96.

Dauzac, J., *et al.* (1982). "A plant vacuolar system - the lutoids from Hevea brasiliensis latex." Physiologie Végétale **20**(2): 311-331.

Dawson, H. G. (1949). "Mechanical Stability Test for Hevea latex." Analytical chemistry **21**(9): 1066-1071.

Dennis, M. S. and D. R. Light (1989). "Rubber elongation-factor from Hevea brasiliensis - identification, characterization, and role in rubber biosynthesis." Journal of Biological Chemistry **264**(31): 18608-18617.

Dukhin, A. S., *et al.* (2007). "Gravity as a factor of aggregative stability and coagulation." Advances in Colloid and Interface Science **134-35**: 35-71.

Duval, J. F. L. and F. Gaboriaud (2010). "Progress in electrohydrodynamics of soft microbial particle interphases." Current Opinion in Colloid & Interface Science **15**(3): 184-195.

Duval, J. F. L. and H. Ohshima (2006). "Electrophoresis of diffuse soft particles." Langmuir **22**(8): 3533-3546.

Farr, R. S. and R. D. Groot (2009). "Close packing density of polydisperse hard spheres." The Journal of Chemical Physics **131**(24): 244104.

Furukawa, A. and H. Tanaka (2010). "Key Role of Hydrodynamic Interactions in Colloidal Gelation." Physical Review Letters **104**(24): 245702.

Gaboriaud, F., *et al.* (2012). "Unravelling the nanometre-scale stimuli-responsive properties of natural rubber latex particles using atomic force microscopy." Soft Matter **8**(9): 2724-2729.

Gidrol, X., *et al.* (1994). "Hevein, a lectin-like protein from Hevea brasiliensis (rubber tree) is involved in the coagulation of latex

" Journal of Biological Chemistry **269**(12): 9278-9283.

Gregory, J. (2009). "Monitoring particle aggregation processes." Advances in Colloid and Interface Science **147–148**(0): 109-123.

Hanower, P., *et al.* (1976). "Étude du mécanisme de la coagulation du latex d'Hevea brasiliensis (Ihnth) Müll. Arg. 1. Facteurs agissant sur la coagulation." Physiologie Végétale **14**(4).

Hemar, Y. and D. N. Pinder (2006). "DWS Microrheology of a Linear Polysaccharide." Biomacromolecules **7**(3): 674-676.

Ho, C. C. (1989). "Changes in eletrokinetic properties of natural-rubber latex after surface chemical modifications." Colloid and Polymer Science **267**(7): 643-647.

Ho, C. C., *et al.* (1996). "Surface Structure of Natural Rubber Latex Particles from Electrophoretic Mobility Data." Journal of Colloid and Interface Science **178**(2): 442-445.

Ho, C. C. and W. L. Ng (1979). "Surface study on the rubber particles in pretreated Hevea latex system." Colloid and Polymer Science **257**(4): 406-412.

Jacob, J. L., *et al.* (1993). "The composition of natutal latex from Hevea-brasiliensis." Clinical Reviews in Allergy **11**(3): 325-337.

Kim, J. M., *et al.* (2013). "Gel Transition in Adhesive Hard-Sphere Colloidal Dispersions: the Role of Fravitational Effects." Physical Review Letters **110**: 208302(208305).

Louie, S. M., *et al.* (2012). "Parameter Identifiability in Application of Soft Particle Electrokinetic Theory To Determine Polymer and Polyelectrolyte Coating Thicknesses on Colloids." Langmuir **28**(28): 10334-10347.

Lu, P. J., *et al.* (2006). "Fluids of clusters in attractive colloids." Physical Review Letters **96**(2): 028306(028304).

Nawamawat, K., *et al.* (2011). "Surface nanostructure of Hevea brasiliensis natural rubber latex particles." Colloids and Surfaces A-Physicochemical and Engineering Aspects **390**(1-3): 157-166.

Nwadinigwe, C. A. (1988). "Some hitherto uncharacterized latex polyisoprenes." Phytochemistry **27**(7): 2135-2136.

Ohshima, H. (1995). "Electrophoresis of soft particles." Advances in Colloid and Interface Science **62**(2-3): 189-235.

Ohshima, H. (2009). "Theory of electrostatics and electrokinetics of soft particles." Science and Technology of Advanced Materials **10**(6): 063001(063013).

Rochette, C. N., *et al.* (2013). "Shell Structure of Natural Rubber Particles: Evidence of Chemical Stratification by Electrokinetics and Cryo-TEM." Langmuir **29**(47): 14655-14665.

Sansatsadeekul, J., *et al.* (2011). "Characterization of associated proteins and phospholipids in natural rubber latex." Journal of Bioscience and Bioengineering **111**(6): 628-634.

Shewan, H. M. and J. R. Stokes (2015). "Viscosity of soft spherical micro-hydrogel suspensions - Supplementary Material." Journal of Colloid and Interface Science **442**(0): 75-81.

Singh, A. P., *et al.* (2003). "Simple and rapid methods for SEM observation and TEM immunolabeling of rubber particles." Journal of Histochemistry & Cytochemistry **51**(8): 1105-1108.

Sorensen, C. M. and A. Chakrabarti (2011). "The sol to gel transition in irreversible particulate systems." Soft Matter **7**(6): 2284-2296.

Toki, S., *et al.* (2008). "Multi-Scaled Microstructures in Natural Rubber Characterized by Synchrotron X-Ray Scattering and Optical Microscopy." Journal of Polymer Science Part B-Polymer Physics **46**(22): 2456-2464.

Tomilov, A., *et al.* (2013). "Aggregation in Colloidal Suspensions: Evaluation of the Role of Hydrodynamic Interactions by Means of Numerical Simulations." The Journal of Physical Chemistry B **117**(46): 14509-14517.

Trappe, V. and D. A. Weitz (2000). "Scaling of the viscoelasticity of weakly attractive particles." Physical Review Letters **85**(2): 449-452.

Wales, M. (1962). "Particle size distribution in rubber latex." Journal Phys. Chem **66**(10): 1768–1772.

Weitz, D. A., *et al.* (1993). " Diffusing-wave spectroscopy - The technique and some applications ." Physica Scripta **T49B**: 610-621.

Whitmer, J. K. and E. Luijten (2011). "Influence of Hydrodynamics on Cluster Formation in Colloid−Polymer Mixtures." The Journal of Physical Chemistry B **115**(22): 7294-7300.

Wisunthorn, S., *et al.* (2012). "SEC-MALS study of dynamic structuring of natural rubber: Comparative study of two Hevea brasiliensis genotypes." Journal of Applied Polymer Science **124**(2): 1570-1577.

Wititsuwannakul, R., *et al.* (2008). "Hevea latex lectin binding protein in C-serum as an anti-latex coagulating factor and its role in a proposed new model for latex coagulation." Phytochemistry **69**(3): 656-662.

Chapter 4

Irreversible restructuration of natural rubber latex gels during hardening under stress

Formation of colloidal gels from natural rubber latex, upon destabilization of the natural suspension after extraction from the *Hevea brasiliensis* tree, is the first step of the production of raw commercial natural rubber (NR). These gels are then submitted to water washing under strong deformations in order to be processed into dried raw commercial NR. In this work, we studied their rheological properties at large deformation and we evidenced a strain hardening behavior. For particles volume fractions below 0.25, of the maximum modulus reached during hardening, just before gel fracture, $G'_{max,}$ scales with $\sim\Phi_v^{1.67}$. For volume fraction larger than 0.25, the fracture occurs at lower strain without any hardening. Unlike others fractal gels, the strain hardening was irreversible. This irreversibility was attributed to the formation of new, irreversible bonds. An irreversible restructuration of the internal structure took place during the hardening under strain with an evolution of the backbone fractal dimensions, D_b, till a maximum value close to the fractal dimension of the gel, D_f. In addition, above a critical strain of 0.5, material properties are slowly degraded with time. A 2D-Ultrasonic speckle velocity (USV) method coupled to a classic rheometer was used and demonstrated that the structural restructurations associated with strain hardening are homogeneously distributed throughout the gap.

This chapter is a paper in preparation.

4.1 Introduction

Natural rubber (NR) made from the *Hevea brasiliensis* latex is used to manufacture popular end-use products (tires, gloves, elastics…). Despite competition from synthetic rubber, this natural material is still irreplaceable in several applications, especially tires, due to its unique mechanical properties (Vaysse *et al.* 2012). These special properties are attributed to the complex structure formed by *cis*-1,4 polyisoprene and non-isoprene components such as proteins and/or lipids and/or minerals (Tanaka 2001; Vaysse *et al.* 2009). The stress-induced crystallization is one of these unique properties, resulting in high elasticity, "green strength" and slower crack propagation. It results in an apparent "hardening" of the material observed from strain values higher than 400 % (Toki *et al.* 2000; Tosaka *et al.* 2004).

In TSR5 or RSS grade NR, the first step of the industrial production of the raw commercial NR is the acid-induced destabilization and coagulation of the latex, resulting in the formation of a colloidal gel. Rubber particles, initially negatively charged, interact and form a fractal colloidal gel with irreversible particle-particle links (Reis *et al.* 2015). These rubber particles, with an average size of 1 µm, display a core-shell morphology with a core of polyisoprene surrounded by a complex shell composed by proteins and phospholipids (Cornish *et al.* 1999; Nawamawat *et al.* 2011; Berthelot *et al.* 2014; Singh *et al.* 2014; Sakdapipanich *et al.* 2015). After coagulation, the colloidal gel is submitted to water washing under strong deformations (creeping) in order to be processed into dried raw commercial NR.

Colloidal gels consist in a percolating network of particles of colloidal size, entrapping a large quantity of solvent, exhibiting a rheological response dominated by elasticity. Gelation can result from different mechanisms such as phase separation and percolation (Tokita 1989; Dickinson 2013). In the latter case, particles diffuse in a suspension, aggregate and form fractal clusters resulting in the formation of a fractal gel (Bremer *et al.* 1993). Viscoelastic properties of these gels were already described in the literature. In the linear regime, models were proposed to explain the behavior of fractal gels by scaling the elastic modulus as a function of the concentration (Bremer *et al.* 1989; Shih *et al.* 1990; Ikeda *et al.* 1999; Wu and Morbidelli 2001; Mellema *et al.* 2002). In recent years, rheological properties of colloidal gels have been studied in the non-linear regime, where the gels break-up, flow or present a strain hardening behavior. The hardening at high values of strain was observed for different gels consisting of either colloidal particles or (bio)polymers, such as polystyrene (Gisler *et al.* 1999), proteins (Pouzot *et al.* 2006; Rohm *et al.* 2014), carrageenan *(Hilliou et al. 2009)*, collagen and polyacrylamide (Storm *et al.* 2005) and DNA (Orakdogen *et al.* 2010). The strain hardening behavior was observed when a deviation of linearity in the stress-strain curves is observed and it followed by a fracture of the network (Gisler *et al.* 1999; Pouzot *et al.* 2006; Brenner *et al.* 2009). In biopolymer gels such as, for instance, those based on collagen or neurofilaments, the strain hardening was attributed to the alignment of polymer chains under shear (Storm *et al.* 2005). For colloidal gels, their elasticity is promoted by the bending (or stretching) of strand of particles which compose the fractal backbone of clusters. This results in a formation of new connections of some strands of particles induced by the shear forces (Colombo and Del Gado 2014). In all cases, the behavior is reversible before

fracture and may be affected by the pH (Sittikijyothin *et al.* 2007) and temperature (Brenner *et al.* 2009). Gisler *et al.* (Gisler *et al.* 1999) proposed a theoretical model to explain strain hardening of fractal colloidal gels. They attributed the hardening to the strengthening of the fractal backbone inside the clusters with the increase of strain. In their model, the internal structure of fractal clusters, fractal dimension (D_f) and backbone fractal dimension (D_b), do not change during strain hardening. Mellema *et al.* (Mellema *et al.* 2002) proposed four categories of kind of deformation inside the clusters depending on the bending or stretching deformation of strands. The type of deformation can be qualitatively estimated from the exponent of the scaling behavior of $G' \sim \Phi_v^{\upsilon/(3-Df)}$ (Shih *et al.* 1990; Wu and Morbidelli 2001). The origin of the deformation is attributed to a bending if $3 < \upsilon < 4$ while is attributed to a stretching if $1 < \upsilon < 2$.

Here, we characterized the linear and non-linear rheological properties of the natural rubber latex colloidal gels, in a wide range of volume fractions ($0.01 < \Phi_v < 0.53$). They present a strain hardening behavior at large deformations for $\Phi_v < 0.25$. This behavior was studied as a function of the volume fraction, using models proposed in the literature. We evidence the irreversible character of this hardening, is probably due to the fact that once two particles come in contact, they are irreversibly bonded. This property allows us to estimate how the structure is affected during hardening. In addition, a 2D-Ultrasonic speckle velocimetry (USV) method was used to study the displacement fields and the local velocity inside the gels during oscillations.

4.2 Material and Methods

4.2.1 Samples

A commercial natural rubber latex from Dalbe (France, ref. 4770002) was used. This latex contained pre-vulcanized rubber particles of natural rubber latex stabilized with ammonia. The particle average diameter measured by static light scattering is 1 µm (Reis *et al.* 2015). The pH of the latex was 10.5, and its dry mass about 59 %wt. The samples were first diluted with an equivalent amount of Tris-HCl buffer (pH 8.5, ionic strength =7 mM). Afterwards, the latex was extensively dialyzed for 7 days against the same buffer using a dialysis tube (SpectraPor, cut-off 12-14kDa, diameter 29 mm). After extensive dialysis, the suspension volume fraction, Φ_v, ranged typically between 0.2 and 0.3. These suspensions were then diluted with the buffer to prepare suspensions with the desired volume fraction. To obtain suspensions with volume fraction higher than 0.3, the commercial latex was directly diluted with the buffer without dialysis, which does not impact the final properties as will be shown in this paper. All prepared suspensions were stored at about 5° C and used within three weeks.

To investigate the origin of the viscoelastic properties of the NRL gels, either from particles or from polyisoprene chains, we measured the viscoelastic properties of dry films of natural rubber latex. The dry films were prepared by evaporation of water from about 3 mL of suspension in a Petri dish, under the fume cupboard. Translucent films of 0.64 mm thickness and a density of 0.91 were obtained after 48 hours.

4.2.2 Gelation procedure

Glucono-δ-lactone (GDL, ref G2164, Sigma-Aldrich) was used to homogeneously and progressively reduce the pH of the medium and therefore induce gel formation (Reis *et al.* 2015). For Φ_v < 0.1, a concentration of 1 %wt GDL set as a standard condition was used to reach a final pH close to 4 in less than 1 h. For Φ_v > 0.1, the amount of GDL was increased to reproduce the standard acidification kinetic. The required amount of GDL was added to the latex suspension under stirring, before loading in the Couette cell of the rheometer. Four hours were needed for the complete gelation to take place *in situ* inside the rheometer before the rheological characterization of gels was carried out.

4.2.3 Rheological characterization

Rheological properties of acid-induced gels from natural rubber latex were obtained using three stress-controlled rheometers: an AR2000ex (TA instrument), equipped with a Couette geometry (inner radius 14 mm, outer radius 15 mm and height 42) and a home-made serrated Couette geometry (same dimensions, with 1 mm depth and 1 mm base on each side), an MCR702 (Anton Paar) equipped with a sanded Couette geometry (inner radius 10 mm, outer radius 11 mm and height 27 mm) and an ARG2 equipped (TA instrument) equipped with a PMMA Couette geometry (inner radius 23 mm, outer radius 25 mm and height 60 mm).

Gelation was first monitored during 4 hours at a constant frequency of 1 Hz and a constant strain of 0.5 %. The results showed no measurable impact of these oscillations on the gelation process and on the final gel properties. Then, the gel was characterized with a frequency sweep from 0.01 to 10 Hz at a constant strain of 0.5 %, which was followed by a stress sweep at a constant frequency of 1 Hz, starting from 0.02 Pa up to the fracture of the gel.

In order to estimate the elastic modulus of natural rubber films, the AR2000ex (TA instrument) equipped with a plate-plate (40 mm) geometry was used. The values of the plateau shear elastic modulus, G'_0, were measured using the manual oscillations mode at 1 Hz and corresponded to the average values of 20 measurements at low normal force values (< 5 N). A dynamic mechanical analysis was also performed with a DMA 1 (Mettler-Toledo, US) where a deformation spectrum was done between 0-750 µm with a constant frequency of 1 Hz at 23° C. G'_0 of the films were estimated from the average of three measurements of the tensile elastic modulus, E', using the following equation 24.

$$G' = \frac{2(1+\nu)}{E'} \qquad \text{Eq. 24}$$

with ν =0.5 for the rubber Poisson coefficient.

4.2.4 Rheo-Ultrasound characterization

Rheo-ultrasound was performed in a stress-controlled rheometer ARG2 (TA instrument) equipped with the PMMA Couette geometry previously described. A 2D-Ultrasonic speckle velocimetry (USV) was coupled to the rheometer (for more details see ref. (Manneville *et al.* 2004)). Polystyrene particles (Dynoseed TS20µm) at 1 %wt total concentration were added before acidification with GDL, and used as an ultrasonic contrast agent. We checked that their addition had no measurable impact on rheological properties. Gelation was monitored during 30 minutes at a constant frequency of 1 Hz and a constant strain of 0.5 %. Then, the successive increases of strain were performed step by step (step duration: 5 min). For each step, a 2D-ultrasonic scan with 20 sequences of 3000 pulses at 350 Hz was performed.

We coupled the classical oscillatory rheology measured in Couette geometry with ultrasonic speckle velocimetry (USV) in order to access local properties of the NRL gel such as its velocity or deformation fields inside the gap. During the strain sweep measurements, we used USV as described in Manneville *et al.* (Manneville *et al.* 2004) to record temporally-resolved velocity profiles. USV is based on the interaction between ultrasound and micron-sized scatterers embedded in the gel. A high-frequency immersed transducer first emits a short ultrasonic pulse and collects the pressure signal backscattered from the gel. The backscattered signal is an ultrasonic speckle that directly reflects the spatial distribution of the scatterers within the gel along the acoustic beam. As the scatterers move with the gel, the cross-correlation of two successive speckle signals over small time windows gives access to the local velocity of the gel.

Velocity profiles during the oscillations were obtained from the displacements images. For this, we used equation 25.

$$v = \sum_{f=1}^{8} v_f \sin\left(2\pi f t - \varphi_f\right) \qquad \text{Eq. 25}$$

$with\ v_f > 0\ and\ \pi > \varphi_f > -\pi$

where v is the velocity, v_f the final velocity, f the frequency, t the time and φ_f the phase.

4.3 Results

4.3.1 Gel characterization in the linear regime: scaling behavior

In a previous work we established that, in the linear regime, the elastic modulus *G'* of NRL gels scales with the volume fraction as $G'_0 \sim \Phi_v^{3.35}$ over more than five decades of Φ_v ($0.01 < \Phi_v < 0.53$) (Reis *et al.* 2015). This scaling behavior, independent of the geometry used, is typical of fractal colloidal gels formed with a fractal dimension D_f, comprised between 1.8 and 2.0 (Buscall *et al.* 1988; Yanez *et al.* 1999). Using the coefficient υ, from the scaling law $G' \sim \Phi_v^{\upsilon/(3-Df)}$, reported by Mellema *et al.* model (Mellema *et al.* 2002), such a behavior ($\upsilon \approx 4$) would be compatible with a bending mode and a network composed by a flexible internal structure formed by the rubber particles.

The values of G'_0 and D_f obtained for the different gels are independent of the final pH, between pH 3 and pH 5.5, (Reis *et al.* 2015); and on the temperature between 4° C and 40° C (results not shown). This suggests that the energy associated with each bond between particles (or between clusters) is much higher than k_bT. This is in agreement with the fact that once formed, gels are not dispersible anymore, even after a strong increase of the pH up to 10. The single particle-particle bond rigidity, κ_0, obtained using the Pantina and Furst model (Pantina and Furst 2005) that states that $G'_0 = \kappa_0 / a\ \Phi_v^{3.35}$, is here about 0.13 N/m for a particle radius a_0 =0.5 µm. The energy of particle-particle bond was estimated ~3.25×10^{-14} J supposing the energy from 2 centers of particles (supposing energy bond $=\kappa_0 a^2$) which is superior to k_bT (~ 4.11×10^{-21} J).

4.3.2 Gel characterization in the non-linear regime: strain hardening behavior

Natural rubber latex gels have been characterized in this study through a continuous increase of the oscillatory stress. Increasing the stress resulted in an increase of the material deformation (strain), and the stress-strain relation obtained is a unique characteristic of each material. As a result, the evolution of the measured moduli could be plot either as a function of the stress or of the strain, independently of the imposed parameter. We validated that by the realization of experiments under increasing values of strain, which resulted in the same evolution as the one observed under conditions where the stress was increased. In the linear regime, at low stresses values, the viscoelastic moduli *G'* and *G"* are constant and independent of the applied stress as expected for a colloidal gel (with $G' \approx 10\ G"$). Then, once a given stress associated with a given strain value is reached, the stress versus strain relationship diverge from linearity at the onset of what we call here the strain hardening. Eventually at even higher strain, the gel fractures macroscopically or comes off from the walls of the Couette geometry.

The evolution of the measured moduli *G'* in function of the stress and the strain is illustrated in Figure 4.1a and 4.1b respectively for several volume fractions. The strain hardening behavior, described by the increase of *G'* and *G"* with the stress (or strain), was observed for Φ_v ranging from 0.01 to 0.25. The limits of linearity of stress (σ_0) and strain (γ_0) were determined once a 5 % deviation of linearity in the stress-strain curves is reached (Hagiwara *et al.* 1998). For these gels, the onset of strain hardening started at values of strain almost around 10 % (Figure 4.1a). Then, during the strain hardening *G'* mostly follows linearly the imposed stress (Figure 4.1a) as recently evidenced on collagen network (Licup *et al.* 2015). This observation suggests that the strain hardening depends on the imposed stress for the NRL gels. On the other hand for $\Phi_v > 0.25$, the gels fractured without any strain hardening phenomenon.

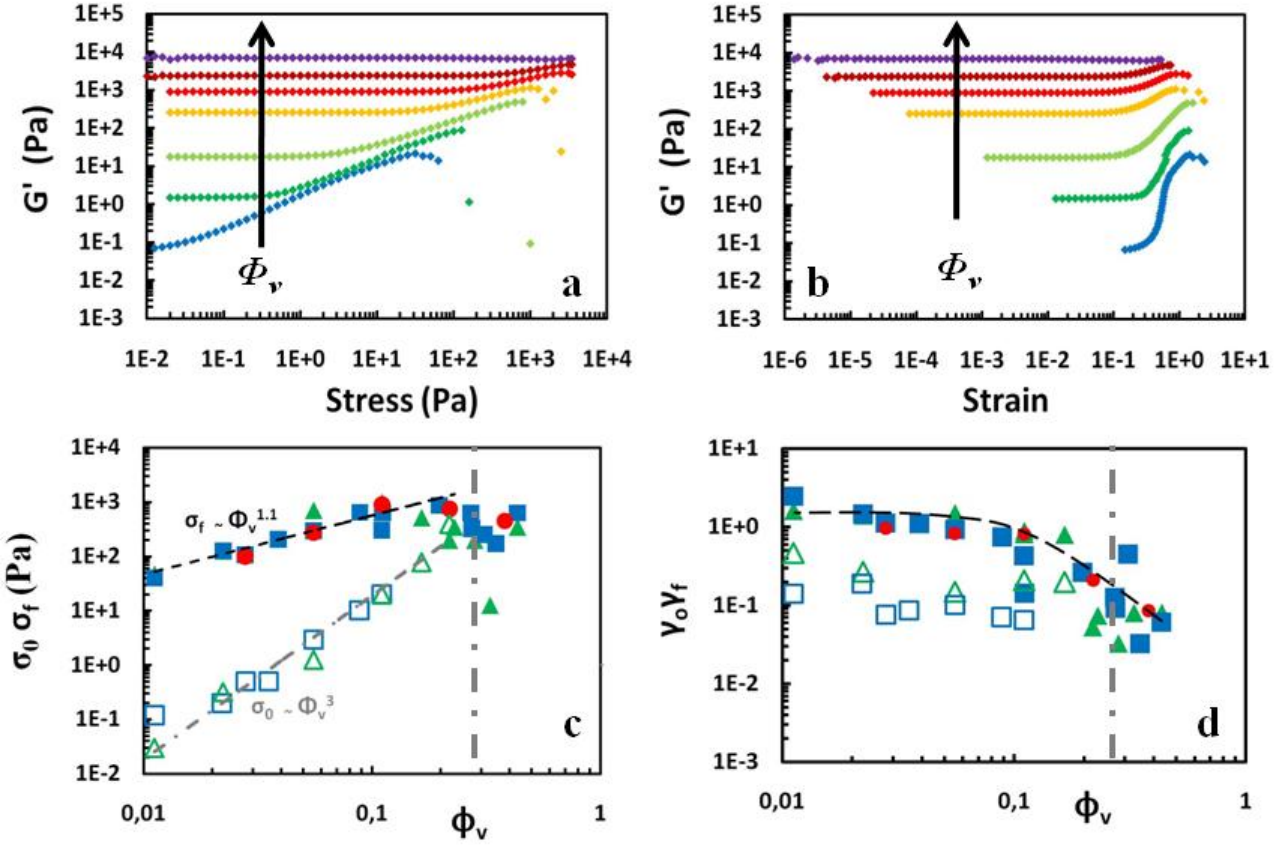

Figure 4.1: (a) Elastic modulus *G'* as a function of applied stress and in (b) as a function of strain using a serrated Couette. In (c) σ_f (filled); σ_0 (empty) and in (d) γ_f (filled); γ_0 (empty) as function of volume fraction estimated from (a) and (b) respectively. In (a) and (b) the volume fraction increases from bottom to the top: blue Φ_v =0.01, green Φ_v =0.025, light green Φ_v =0.05, yellow Φ_v =0.1, red Φ_v =0.15, burgundy Φ_v =0.2 and purple Φ_v =0.4. In (c) and (d) the symbols represent the different Couette geometries: smooth Couette in blues square, serrated Couette in green triangles and PMMA Couette in red (γ_0 and σ_0 cannot be determined in this geometry due to the use of a step to step procedure). The grey vertical dashed line represents the limit of fractality.

For gels exhibiting the strain hardening behavior ($\Phi_v < 0.25$), the limit of linearity of stress (σ_0) increases with the volume fraction with a power law $\sigma_0 \sim \Phi_v^{3.0}$ (Figure 4.1c) while the stress at the fracture (σ_f) increase with a power law $\sigma_f \sim \Phi_v^{1.1}$ (Figure 4.1c). The difference between σ_f and σ_0 decreased with the increase of the volume fraction (Figure 4.1c). In return, the limit of linearity of strain (γ_0) was tilled almost constant around 10 % as mentioned before (Figure 4.1d). In, this line the strain at the fracture (γ_f), determined when the *G'* decrease, was mostly constant around 1 up to Φ_v =0.1, in accordance with values reported for others colloidal gels (Gisler *et al.* 1999; Pouzot *et al.* 2006) (Figure 4.1d). By contrast, for gels where the strain hardening behavior is not observed (for $\Phi_v > 0.25$), the γ_f decreased with the volume fraction (Figure 4.1d) while σ_f were constant (despite the scatter of the data points).

The strain hardening was also observed in rotational measurements using a constant shear rate of 10^{-4} s^{-1}. This confirmed the non dependence of this behavior with the oscillatory movements. The strain hardening is independent of the frequency of oscillations (0.01 Hz to 10 Hz), of the temperature (4° C to 40° C) and of the surface of Couette geometry (smoothed, serrated, sanded and plastic). Those results strongly support the absence of wall slip in the non-linear regime investigated here.

As mentioned before, when strain hardening is observed, *G'* increases with the stress (or strain) until a limit passing through a maximum (G'_{max}) (Figure 4.1a and 4.1b). Figure 4.2 shows that G'_{max}, obtained at the maximum of the amplitude of the strain hardening, scales with the volume fraction as $\sim\Phi_v^{1.67}$, *i.e.* much less than the plateau modulus G'_0, which scales as $\sim\Phi_v^{3.35}$. The relative amplitude of the strain hardening, $G'_{max} - G'_0$, decreases with the volume fraction as shows in Figure 4.2. The decreases of the strain hardening behavior with the volume fraction can be explained by the variation of the radius of the clusters when clusters random close packing is reached (R_c). In fact, in the fractal model the cluster radius exhibited a scaling behavior with the volume fraction $R_c = a_0 \Phi_v^{-1/Df}$. The capacity to restructure (that corresponds to the amplitude of the strain hardening) decreases with Φ_v and therefore R_c up to the mentioned limit ($\Phi_v < 0.25$). Above this limit, the system does not show any hardening. For these gels, gelation is very quick due to the high particles density, "clusters" consist of only one or two particles, and the concept of fractality is not pertinent anymore. In these gels the fracture occurs for smaller values of strain. It has to be noticed that the moduli reached by the gels tend to approach the modulus of natural rubber dense films when their volume fraction approach the random close packing of rubber particles (Φ_{rcp}). For the system studied here, Φ_{rcp} can be estimated to be Φ_v =0.715 from the particle size distribution (supplementary data). Due to the particles polydispersity, this value is higher than for monodisperse hard sphere particles, *i.e.* 0.68 (Shewan and Stokes 2015).

In order to determine the origin of the viscoelastic properties of the natural rubber latex gels, we characterized by DMA and oscillatory shear measurements the viscoelastic properties of dense natural rubber latex films prepared by the drying of a latex suspension. Both values of G'_0 are equal and plotted at a volume fraction close to 0.87 according the dry percentage of polyisoprene in the natural rubber latex as mentioned in chapter 1 (Figure 4.2). These values of *G'* obtained for the rubber films are in the same order of magnitude than the maximum

values of G'_0 obtained for the highest concentrated natural rubber latex gels. This tentatively suggests a key role of the intrinsic material properties, probed in the dense film, in the overall properties of the fractal gels. However, such hypothesis should be carefully tested. Indeed, Ho *et al.* (Ho and Khew 1999) and Sakdapipanich et *al.* (Sakdapipanich *et al.* 2015) showed that rubber particles of a film made with NR latex needed several weeks to coalesce at room temperature. In the first days of film formation, they showed by AFM that the spherical particles would be still present in the rubber films (Ho and Khew 1999; Sakdapipanich *et al.* 2015). Then, a homogenous rubber film would be obtained after some weeks due to the coalescence of particles (Sakdapipanich *et al.* 2015). As it is possible that our "dense" films still contain individual particles, our results cannot demonstrate unambiguously the participation of particle core on the viscoelastic properties of natural rubber latex gels.

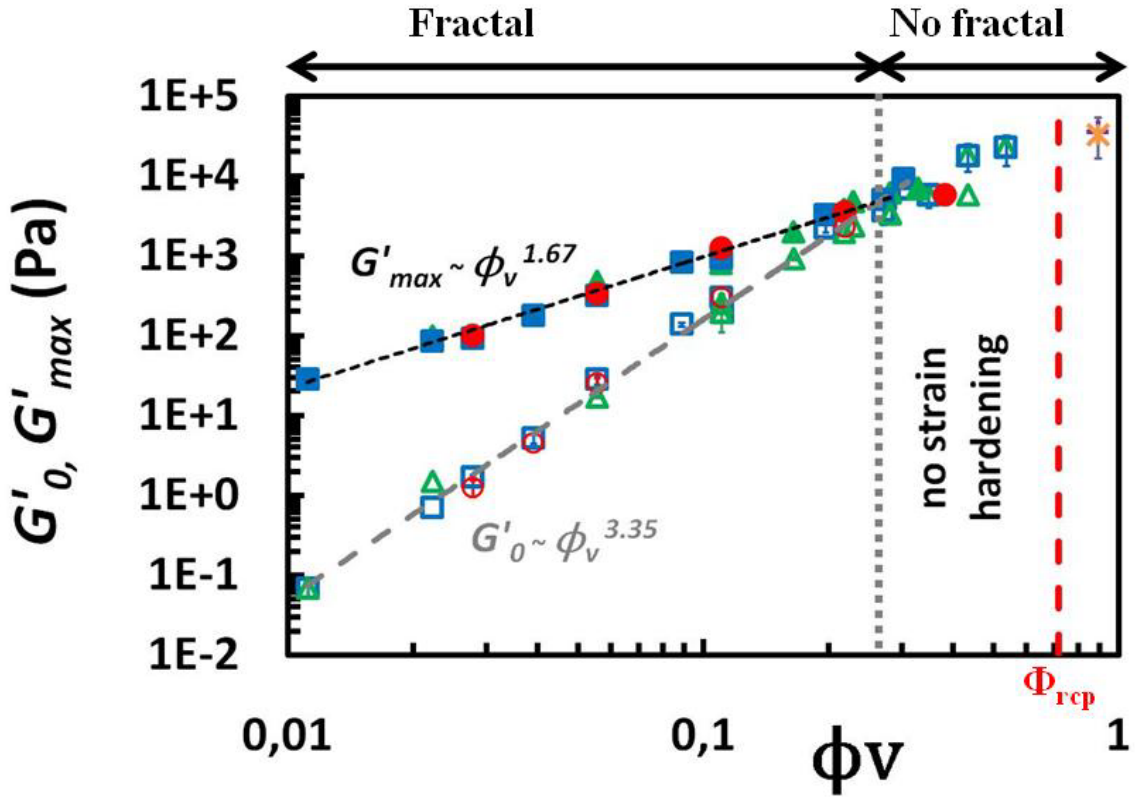

Figure 4.2: G'_{max} (filled symbols) and G'_0 (open symbols) as function of volume fraction. Scaling laws behavior of $G'_{max} \sim \Phi_v^{1.67}$ and $G'_0 \sim \Phi_v^{3.35}$ are represented by the dark dashed line and grey dashed line respectively. The symbols and colors represent the different Couette geometries: smooth Couette (blues square), serrated Couette (green triangles) and PMMA Couette (red circles). For dense natural rubber films, G' estimated from DMA measurements (orange start) and G'_0 using a plate-plate geometry (purple plus) are plotted. Vertical grey dashed curve represent the limit of fractality ($\Phi_v \sim$ 0.25-0.3) and the vertical red dashed curve represent the volume fraction at random close packing.

The tan δ (equal to G''/G') parameter quantifies the balance between the loss (G'') and storage moduli (G'). In this line, the fracture is characterized by the increase of the tan δ with the decrease of the G'. Figure 4.3 shows normalized tan δ (tan $\delta(\gamma)/\tan\delta_0$) and normalized elastic modulus ($G'(\gamma)/G'_0$) as a function of strain during oscillations for three distinct behaviors depending on the volume fraction (Φ_v =0.025, Φ_v =0.1 and Φ_v =0.4). For gels formed at Φ_v < 0.1, tan $\delta(\gamma)/$ tan δ_0 exhibited a minimum before the fracture of gels occurred at the maximum of $G'(\gamma)/G'_0$), which is attributed to the energy dissipation in the weak gels (Gisler *et al.* 1999; Pouzot *et al.* 2006). Gels formed at Φ_v between 0.1 and 0.25, exhibit a constant tan $\delta(\gamma)/$ tan δ_0 during the strain hardening without any signs of an increase in energy dissipation. Then, the tan $\delta(\gamma)/$tan δ_0 increased when the gel fracture. In contrast, for the gels formed at Φ_v > 0.25 (where strain hardening is not observed), G' decreased at small strain (until a strain of 0.02) and therefore tan $\delta(\gamma)/$ tan δ_0 increased.

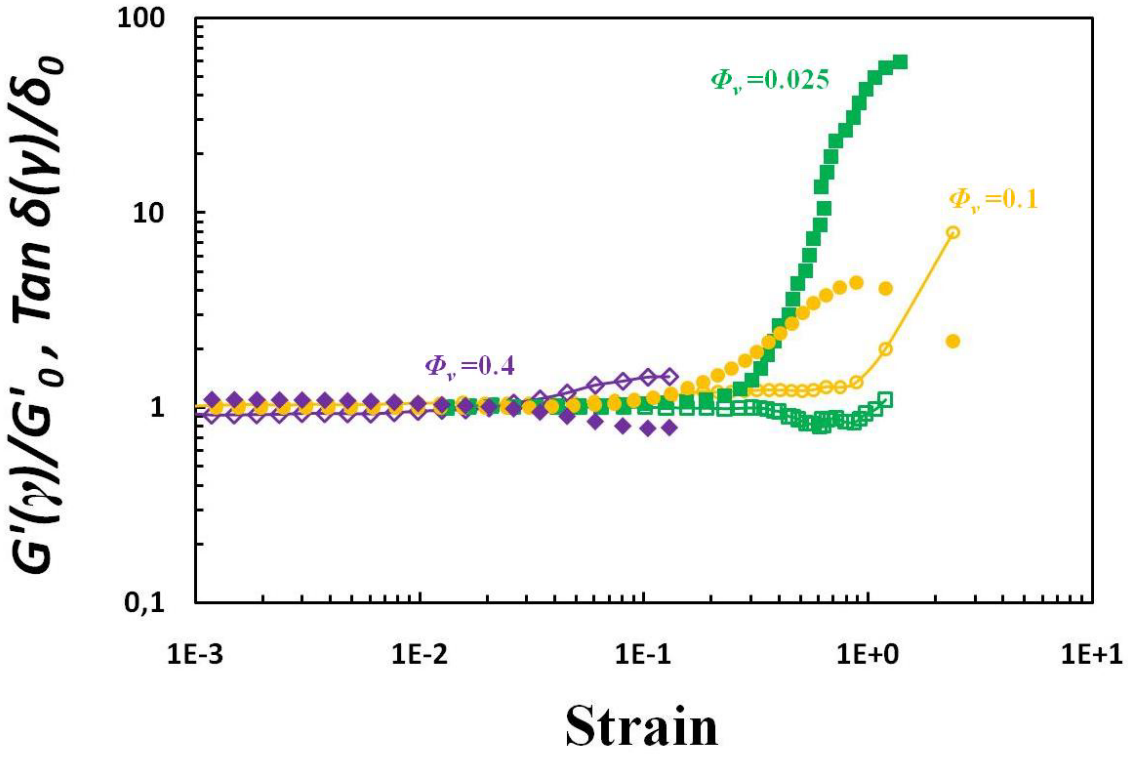

Figure 4.3: Relative $G'(\gamma)/G'_0$ (filled symbols) and tan $\delta(\gamma)/$ tan δ_0 (empty symbols) as function of strain for different volume fraction using a serrated Couette. Three different behaviors: weakly gels for Φ_v =0.025 (green squares), constant tan $\delta(\gamma)/$ tan δ_0 for Φ_v =0.1 (yellow circles) and no strain hardening for Φ_v =0.4 (purple diamonds).

Whatever the volume fraction, the strain hardening is well fitted using the model proposed by Gisler *et al.* (Gisler *et al.* 1999) for colloidal gels, and extended by the polynomials proposed by Pouzot *et al.* (Pouzot *et al.* 2006) where $G'(\gamma)/G'_0$ is function of both strain and backbone fractal dimensions (D_b). This model assumes that strain hardening occurs mostly because of bending associated with extension rather than compression or rotation of particles network. We plotted the master curve $G'(\gamma)/G'_0$ as a function of strain for a large range of volume fraction (Figure 4.4). We used the model varying the values of D_b between 1.1 - 1.4 according to the typical values for colloidal gels (the values of 1.13 and 1.3 are represented in Figure 4.4). In agreement with these fractal colloidal models, we determined D_b =1.13 being the best fit for the master curve of the strain hardening for the natural rubber latex gel. This value of D_b defined a fractal backbone almost linear inside the cluster.

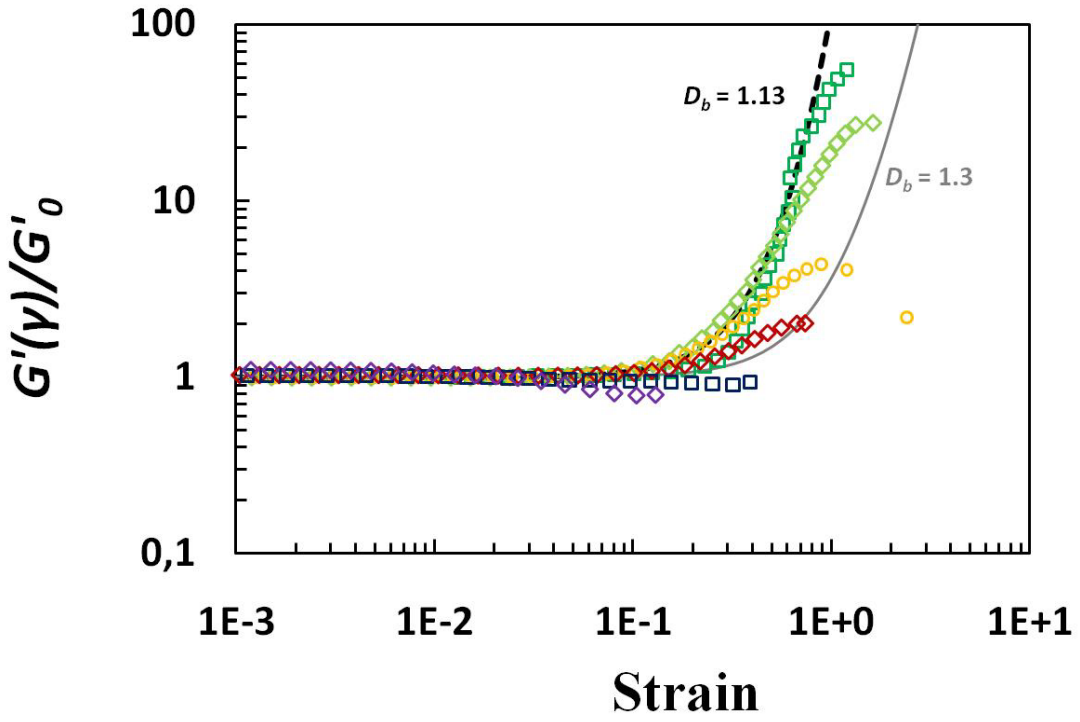

Figure 4.4: Normalized elastic modulus $G'(\gamma)/G'_0$ as a function of strain using a serrated Couette. Fits from Gisler *et al.* model using the polynomials proposed by Pouzot *et al.* are represented by the dark dashed line using D_b =1.13 and grey solid line using D_b =1.3. The volume fractions decrease from the top to the bottom: green Φ_v =0.025, light green Φ_v =0.05, yellow Φ_v =0.1, burgundy Φ_v =0.2, dark blue Φ_v =0.3 and purple Φ_v =0.4.

4.3.3 Strain hardening in NRL gels is irreversible

The reversibility of strain hardening of the NRL gel was studied varying the maximum value of stress imposed during an oscillation. This maximum value of stress was successively increased and decreased step by step. This is illustrated in Figure 4.5. The stress (here we analyzed the *G'* as function of strain) is first continuously increased (Figure 4.5a), then continuously decreased towards its initial lower value (Figure 4.5b), then increased again towards a higher strain than the one reached in step a (Figure 4.5c), and so on till the fracture of the gel (Figure 4.5d-e). For strains smaller than 0.1, *G'* is constant whatever the value of the strain, as expected from a linear regime. However, when the strain exceeds 10%, strain hardening irreversibly occurs, in the sense that a further decrease of the strain is not associated with a return to the initial modulus plateau. Instead, the material exhibits a new *G'* at a plateau higher than G'_0 even at very low strain. We tentatively suggest that irreversibility of strain hardening could be associated to the appearance of new irreversible bonds between particles. In our previous study of NRL aggregation, we observed that once particles are associated in a cluster, interparticles bonds are irreversible, whatever the physical-chemical conditions (Reis *et al.* 2015. It is therefore likely that if during a deformation, particles that were far apart at rest come to contact, they can form a new bond that will stay even after the release of the deformation.

Similarly to the properties in the linear regime, strain hardening appeared to be very robust, independently of the number of steps of the characterization procedure and theirs durations, of the frequency (varied between 0.01 and 10 Hz) or of the temperature (varied between 4°C and 40°C). It has been also observed in the absence of mechanical oscillations, when the strain is only continuously increased. This behavior is unusual because of its irreversibility, it appears as a characteristic of this material, and, to our knowledge, was not reported previously with another type of colloidal gel.

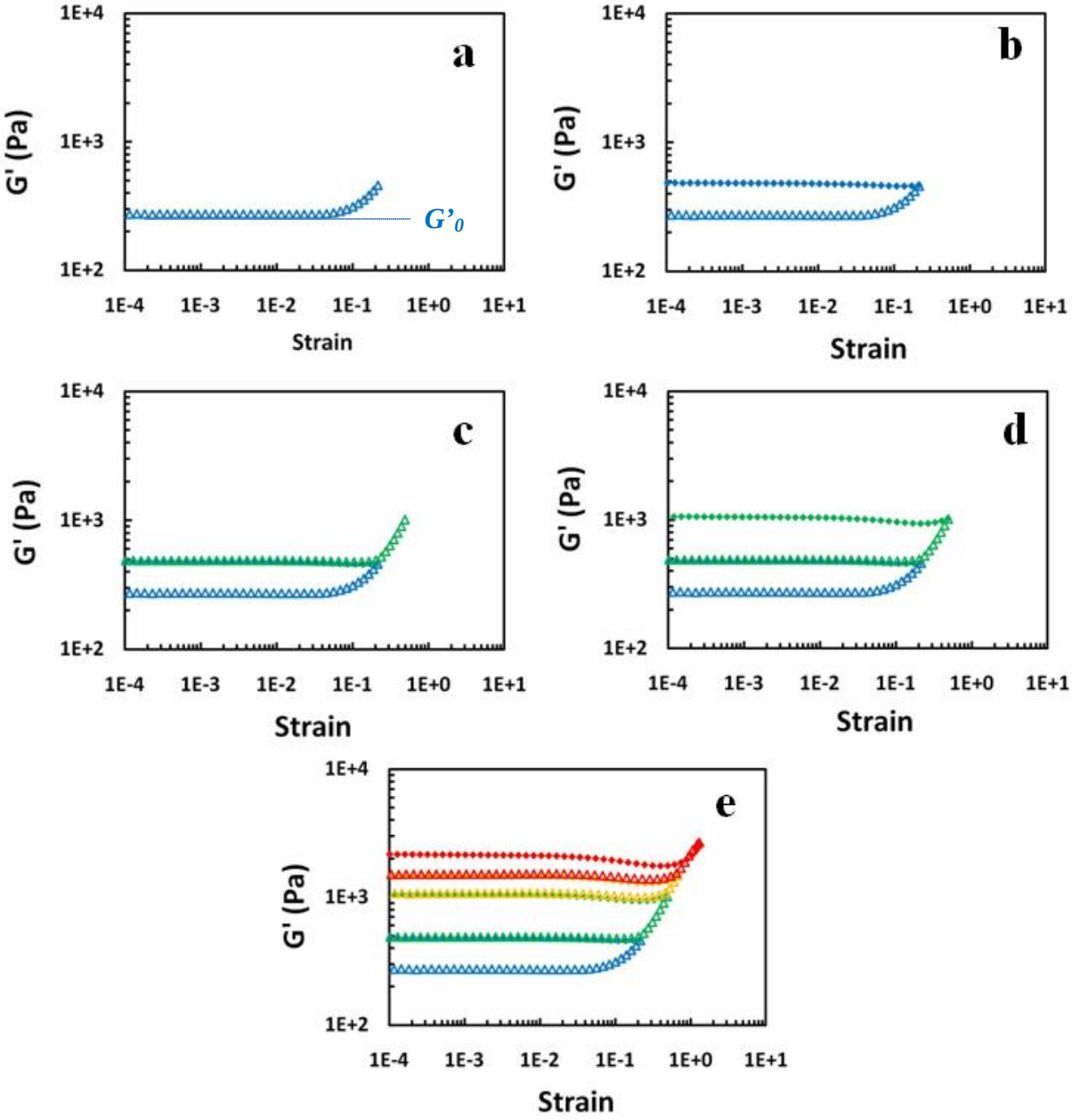

Figure 4.5: *G'* as a function of strain during the successive increase and decrease of strain for Φ_v =0.1 using a serrated Couette. (a) Increase of strain till γ_{max} =20 %, (b) then decrease from γ_{max} =20 % to γ =0.01 %, (c) increase of strain from γ =0.01 % to γ_{max} =50 % (d) then decrease from γ_{max} =50 % to γ =0.01 % and (e) successive increase/decrease with several plateaus of *G'* until fracture at γ_f > 100 %.

The model proposed by Gisler *et al.* (Gisler *et al.* 1999), previously presented in Figure 4.4, was used to characterize the evolution of the different *G'* plateaus obtained for different strain values ($G'_{0\text{-}\gamma max}$) observed during the irreversible hardening (Figure 4.5). The values of $G'(\gamma)/G'_{0\text{-}\gamma max}$ were estimated for each step, during the increase, for a volume fraction between Φ_v =0.035 and Φ_v =0.1. In figure 4.6, we observe a shift of curves with the increase of the maximum strain value for all volume fractions. The experimental curves nicely follow the fit. This analysis showed that, the values of D_b increase with values of γ_{max} above about 0.5. This behavior suggests an evolution of D_b during strain hardening in two-step (Inset Figure 4.6).

For strain values below 0.5, the initial backbone fractal dimension remained mostly constant. In return, for strains above 0.5, the values of D_b increased following a power law relation with the strain. Then for $D_b \approx 1.8$, a value close to the overall gel fractal dimension (*i.e.* 1.8-2.0), the network fracture which represents the maximum deformation supported by the strand of particles forming the backbone.

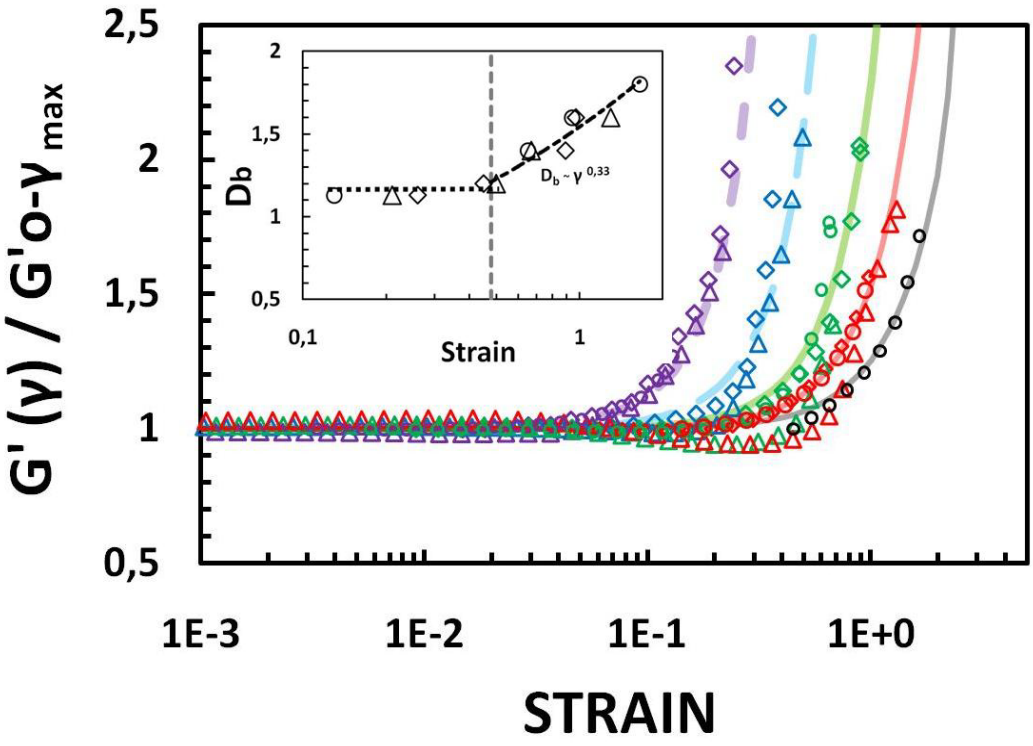

Figure 4.6: *G'(y)/G'*$_{0\text{-}}\gamma_{max}$ as a function of strain during the increases/decreases for different step using a serrated Couette. The colors represent the maximum strain attempted applied at each step: Purple: γ_{max} =0.25, blue: γ_{max}=0.5, green: γ_{max}=0.9, red: γ_{max}=1.2 and black: γ_{max}= 1.65. The curves are fitted using from left to the right: D_b =1.13 (purple line), 1.2 (blue line), 1.4 (green line), 1.6 (red line) and 1.8 (black line) using Gisler *et al.* model (Gisler *et al.* 1999). Inset: evolution of the backbone fractal dimension D_b function of strain. The symbols represent the three different volume fractions used: Φ_v =0.035 (diamonds), Φ_v =0.05 (circles) and Φ_v =0.1 (triangles).

For high values of strain, we observed a deviation from the fit: just before strain hardening, *G'* slightly decreases before to increase. These deviations are illustrated by the troughs observed in Figure 4.5. They allow to distinguished newly hardened materials to a non-hardened gel (same *G'*) prepared with a higher particle volume fraction: they could exhibit the same plateau modulus, by hardened gels and only then will exhibit the slight modulus decrease before hardening. This deviation observed when the maximum strain imposed during hardening exceeded 0.5 is repeatable. Troughs depth increases with the maximum value of strain applied. In addition, a bump was observed in the *G"* curves (data not show) at the same strain values.

To check the temporal stability of hardened gels, we stopped the stress increase during an oscillatory sweep in the hardening region and then maintained the material under a constant oscillatory strain for 3 hours. We did this kind of experiment for different values of strain, as illustrated in Figure 4.7. *G'* of hardened gel was constant during 3 hours when a constant strain below 0.6 was applied. On the other hand, for the higher than 0.6 applied strain, *G'* decreased continuously and the fracture of the gel was eventually observed. The critical strain that have to be applied to observe this progressive de-structuration of the gel is similar to the critical strain for which D_b begin to increase and for which troughs appeared before material hardening in stress sweep. So, if a critical strain of 0.5 is reached the gel structure is progressively destroyers till the gel fractures. Moreover, when this critical strain is reached, D_b approaches D_f and its represents the maximum stress supported by the network. This evolution rise the question of the origin of this materials properties evolution. Is this de-structuring homogeneously distributed in the sample, or is it for example localized at the wall interface? We try to answer to this question using the rheo-ultrasound technic.

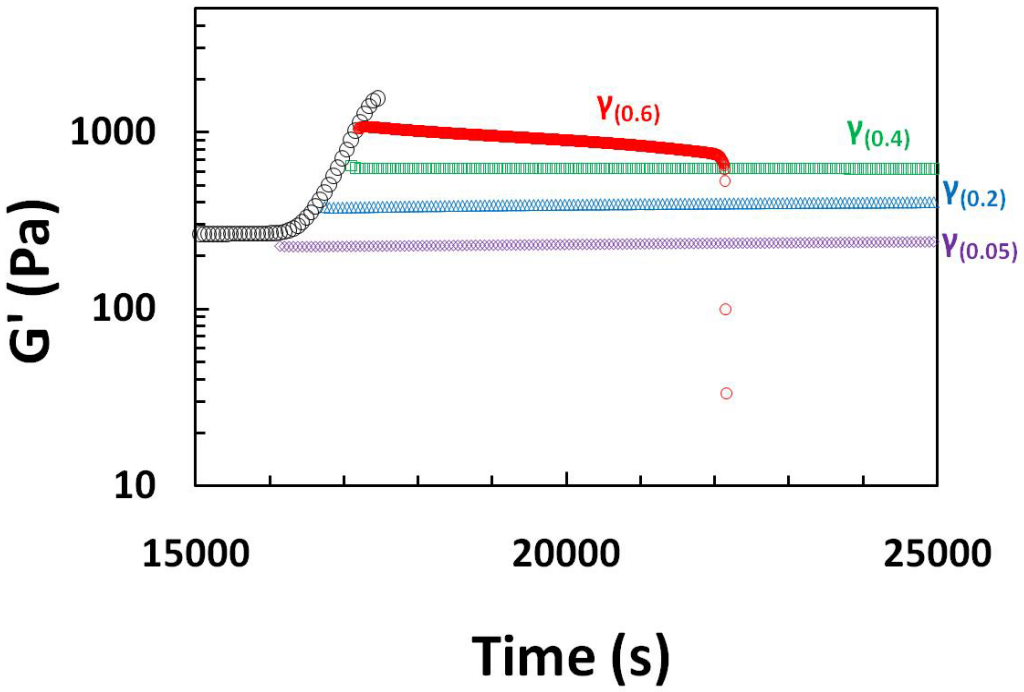

Figure 4.7: Standard strain hardening (up to fracture) obtained from the stress sweep is represented in black circles for Φ_v =0.1 using a serrated Couette. In colors the continuous strain applied at different strain values during the strain hardening: the constant *G'* for γ =0.05 in purple diamonds, γ =0.2 in blues triangles, γ =0.4 in green squares and the fracture of the gel for γ =0.6 in red circles.

4.3.4 Gel hardening or degradation under strain is homogenously distributed in the sample

We used the 2D-Ultrasonic speckle velocity (USV) technic to observe the displacement fields inside the gel during the oscillatory strain. In this study, the strain (and not any more the stress) was applied to the gel due to the high inertia and also the large radius of the PMMA Couette geometry. Figure 4.8a, 4.8b and 4.8c show the displacement fields inside the gel obtained by USV for 0.1, 0.4 and 0.8 imposed strain values, respectively. Figures 4.8d, 4.8e, 4.8f show the local velocity inside the gel during the oscillations obtained from the Figure 4.8a, 4.8b and 4.8c, respectively. The black signal is obtained by the rheometer and the color signals by USV at different places on the gap.

At low strain (0.1) in the linear regime, we observed a sinusoidal signal as expected (Figure 4.8d). This signal confirmed the linear character of the strain-stress response. Instead, when the strain is increased at 0.4 (Figure 4.8e), the strain signal imposed by the rheometer is triangular and not anymore sinusoidal, and so is the deformation field inside the gel. Beside the rheometer cannot impose a sinusoidal signal it is interesting to notice that the USV data clearly showed that the material response to the solicitation is linear, *i.e.* it exhibits the exact same triangular shape, whatever the depth is considered. For values of strain about 0.8, when nearby the gel fracture, signals become heterogeneous. The Fast Fourier Transform (FFT) of the local velocity as a function of time was then used to obtain the different harmonics from the local velocity profile function of time. At low strain, we observed only a first harmonic as expected for the sinusoidal signal (Figure 4.8g). When the strain is increased, a third harmonic was observed which is reported to appear in the non-linear regime (Figure 4.8h) (Hyun *et al.* 2011). In that case, we can note that the 3^{rd} harmonic is already present in the output signal of the rheometer (plotted in grey in the figure).

For even higher strain value (0.8), a 2^{nd} harmonic was observed in USV data but not in the input signal from rheometer. The physical meaning of the emergence of a 2^{nd} harmonic is still unclear in the literature (Hilliou *et al.* 2009; Hyun *et al.* 2011). Some authors link the absence of the 2^{nd} harmonic with the absence of wall slip. However, in your system the wall-slip is absent and the 2^{nd} harmonic appears very close to the fracture of the gel, which suggests that it could be associated with internal and irreversible ruptures inside the gel structure.

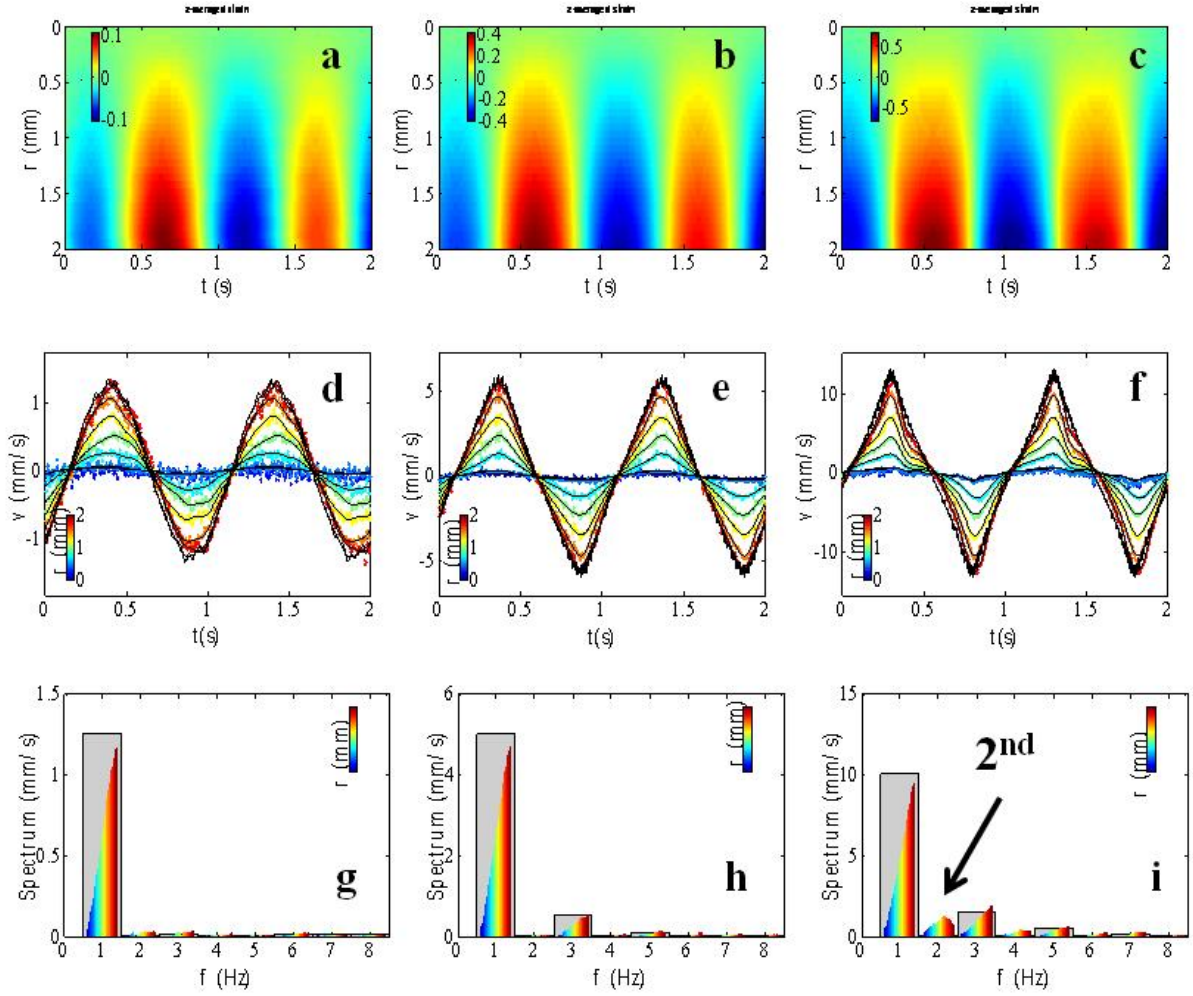

Figure 4.8: Rheo-ultrasound measurements of the natural rubber latex gels for Φ_v =0.025. Figure 8a, 8b and 8c: displacements obtained from USV speckles gel with stator r =0 and rotor r =2. Colors represent the displacement (blue and red represent the different direction of displacements). Figures 8d, 8e and 8f: velocity obtained from the rheometer (black signal) and from USV (colors signals) inside the gel. Figure 8g, 8h and 8i: harmonics obtained after FFT of the velocity from USV (colors) and from input signal from rheometer (grey cases). Left (a, d, g): 0.1 of strain, center (b, e, h): 0.4 of strain and right (c, f, i): 0.8 of strain.

The velocity profiles inside the gel are linear for all values of strain imposed, as illustrated in Figure 4.9. Despite the fact that the 2nd harmonic appears close to the fracture, the velocity profiles inside the gel are homogenous into the gap, which suggest that the restructuration mechanism at the origin of the irreversible strain hardening is homogenously distributed in the material. There is no apparent transient evolution once a new strain is imposed. Local rearrangements are quasi-instantaneous upon strain increase, and homogeneously distributed in the sample. The USV scale is around 100 µm, so this indicates that the rearrangement associated with strain hardening takes place on a smaller scale, probably close to the particle or a few particle scale.

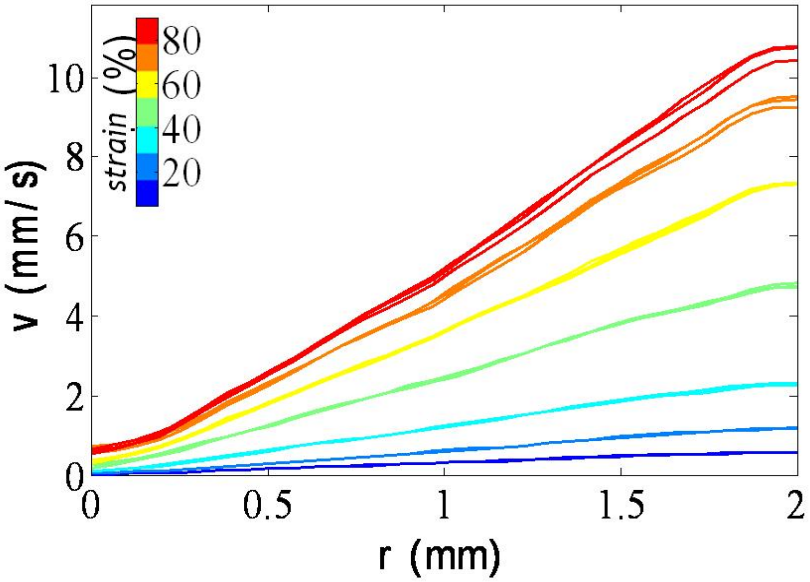

Figure 4.9: Linear velocity profiles, v (mm/s), as function of the gap between the stator (r =0 mm) and the rotor (r =2 mm) obtained from USV data for Φ_v = 0.025. Strain increase from the bottom to the top: γ =0.1 (dark blue), γ =0.2 (blue), γ =0.3 (light blue), γ =0.4 (green), γ =0.6 (yellow), γ =0.7 (orange) and γ =0.8 (red).

4.4 Conclusions

We investigated the rheological behavior of natural rubber latex gels, acid-coagulated with the GDL, in the rheological non-linear regime in a wide range of volume fraction (0.01 to 0.53). For $\Phi_v < 0.25$, these fractal colloidal gels presented a strain hardening behavior at high values of strains. Scaling behavior of $G'_0 \sim \Phi_v^{3.35}$ and $G'_{max} \sim \Phi_v^{1.67}$ are observed. Both moduli merge for Φ_v =0.25, above which no hardening is observed ($G'_0 = G'_{max}$). Interestingly, for $\Phi_v > 0.25$, the moduli continue to increase with volume fraction, till it reaches the valued measured on a rubber film.

For all samples formed for $\Phi_v < 0.25$, the strain hardening behavior appeared at the values of strain around 10 % and the network fracture almost at the same strain (~100 %) independently on the volume fraction. The strain hardening of natural rubber latex gels occurs by the rearrangements of particles due to the bending where new irreversible bonds were formed during the oscillation according the colloidal fractal model. For all gels formed at high volume fractions, $\Phi_v > 0.25$, the strain hardening is not observed due to the loss of fractality. These gels exhibited a fracture at lower strain which decreased with the increase of the volume fraction.

Strain hardening of natural rubber latex gels is irreversible in agreement with the irreversibility of the interactions between the rubber particles since the aggregation step. This irreversible restructuration of the gel is related to the increased of the backbone fractal dimensions D_b with the increased of strain using the colloidal fractal models. Gel hardening was still stable for moderate values of strain, inferior to 0.5. For higher values of strain the

materials does not support the oscillatory strain over a long period of time, its modulus progressively decrease and it eventually fracture. We suggest a breaking of some interactions as related for colloidal gels (Wessel and Ball 1992; Colombo and Del Gado 2014). These breaking are associated with the development of the troughs during the hardening and correlated to the increases of the $D_{b.}$ This supposed a fracture of the network where the fractal backbone reaches the maximal deformation (stress supported). Moreover, the progressive de-structuration could be explained by a local heterogeneity of the stress distributed in the network at scale of particles (Colombo and Del Gado 2014).

The original combination of the classic rheology and ultrasound turns out to be very efficient to follow the deformation fields both spatially and temporally inside the gel. The linear displacement profile within the gel confirms that the strain hardening behavior occurs on the scale of particles. Moreover, the fracture mostly occurs homogeneously in all space for the scale of this method, *i.e.* 100-200 µm. For the future studies, rheology coupled with imaging techniques could be used to analyze the particles during the strain hardening.

Acknowledgment

This work was carried out with support from CNPq – National Council for Scientific and Technological Development – Brazil and CIRAD-DRS (France).

References

Berthelot, K., *et al.* (2014). "Rubber particle proteins, HbREF and HbSRPP, show different interactions with model membranes." Biochimica et Biophysica Acta (BBA) - Biomembranes **1838**(1, Part B): 287-299.

Bremer, L. G. B., *et al.* (1993). "Formation, properties and fractal structure of particle gels." Advances in Colloid and Interface Science **46**(0): 117-128.

Bremer, L. G. B., *et al.* (1989). "Theoretical and experimental study of the fractal nature of the structure of casein gels." Journal of the Chemical Society, Faraday Transactions 1: Physical Chemistry in Condensed Phases **85**(10): 3359-3372.

Brenner, T., *et al.* (2009). "Rheology of thermo-reversible fish protein isolate gels." Food Research International **42**(8): 915-924.

Buscall, R., *et al.* (1988). "Scaling behaviour of the rheology of aggregate networks formed from colloidal particles." Journal of the Chemical Society, Faraday Transactions 1: Physical Chemistry in Condensed Phases **84**(12): 4249-4260.

Cornish, K., *et al.* (1999). "Rubber particles from four different species, examined by transmission electron microscopy and electron-paramagnetic-resonance spin labeling, are found to consist of a homogeneous rubber core enclosed by a contiguous, monolayer biomembrane." Planta **210**(1): 85-96.

Dickinson, E. (2013). "Structure and rheology of colloidal particle gels: Insight from computer simulation." Advances in Colloid and Interface Science **199–200**(0): 114-127.

Farr, R. S. and R. D. Groot (2009). "Close packing density of polydisperse hard spheres." The Journal of Chemical Physics **131**(24): 244104.

Gisler, T., *et al.* (1999). "Strain Hardening of Fractal Colloidal Gels." Physical Review Letters **82**(5): 1064-1067.

Hagiwara, T., *et al.* (1998). "Fractal analysis of aggregates in heat-induced BSA gels." Food Hydrocolloids **12**(1): 29-36.

Hilliou, L., *et al.* (2009). "Structural and mechanical characterization of kappa/iota-hybrid carrageenan gels in potassium salt using Fourier Transform rheology." Food Hydrocolloids **23**(8): 2322-2330.

Ho, C. C. and M. C. Khew (1999). "Surface Morphology of Prevulcanized Natural Rubber Latex Films by Atomic Force Microscopy: New Insight into the Prevulcanization Mechanism." Langmuir **15**(19): 6208-6219.

Hyun, K., *et al.* (2011). "A review of nonlinear oscillatory shear tests: Analysis and application of large amplitude oscillatory shear (LAOS)." Progress in Polymer Science **36**(12): 1697-1753.

Ikeda, S., *et al.* (1999). "Rheological Study on the Fractal Nature of the Protein Gel Structure." Langmuir **15**(25): 8584-8589.

Krieger, I. M. and T. J. Dougherty (1959). "A Mechanism for Non -Newtonian F Suspensions of Rigid Spheres." Transactions of The Society of Rheology (1957-1977) **3**(1): 137-152.

Licup, A. J., *et al.* (2015). "Stress controls the mechanics of collagen networks." Proceedings of the National Academy of Sciences of the United States of America **112**(31): 9573-9578.

Manneville, S., *et al.* (2004). "High-frequency ultrasonic speckle velocimetry in sheared complex fluids." European Physical Journal-Applied Physics **28**(3): 361-373.

Mellema, M., *et al.* (2002). "Effects of structural rearrangements on the rheology of rennet-induced casein particle gels." Advances in Colloid and Interface Science **98**(1): 25-50.

Nawamawat, K., *et al.* (2011). "Surface nanostructure of Hevea brasiliensis natural rubber latex particles." Colloids and Surfaces A: Physicochemical and Engineering Aspects **390**(1–3): 157-166.

Orakdogen, N., *et al.* (2010). "Evidence of Strain Hardening in DNA Gels." Macromolecules **43**(3): 1530-1538.

Pantina, J. P. and E. M. Furst (2005). "Elasticity and critical bending moment of model colloidal aggregates." Physical Review Letters **94**(13).

Pouzot, M., *et al.* (2006). "Strain hardening and fracture of heat-set fractal globular protein gels." Journal of Colloid and Interface Science **293**(2): 376-383.

Reis, G. D., *et al.* (2015). "Acid-induced aggregation and gelation of natural rubber latex particles." Colloids and Surfaces a-Physicochemical and Engineering Aspects **482**: 9-17.

Rohm, H., *et al.* (2014). "Gelation of Cross-Linked Casein under Small and Large Shear Strain." Journal of Texture Studies **45**(2): 130-137.

Sakdapipanich, J., *et al.* (2015). "Influence of mixed layer of proteins and phospholipids on the unique film formation behavior of Hevea natural rubber latex." Colloids and Surfaces A: Physicochemical and Engineering Aspects **466**(0): 100-106.

Shewan, H. M. and J. R. Stokes (2015). "Analytically predicting the viscosity of hard sphere suspensions from the particle size distribution." Journal of Non-Newtonian Fluid Mechanics(0).

Shih, W.-H., *et al.* (1990). "Scaling behavior of the elastic properties of colloidal gels." Physical Review A **42**(8): 4772-4779.

Singh, M., *et al.* (2014). "Influence of hydrophobically modified inulin (INUTEC NRA) on the stability of vulcanized natural rubber latex." Colloids and Surfaces A: Physicochemical and Engineering Aspects **451**(0): 90-100.

Sittikijyothin, W., *et al.* (2007). "Heat-induced gelation of beta-lactoglobulin at varying pH: Effect of tara gum on the rheological and structural properties of the gels." Food Hydrocolloids **21**(7): 1046-1055.

Sridee, J. (2006). Rheological properties of natural rubber latex

Suranaree University of Technology, Thailand. **Thesis**.

Storm, C., *et al.* (2005). "Nonlinear elasticity in biological gels." Nature **435**(7039): 191-194.

Tanaka, Y. (2001). "Structural characterization of natural polyisoprenes: Solve the mystery of natural rubber based on structural study." Rubber Chemistry and Technology **74**(3): 355-375.

Toki, S., *et al.* (2000). "Strain-induced crystallization of natural rubber as detected real-time by wide-angle X-ray diffraction technique." Polymer **41**(14): 5423-5429.

Tokita, M. (1989). "Gelation mechanism and percolation." Food Hydrocolloids **3**(4): 263-274.

Tosaka, M., *et al.* (2004). "Orientation and crystallization of natural rubber network as revealed by WAXD using synchrotron radiation." Macromolecules **37**(9): 3299-3309.

Vaysse, L., *et al.* (2012). Natural rubber in Polymer Science: A Comprehensive Reference. Amsterdam, Elsevier BV.

Vaysse, L., *et al.* (2009). Natural Rubber in Sustainable Solutions for Modern Economies,Coord. Dr Rainer Höfer, The Royal Society of Chemistry. Cambridge, UK**:** 339-367.

Wu, H. and M. Morbidelli (2001). "A Model Relating Structure of Colloidal Gels to Their Elastic Properties." Langmuir **17**(4): 1030-1036.

Yanez, J. A., *et al.* (1999). "Viscoelastic Properties of Particle Gels." Journal of Colloid and Interface Science **209**(1): 162-172.

Supplementary Material

Viscosity measurements were conducted on stable latex suspensions (without acidification). For low volume fraction ($\Phi_v < 0.1$), we used a Schott U-tube capillary viscometer (ref. # Tyn 51813), for which the flow time was digitally recorded using the Schott timer AVS400. For volume fraction $\Phi_v > 0.1$ an MCR702 (Anton Paar) equipped with a sanded Couette (inner radius 10 mm, outer radius 11 mm and height 27 mm) was used with a shear rate from 500 s^{-1} to 0.01 s^{-1}. The viscosity is determined at the plateau observed when viscosity is plotted as a function of the shear rate. All measurements were performed three times at a constant temperature of 20° C. The resulting dependence of the suspension relative viscosity on the particles volume fraction from Φ_v =0.0048 to Φ_v =0.61, is plotted on Figure 4.10.

This evolution can be fitted using the Krieger-Dougherty (Krieger and Dougherty 1959) model, which gives an estimate of the volume fraction at maximum packing is Φ_{max} =0.72, and a value of 2.86 for the intrinsic viscosity (see table 4.1). The Krieger-Dougherty fit results in values closed to the ones found in the literature (Sridee 2006). Φ_m is here much higher than the theoretical value for monodisperse hard spheres, Φ_m^{HS} =0.58, which can be explained by the polydispersity of the rubber particles (Shewan and Stokes 2015).

The evolution of relative viscosity with the volume fraction can also be fitted by the Maron–Pierce–Quemada (MPQ) (Shewan and Stokes 2015) model, which requires the knowledge of Φ_{rcp}, the volume fraction at the random close packing. It can be determined independently by the ratio of the volume diameter mean and surface diameter mean of particles, $D_{4.3}/D_{3.2}$, (Farr and Groot 2009), that we obtained by static light scattering. From the particle size distribution, we determined that Φ_{rcp} =0.715 (Reis *et al.* 2015). (Figure S1).

Table 4.1 – Parameters estimated from the Krieger-Dougherty and Maron-Pierce-Quemada models.

Models	Equations	Parameters
Krieger-Dougherty (Krieger and Dougherty 1959)	$\frac{\eta_d}{\eta_0} = \left[1 - \frac{\Phi_v}{\Phi_{max}}\right]^{-[\eta]\Phi_{max}}$	$[\eta] = 2.86$ $\Phi_{max} = 0.72$
Maron–Pierce–Quemada (MPQ) (Shewan and Stokes 2015)	$\frac{\eta_d}{\eta_0} = \left[1 - \frac{\Phi_v}{\Phi_{rcp}}\right]^{-2}$	$\Phi_{rcp} = 0.715$

where η_d and η_0 are the viscosity of the suspension and the viscosity of the solvent respectively, Φ_{max} the volume fraction at maximum packing, Φ_{rcp} is the random close packing volume fraction and $[\eta]$ is the intrinsic viscosity.

The coherence of our experimental results with the MPQ model, which do not requires any adjustable parameters, is remarkable. It allows us to estimate if particles are deformed under the conditions of measurements. Indeed, the soft character of the particles can be estimated from the relation between $1/(\eta_r)^{0.5}$ against Φ_v/Φ_{rcp} (Shewan and Stokes 2015) where the softening of particles is characterized by a deviation of linearity of data. Replotting our data in

this context (Figure 4.11) demonstrate that NRL suspension follow this linear relationship: in the conditions of viscosity measurements (up to shear stress close to 0.2-0.6 Pa depending on volume fraction), rubber particles exhibit a hard sphere behavior

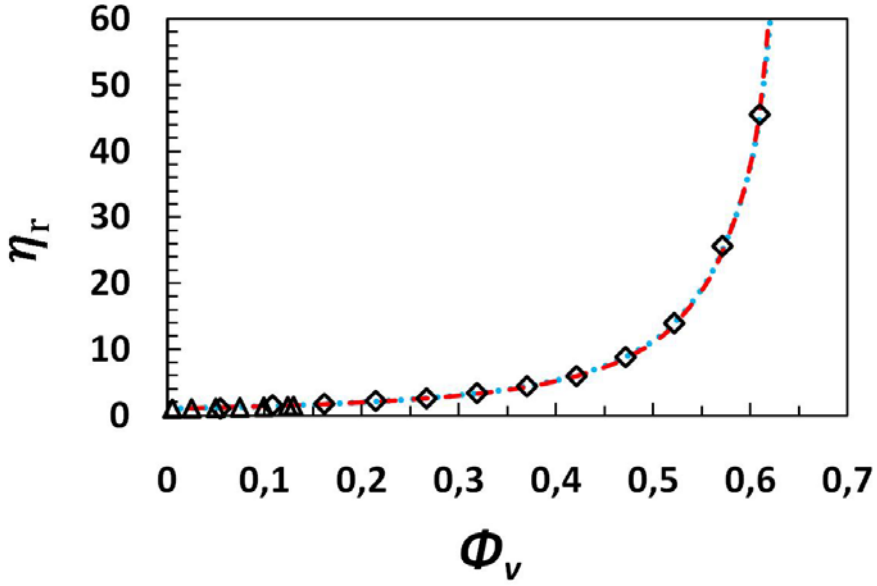

Figure 4.10: Relative viscosity of NRL suspension as a function of volume fraction. Measurements are obtained with an MCR702 rheometer (diamonds) and a capillary viscometer (triangles). Dashed line (---): Krieger-Dougherty equation with two fitting parameters, Φ_{max} =0.72 and [η] =2.86. Bleu dashed points (···): MPQ model with Φ_{rcp} =0.715 determined independently by static light scattering.

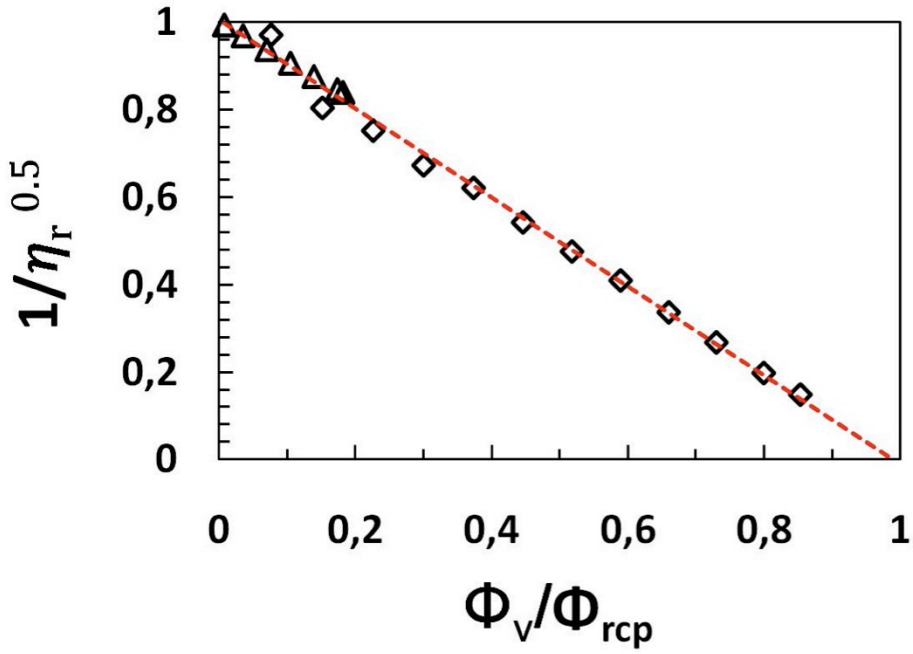

Figure 4.11: $1/(\eta_r)^{0.5}$ function of Φ_v/Φ_{rcp}. Measurements are obtained with an MCR702 rheometer (diamonds) and a capillary viscometer (triangles). The MPQ model for hard sphere is represented by the red dashed line.

Chapter 5

Gelation under an oscillatory shear: influence of the strain amplitude on the structural properties

In the previous chapters, gelation was monitored under a small, constant oscillatory strain which value was set at 0.5 %. Rheological investigations of the final gel properties showed that such oscillatory strain had no apparent impact on the material structure. Such structure, once formed, exhibits strain hardening if submitted to an increasing oscillatory strain, when its value exceeded about 10 % in amplitude. As this hardening was irreversible, it constitutes a simple and efficient opportunity to strengthen materials and reach elastic moduli equivalent to the ones obtained at much higher volume fraction. In this chapter, we study the impact of an oscillatory strain imposed directly during the gelation on the network structure. We wish to establish if such conditions would allow the formation of strengthen materials similarly to a deformation imposed on an already formed gel. We therefore monitored the gel formation at a given initial oscillatory strain, and then characterized through a strain sweep the rheological properties of the resulting gels.

Acidification of NRL was performed using glucono-delta-lactone (GDL). Viscoelastic properties of the gels resulting from this coagulation (pH 4) were characterized in the linear and non-linear regimes. For gels prepared at high volume fractions, for $\Phi_v > 0.25$, application of an oscillating strain during gelation result in a degradation of the material properties as assessed by a decrease of the gel modulus. For $\Phi_v < 0.25$, four different behaviors were observed depending on the initial oscillatory strain, *i.e.* the oscillatory strain applied during gelation. For small initial strain ($0.5\ \% < \gamma < 10\ \%$), gels exhibited the same behavior as for the reference. For strain between 10 and 50 %, gels hardened during gelation and always exhibited strain hardening in the subsequent strain sweep. For strain $\geq 50\ \%$), the gel did not exhibit anymore strain hardening. Finally, for very high strain values ($\gamma > 90\ \%$), a macroscopic heterogeneous gel was observed. In this chapter, we will specifically focus on these different behaviors through a systematic comparison with gels prepared at rest (or under low oscillating strain).

This chapter is a paper under preparation.

5.1 Introduction

Natural rubber latex, composed mostly by rubber particles, is used worldwide since many years (Blackley 1996; Vaysse *et al.* 2009; Vaysse *et al.* 2012). Rubber particles are initially negatively charged due to the existence of a mixed membrane of lipids and proteins surrounding a polyisoprene core (Cornish *et al.* 1999; Nawamawat *et al.* 2011; Gaboriaud *et al.* 2012; Berthelot *et al.* 2014). They aggregate during acidification and form a fractal colloidal gel. In our recent work, we studied the acid-induced gelation of the rubber particles and the viscoelastic properties of the resulting colloidal gel (Reis *et al.* 2015). They exhibit an irreversible strain hardening under large deformation due to internal restructuration of interactions network. This restructuration induced a formation of new connections between the strands of particles (Wessel and Ball 1992). The elastic modulus *G'* increased irreversibly with the strain (or stress) imposed. A critical strain around 50 % was observed: above it, a progressive de-structuration of the network occurred.

Colloidal particles aggregate if their pair-potential is attractive. In absence of external forces, aggregation kinetics are controlled by the strength of the attractive interaction and their diffusion coefficient in the medium. External forces such as shear or gravitational forces can however affect the aggregation rate. The shear rate can accelerate particles aggregation or clusters rupture (Vermant and Solomon 2005).It can also change the aggregation mechanism since aggregates are rather formed through *diffusion limited cluster aggregation* (DLCA) at small shear rate but through *reaction limited cluster aggregation* (RLCA) regime at high shear rate. This results in the formation of superaggregates induced by high shear rates was reported for dense colloidal systems (Mokhtari *et al.* 2008). Recently, the control of the design of colloidal gel structure by shear rate was demonstrated (Koumakis *et al.* 2015). Depending on the volume fraction (and/or interactions forces between particles) and on the shear rate, heterogeneous or homogeneous gels can be obtained. The heterogeneity of network of a colloidal gel induced by the shear rate was also reported (Hsiao *et al.* 2014). Recently, the impact of the shear rate on the network structure was described on a model colloidal gel developed by Colombo and Del Gado (Colombo and Del Gado 2014). These authors demonstrated, by numerical simulations, the relation between the shear rate and the balance between the formation of new bonds and the breaking of existing ones.

In this paper, we investigate the impact of an initial oscillatory shear applied during gelation on the acid-induced gelation of natural rubber latex. For this, the initial oscillatory strain, maintained constant during the gelation, was varied between 0.5 and 150 %. The impact of this initial strain amplitude on the network structure and viscoelastic properties of resulting gels was studied. In order to compare with the hardening observed at large deformation for a gel at equilibrium, the viscoelastic properties were characterized in the linear and non-linear regimes through a complete strain sweep.

5.2 Material & Methods

5.2.1 Samples

We used a commercial natural rubber latex product from Dalbe, France (ref. 4770002), which contained pre-vulcanized rubber particles of natural rubber latex stabilized with ammonia. The pH of the product was 10.5 and its dry mass around 59 %wt. The particle average diameter is centered at 1 µm as measured by static light scattering (Reis *et al.* 2015). Samples were first diluted with an equivalent amount of Tris-HCl buffer (pH 8.5, ionic strength =7 mM) and then extensively dialyzed for 7 days against the same buffer using a dialysis tube (SpectraPor, cut-off 12-14kDa, diameter 29 mm). After dialysis, the suspension volume fractions, Φ_v, ranged typically between 0.20 and 0.30. Suspensions were stored in a fridge and used within three weeks. Suspensions with $\Phi_v \leq 0.3$ were prepared by dilution of the stock solutions, while suspensions with higher volume fraction were prepared by direct dilution of the commercial suspension, without dialysis, which had no impact on the rheological properties (Reis *et al.* 2015).

5.2.2 Gelation procedure

Glucono-δ-lactone (GDL, ref G2164, Sigma-Aldrich) was used to decrease the pH, as described in chapter 3 (Reis *et al.* 2015). For $\Phi_v < 0.1$, a concentration of 1 %wt GDL as a standard condition was used to ensure a final pH close to 4 in less than 1 h. For $\Phi_v > 0.1$, the amount of GDL was increased to reproduce standard acidification conditions. The required amount of GDL was added under stirring to ensure a good dispersion of the GDL, before loading on the rheometer. Then gelation takes place *in situ* inside the rheometer and was monitored for 4 hours in an oscillatory mode.

5.2.3 Rheological characterization

The gel rheological properties were obtained using two stress-controlled rheometers: a MCR702 (Anton Paar) and an AR2000ex (TA instrument) equipped respectively with a sanded Couette (inner radius 10 mm, outer radius 11 mm and height 27 mm) and a home-made serrated Couette (inner radius 14 mm, outer radius 15 mm and height 42 with 1 mm depth and 1 mm base on each side).

During gelation, a constant oscillatory strain was applied with a frequency of 1 Hz. Amplitude was varied between 0.5 % and 150 %. Then, the viscoelastic properties of the gels were characterized using a stress sweep from 0.01 to 10 Pa at a constant frequency of 1 Hz.

5.3 Results

We previously evidenced that imposing an oscillatory strain of 0.5 % during gelation did not affect the structure of the colloidal gel, as those gels exhibited the same properties as gels formed at rest. Those conditions of preparation will therefore be considered in the following as the reference conditions. Here, we focused on the effect of stronger oscillatory strain imposed during gelation on the final gel structural properties. It is worth noting that we observed that the gelation time decreased while increasing the imposed strain. However, this point will not be discussed here as studying aggregation kinetics is not the object of this chapter. Generally speaking, we observed that imposing an oscillatory strain result in different effects depending on both the particles volume fraction and the amplitude of the oscillating strain. They are systematically investigated though a characterization of the materials through a continuous strain sweep, covering both the linear and non-linear regime of the materials.

First, for $\Phi_v < 0.25$ three regimes were observed depending on the imposed strain values: *i*) for strain < 10 %, the material properties were similar to the reference sample, *ii*) for strain between 10 and 50 %, the increase of the oscillating strain imposed during gelation result in the formation of strengthen materials, *iii*) for strain values between 50 and 80 %, the increase of the oscillatory strain is associate with the observation of an over-shoot of *G'* during gelation and *iv*) for the highest strain values > 90 %, heterogeneous gel which moduli *G'* and *G"* are equivalents were formed. In the following section, we will describe independently each regime observed for the fractal gels. This will be followed by a general discussion which will include also the specific behavior of gels formed at high volume fraction, for $\Phi_v > 0.25$.

5.3.1 Regime I: absence of effects of the oscillating strain

Regime I was observed for the initial strain values imposed during the gelation inferior to 10 %. For these strain values, the viscoelastic properties have not shown a significant variation (Figure 5.1a). This is in accordance with the limit of linearity of strain around 10 % as mentioned in previously chapters. Then, these gels already hardened during gelation were characterized by a stress sweep. Those gels show evidence of a strain hardening behavior during the oscillatory deformation (Figure 5.1b). This strain hardening behavior was also equivalent to the strain hardening observed for the reference, i.e. $\gamma = 0.5$ %. These results confirm the absence of effects of the oscillatory strain up to 10 % on the structure of the NRL gels.

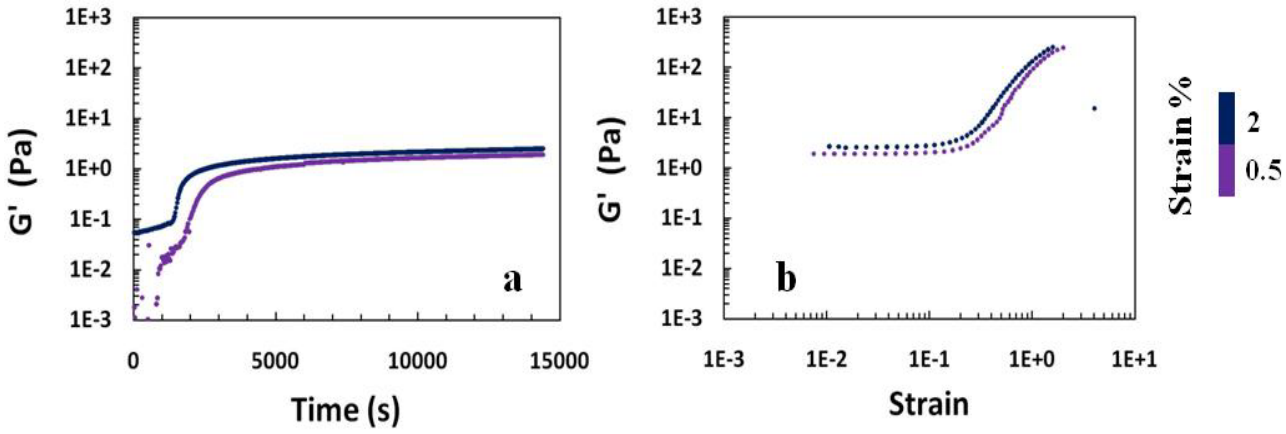

Figure 5.1: (a) *G'* as a function of time during gelation for different initial strain and (b) *G'* as a function of strain in the subsequent strain sweep for Φ_v =0.025 in regime I.

5.3.2 Regime II: hardening under shear

Regime II was obtained for gels formed under a constant oscillatory strain between 10 and 50 %. In this regime, the general evolution of *G'* and *G"* was similar to the one observed under reference conditions (0.5 % of strain). Thereby, both moduli *G'* and *G"* drastically increased during gelation and reached a plateau. However, the larger the oscillatory strain imposed during gelation, the larger the final elastic modulus will be (Figure 5.2a). For example for a volume fraction of 0.025, while the modulus for a gel obtained under reference conditions was 1.9 Pa, it reached 57 Pa under 40 % of strain (Figure 5.2a), *i.e.* a 3000 % increase. This increase suggest that a higher density of contact between strands of particles was reached (Wessel and Ball 1992).

Then, these gels already hardened during gelation were characterized by a stress sweep. Those hardened gels show evidence of a strain hardening behavior during the oscillatory deformation (Figure 5.2b). However, the relative amplitude of this behavior decrease with the initial strain applied during the gelation due to the previous increase of G'_0. Interestingly, the maximum value of elastic modulus (G'_{max}) attempted for these volume fractions was almost the same for all samples. The strain at which the onset of hardening occurs is delayed to higher values, so that during hardening the curves almost perfectly superimposed with the one of the reference.

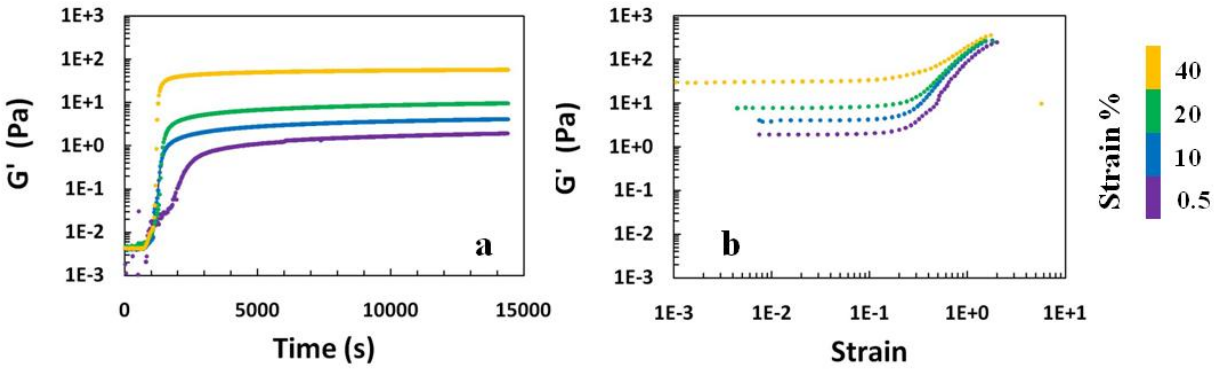

Figure 5.2: (a) *G'* as a function of time during gelation for different initial strain and (b) *G'* as a function of strain in the subsequent strain sweep for Φ_v =0.025 in regime II.

We compared the hardening obtained during the gelation at different initial strains to that obtained with a gel already formed, in reference conditions. For that, we plotted the plateau modulus G'_0 measured on samples prepared under different oscillatory strain on the strain sweep curve obtained on the reference sample (Figure 5.3). Interestingly, we observed a correlation between them: the plateau modulus obtained after a gelation conducted under a given oscillatory strain (colors circles) is similar to the value of the modulus measured on the reference sample submitted to a similar oscillatory strain (purple diamonds), and this is valid in both the linear and non-linear regimes. It suggest that the hardening obtained during the gelation occurs through the same mechanisms as the strain hardening observed for gels formed under standard conditions at high strain.

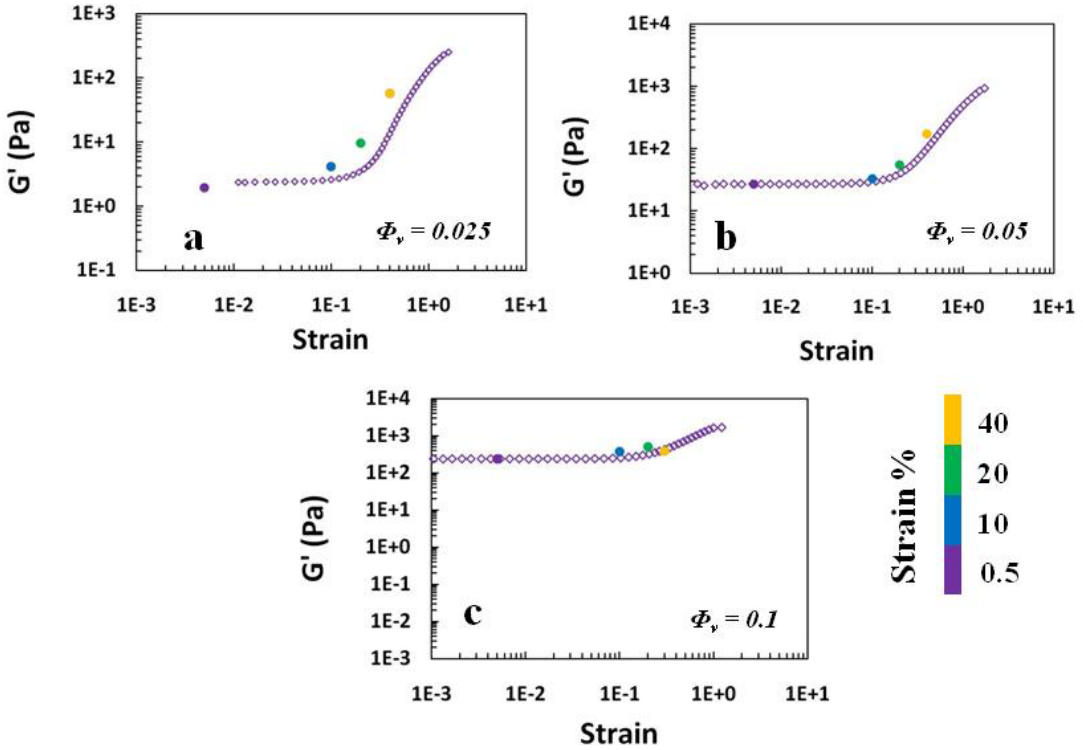

Figure 5.3: G'_0 obtained for different initial strain during the gelation superposed to the strain sweep obtained under reference conditions for different volume fractions in the regime II: (a) Φ_v =0.025, (b) Φ_v =0.05 and (c) Φ_v =0.1. The colors represent the different strain applied during the gelation: 0.5 % in purple (reference), 10 % in blue, 20 % in green and 40 % in yellow.

5.3.3 Regime III: hardening and over-shoot

Regime III was observed for initial oscillatory strain ranging from 50 % to 80 %. As observed in regime II, such materials exhibit a plateau modulus significantly higher than the one of the reference (Figure 5.4a). However, the evolution of the measured modulus during gelation is atypical: an over-shoot of *G'* was observed, which passes through a maximum G'_{max} and then decreases (Figure 5.4a). Such an evolution suggests that after a first stage in which the oscillatory strain strengthen the material, in a second stage a mechanism of fatigue, associated with a decrease of the material elastic modulus, dominates. While the time scale associated with the strengthening is very short, the fatigue occurs on longer period. We can hypothesize that if pursued on a loner time, we would observe a continuous decrease of *G'* till the fracture of the colloidal gel. For gels formed under 80 % of strain, for which the decrease of the elastic modulus is more pronounced, we observed that subsequent strain sweep do not lead anymore to strain hardening (Figure 5.4b).

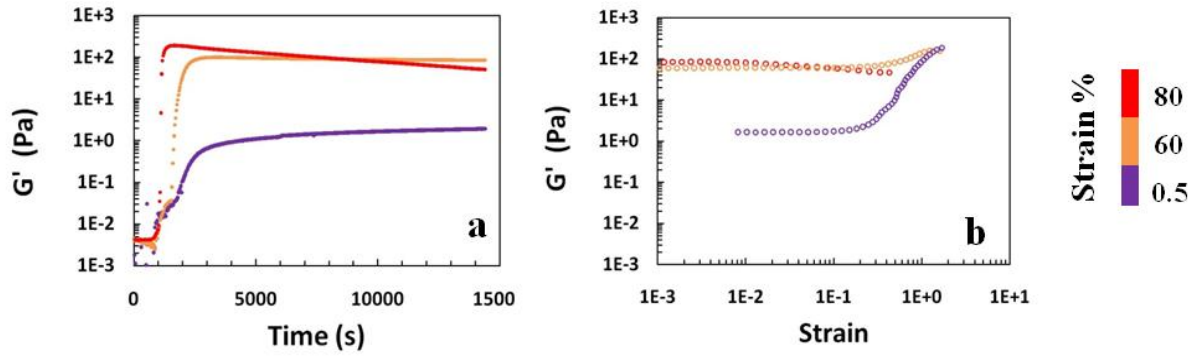

Figure 5.4: (a) *G'* as a function of time during gelation under different strain values in the regime III (red and orange) and to the reference (purple) and (b) *G'* as a function of strain for gel formed in (a) for Φ_v =0.025.

The mechanical spectrum as a function of strain of the gels formed in the regime III are plotted in Figure 5.3b. We clearly observed two different behaviors depending on the applied initial strain. For the gels formed at Φ_v =0.025 under 60 % of strain, the strain hardening was still observed (Figure 5.4b). On the other hand, gels formed under 80 % of strain did not exhibit strain hardening (Figure 5.4b). This can be an effect of the decrease of *G'* observed during the gelation (Figure 5.4a). For this strain, a progressive breaking of some connections between strand of particles could be suggested, in accordance with the model colloidal gel recently proposed (Colombo and Del Gado 2014). Indeed, for high shear rate, the connections in the network structure could be broken before the formation of new connections between strands of particles (Wessel and Ball 1992). Moreover, for gels formed at Φ_v =0.025 in the regime III had a modulus G'_0 around 100 Pa in the stress sweep step (Figure 5.4b).

We plotted the values of G'_{max} and G'_0 obtained during the gelation under different initial strains with the strain sweep curves obtained on the sample prepared under reference conditions for different volume fractions (Figure 5.5). The overshoot amplitude (G'_{max} - G'_0) increased with the value of the imposed strain (Figure 5.5). For Φ_v =0.1 the values of G'_0 obtained under a gelation with an imposed strain of 50 % and 80 % (Figure 5.5c) were close

to the values of G'_0 obtained under very small strain (reference conditions). Indeed, if the gelation was performed under a strain higher than 50 %, the overshoot was observed and the strain hardening (restructuration) was no longer observed.

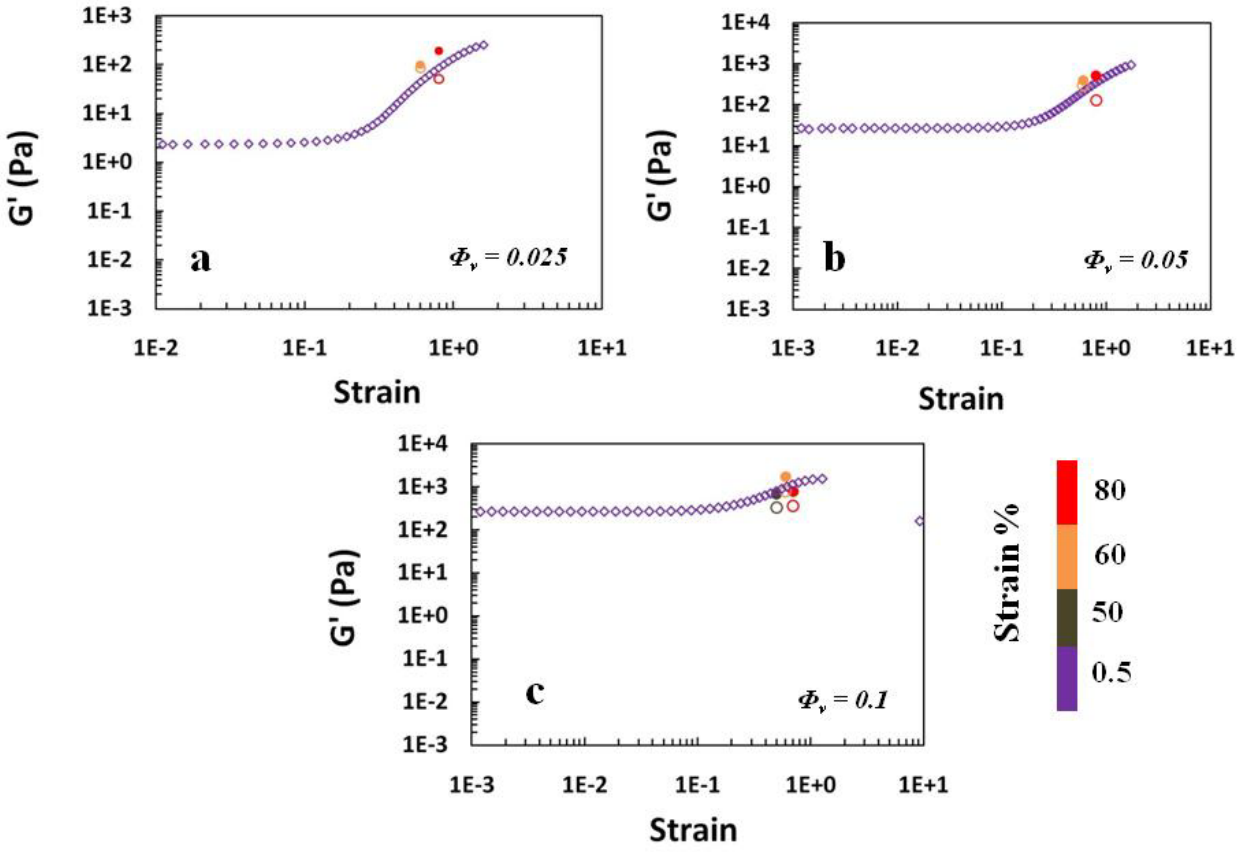

Figure 5.5: G'_0 (empty circles) and G'_{max} (filled circles) obtained during the gelation under strain, in the regime III, for three different volume fraction superposed to the strain hardening curve at reference conditions. The volume fractions are (a) Φ_v =0.025, (b) Φ_v =0.05 and (c) Φ_v =0.1. The colors represent the different strain: 0.5 % in purple (reference), 50 % in brown, 60 % in orange and 80 % in red.

5.3.4 Regime IV: heterogeneous gels

Regime IV was obtained when an initial oscillatory strain higher than 90 % was applied during the gelation step. In this regime, a modulus overshoot was observed during gelation as previously described in regime III. In terms of viscoelastic properties, *G'* and *G"* were equivalent or very closed during the gelation step and in the obtained gel (Figure 5.6a). In some cases, *G'* and *G"* obtained after 4 hours were lower than G'_0 obtained under the reference conditions (0.5 % of strain). Then, for theses gels the strain hardening was never observed during the stress sweep step. Indeed, they present a small plateau at low strain and then the elastic modulus decreases progressively with the strain due to the destructuration of the heterogeneous gel (Figure 5.6b). Interestingly, the values of *G'* at the plateau during the stress sweep are increased if compared with the values of G'_0.

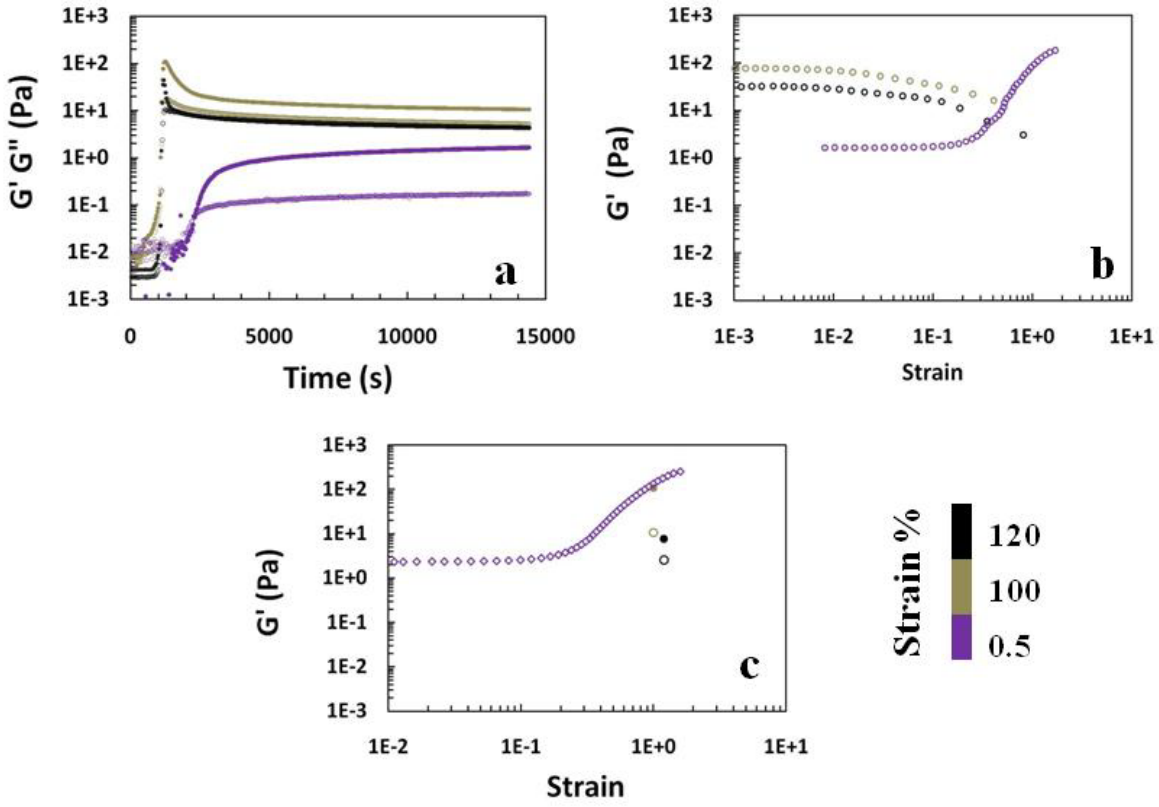

Figure 5.6: (a) *G'* (filled symbols) and *G"* (empty symbols) as a function of time during gelation for different initial strain, (b) *G'* as a function of strain in the subsequent strain sweep for Φ_v =0.025 and (c) G'_0 (empty circles) and G'_{max} (filled circles) obtained during the gelation under strain for two different volume fraction superposed to the strain hardening curve at reference conditions in the regime IV for Φ_v =0.025. The colors represent the different strain: 0.5 % in purple (reference), 100 % in bronze and 120 % in dark.

5.4 General discussion

The visual state of natural rubber latex gels prepared under shear is illustrated in Figure 5.7. For regimes I, II and III, a macroscopic homogenous gel (Figure 5.7 left) was observed for all samples. In return, the macroscopic heterogeneity of gels prepared in regime IV is very different (Figure 5.7 right). We observe the formation of large strands of gel due to the high amplitude of oscillations. We suggest that the liquid descends to the bottom of the cup when the mobile is moved up. The formation of these strands was repeatable and was obtained for all samples in the regime IV.

Figure 5.7: Pictures taken after 4 hours of gelation Φ_v =0.05. Left: homogenous gel in the regime I to III (< 90 % of strain) and right: heterogeneous gel in the regime IV (> 90 % of strain).

In conclusion, we observed four different regimes depending on the strain applied during the gelation. These four regimes were observed for volume fractions below 0.25. Figure 5.8 shows the values of G'_0 obtained during gelation under different strains and different volume fractions superposed on the strain hardening curves obtained under reference conditions (*i.e.* 0.5 % of strain). For the volume fractions 0.025, 0.05 and 0.1, the same behavior for the four regimes was observed (Figure 5.8a, b and c). The frontier between regimes II and III was observed at a critical strain around 50 %. This limit corresponds to the same critical strain observed at the onset of the progressive destructuration of the gel previously described in chapter 4. It suggests that at this critical strain the network cannot support the stress imposed and some breaking of strand of particles occurs. Moreover, if the oscillatory strain applied during gelation is above 50 %, the gels lost the ability for strain hardening during the stress (or strain) sweep.

Interestingly, for Φ_v =0.1, the overshoot was not observed for a gelation under 150 % of strain. In this case, G' was still constant despite the heterogeneous surface of the colloidal gels (Figure 5.8c). For non fractal gels, Φ_v > 0.25, the high oscillatory amplitude always contribute to a decrease of the material elastic modulus, (Figure 5.8d).

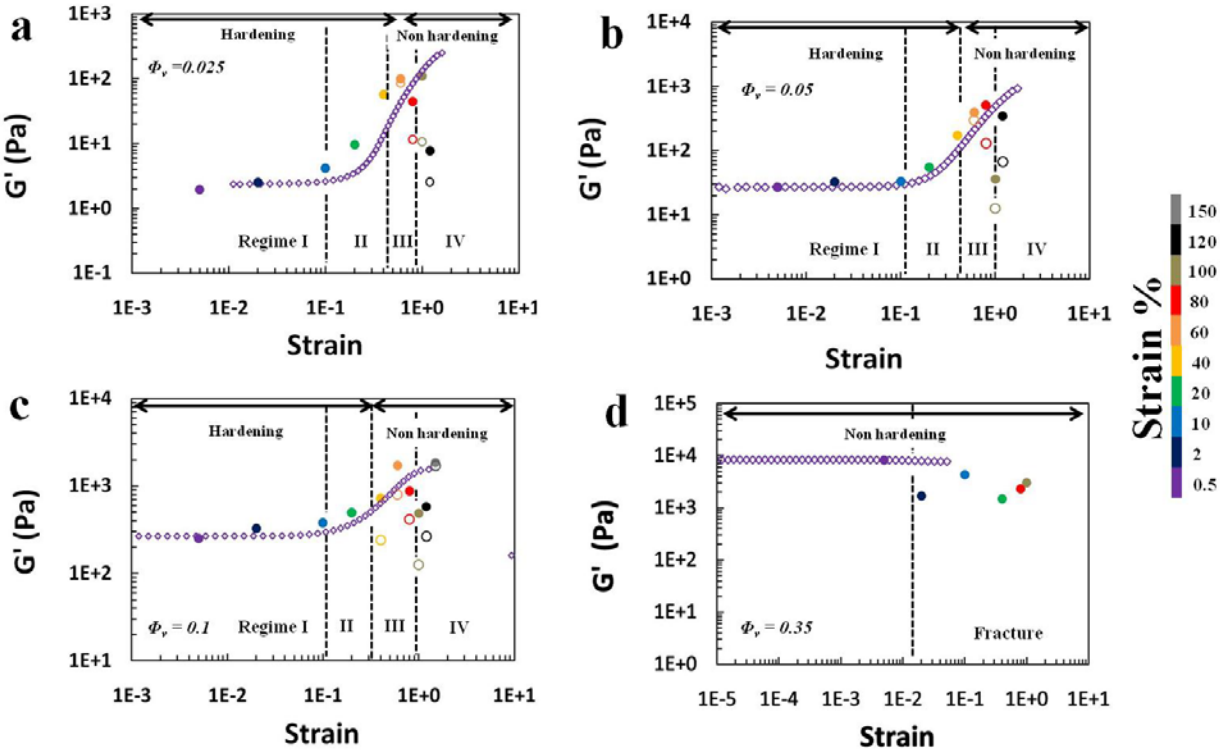

Figure 5.8: G'_0 (empty circles) and G'_{max} (filled circles) obtained during gelation under different strain (colors) values plotted on the strain hardening curve obtained at reference conditions (purple diamonds) for (a) Φ_v =0.025, (b) Φ_v =0.05, (c) Φ_v =0.1 and (d) Φ_v =0.35. In regime I: 0.5 % in purple, and 2 % in dark blue. In regime II: 10 % in blue, 20 % in green and 40 % in yellow. Regime III: 60 % in orange and 80 % in red. In regime IV: 100 % in bronze, 120 % in dark and 150 % in grey.

5.5 Conclusions

Rubber particles from natural rubber latex aggregate due to the acidification of the medium and form a fractal colloidal gel. This colloidal gel, formed by a percolated network of rubber particles, was obtained without any impact of shear forces (reference conditions). These gels exhibited an irreversible strain hardening behavior (irreversible restructuration) under large deformation due to the formation of new irreversible bonds.

In this work we studied the impact of the oscillatory strain imposed during the acid-induced gelation of the natural rubber particles. The impact of the oscillatory shear during the gelation was studied in a large range of volume fraction and oscillatory strain. For Φ_v < 0.25, four distinct regimes were obtained depending on the initial oscillatory strain. For γ < 10%, the oscillatory strain has no impact on the gel structure formation, so that we called this the Regime I. In the regime II, observed for γ < 50 %, the gels hardened during the gelation: G'_0 increases with the initial strain due to the formation of new connections between strands of particles. All samples in regime II exhibited the ability to harden under a further strain sweep. This hardening is equivalent to the strain hardening observed for gels formed in reference conditions (γ =0.5 %). In regime III, for 50 % ≤ γ ≤ 80 %, gels hardened but an over-shoot of

G' was observed in the first step of gelation. This over-shoot is associated with a break-up of some interactions resulting in a loss of the capacity to generate a strain hardening under large deformation. Finally, in regime IV, for $\gamma > 90$ %, the gels are macroscopically heterogeneous due to the very high oscillatory amplitudes. Strain hardening is no longer observed for such gels. The results suggest a capacity of hardening of natural rubber latex gel until a critical strain around 50 %. If this critical strain is reached the strain will impact the stability of the structure and the reorganization of the particles inside the gel is lost. De-structuration of some connections starts at this critical strain.

On the other hands, for $\Phi_v > 0.25$, gels begin to de-structure during the gelation for the first increase of oscillatory strain. For these gels, the maximum stress supported by the network was exceeded and the decrease of elastic modulus was observed. The breaking of the network occurs before the formation of new connections.

Acknowledgment

This work was carried out with support from CNPq – National Council for Scientific and Technological Development – Brazil and CIRAD-DRS (France).

References

Berthelot, K., *et al.* (2014). "Hevea brasiliensis REF (Hev b 1) and SRPP (Hev b 3): An overview on rubber particle proteins." Biochimie 106(0): 1-9.

Blackley, D. C. (1996). Polymer Latices: Science and Technology. London, Chapman & Hall.

Colombo, J. and E. Del Gado (2014). "Stress localization, stiffening, and yielding in a model colloidal gel." Journal of Rheology 58(5): 1089-1116.

Cornish, K., *et al.* (1999). "Rubber particles from four different species, examined by transmission electron microscopy and electron-paramagnetic-resonance spin labeling, are found to consist of a homogeneous rubber core enclosed by a contiguous, monolayer biomembrane." Planta 210(1): 85-96.

Gaboriaud, F., *et al.* (2012). "Unravelling the nanometre-scale stimuli-responsive properties of natural rubber latex particles using atomic force microscopy." Soft Matter 8(9): 2724-2729.

Hsiao, L. C., *et al.* (2014). "Role of shear-induced dynamical heterogeneity in the nonlinear rheology of colloidal gels." Soft Matter 10(46): 9254-9259.

Koumakis, N., *et al.* (2015). "Tuning colloidal gels by shear." Soft Matter 11(23): 4640-4648.

Mokhtari, T., *et al.* (2008). "The effect of shear on colloidal aggregation and gelation studied using small-angle light scattering." Journal of Colloid and Interface Science 327(1): 216-223.

Nawamawat, K., *et al.* (2011). "Surface nanostructure of Hevea brasiliensis natural rubber latex particles." Colloids and Surfaces A: Physicochemical and Engineering Aspects 390(1–3): 157-166.

Reis, G. D., *et al.* (2015). "Acid-induced aggregation and gelation of natural rubber latex particles." Colloids and Surfaces a-Physicochemical and Engineering Aspects 482: 9-17.

Swift, D. L. and S. K. Friedlander (1964). "The coagulation of hydrosols by brownian motion and laminar shear flow." Journal of Colloid Science 19(7): 621-647.

Vaysse, L., *et al.* (2012). Natural rubber in Polymer Science: A Comprehensive Reference. Amsterdam, Elsevier BV.

Vaysse, L., *et al.* (2009). Natural Rubber in Sustainable Solutions for Modern Economies,Coord. Dr Rainer Höfer, The Royal Society of Chemistry. Cambridge, UK: 339-367.

Vermant, J. and M. J. Solomon (2005). "Flow-induced structure in colloidal suspensions." Journal of Physics-Condensed Matter 17(4): R187-R216.

Wang, L., *et al.* (2005). "CFD simulation of aggregation and breakage processes in laminar Taylor–Couette flow." Journal of Colloid and Interface Science 282(2): 380-396.

Wessel, R. and R. C. Ball (1992). "Fractal aggregates abd gels in shear-flow." Physical Review A 46(6): R3008-R3011.

Chapter 6

Discussion & Conclusions

The focus of this PhD thesis was to study the structuration of the natural rubber latex into natural rubber during the first step (acid-coagulation) of the transformation. In order to investigate this structuration, the aggregation and gelation of natural rubber latex particles was induced following *in situ* acidification. The viscoelastic properties of the resulting colloidal gels were characterized by rheological measurements in the linear and non-linear regimes. During this thesis we used a soft matter physics approach, and colloidal gel models to analyze the structuration processes during acidification and/or under shear. However, it has to be keep in mind that aggregates formed by rubber particles have a size larger than 1 µm, and therefore at the limit between colloidal and granular domains.

In this chapter, a general discussion of the results and a comparison with those reported in the literature with other types of colloidal gels is done. Moreover, perspectives on this work are also proposed and discussed

Aggregation and gelation of NRL

In chapter 3, we reported the study of the acid-induced aggregation of the natural rubber particles. We demonstrated a pH dependence of the onset of aggregation in a large range of volume fraction ($5x10^{-4}$ to $5x10^{-1}$). A state diagram in the pH / volume fraction space was established over 5 weeks. Three different states were observed: *i*) stable suspension, *ii*) macroscopic phase separation between a suspension and a gel and *iii*) a gel. The competition between gravitational forces and Brownian motion are visualized for intermediary values of pH and volume fraction (Figure 6.1, between black and blue curves). It is the area where the first aggregates formed tend to cream because they become sensitive to the gravity due to their large sizes (> 3µm). A phase separation takes place, with a gel that is formed on the top of the tube, due to the increase of the local volume fraction, and a stable suspension at the bottom of the tube. The volume fraction-pH zone of this macroscopic phase separation increases with time of storage of the tube after acidification (Figure 6.1). For 4 hours of acidification, the aggregation (dark line) and gelation (red line) limits were determined experimentally using a combination of three different methods based on light scattering: turbidity, DWS and SLS. Interestingly, the critical pH of aggregation or gelation depended on the volume fraction. Then, in this PhD thesis, we focused on the rheological characterization of the gels formed at pH 4.

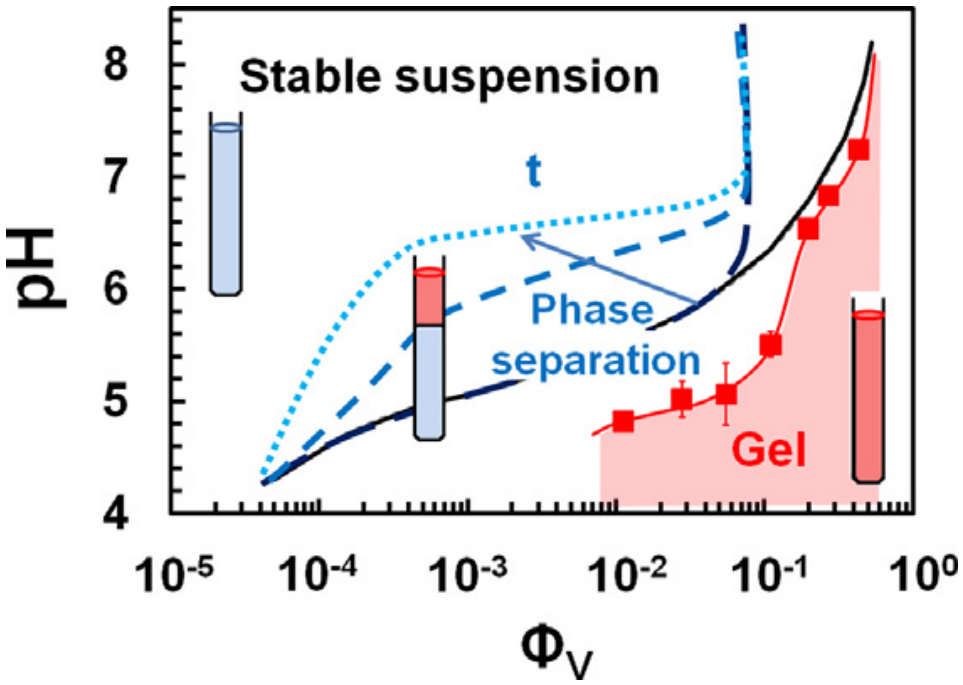

Figure 6.1: State diagram of natural rubber latex in pH- Φ_v space. Red square: pH at gelation obtained by rheology. Black line: onset of aggregation observed after 4 hours. Dashed and dotted blues lines represent the limits of the macroscopic phase separation between 1 and 5 weeks.

The viscoelastic properties of colloidal gels formed at pH 4, after 4 hours, were characterized by rheology in the linear regime. A typical fractal scaling law between the elastic modulus *G'* and the volume fraction was established, *i.e.* $G'_0 \sim \Phi_v^{3.35}$, for a range of volume fractions between $1x10^{-2}$ and $5x10^{-1}$. Moreover, the elastic modulus *G'* of these gels was independent of the kinetics of acidification, the temperature and of the measurement frequency used. This suggests that the energy associated with each bond between particles (or between clusters), is much higher than k_bT, in agreement with the fact that once formed, gels are not dispersible anymore. At equilibrium, these fractal colloidal gels have a network structure formed in the DLCA regime, according to the colloidal fractal model. An open question in this chapter 3 is about the evolution of the gelation time with the volume fraction. Unexpectedly for a colloidal gel, a two step evolution was observed from rheological measurements, instead of a decreasing scaling law evolution, which is characteristic of a pure DLCA mechanism. Later, in order to check this unusual two-step evolution of gelation time with the volume fraction, observed by rheology, we determined the gelation times by other methods. We used two light scattering equipments, namely Turbiscan Tower (Formulaction, France) and Rheolaser® Master (Formulaction, France) (annex I). The gelation times obtained with both techniques were equivalents to those obtained by rheology (Figure 6.2).

The reason of this two-step evolution is still unclear We can assume an impact of gravitational and/or hydrodynamics forces. This behavior could also be due to the nature of the membrane surrounding the rubber particles (due to changes in charge distribution due to the evolution of the pH). Indeed, one or more forces can affect the aggregation and decrease the gelation time.

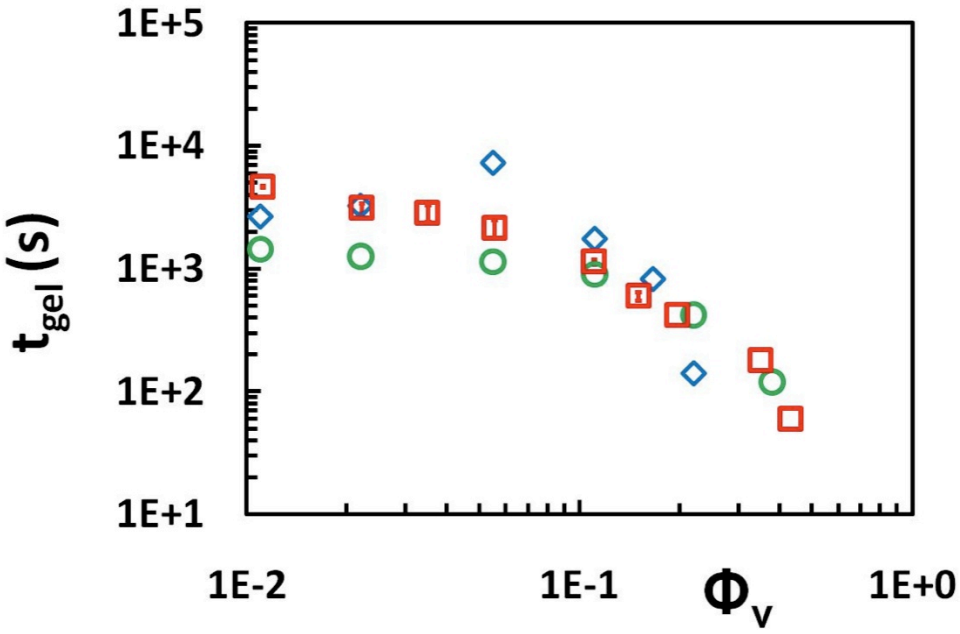

Figure 6.2: Evolution of the experimental gelation time (t_{gel}) as a function of volume fraction. Red squares: obtained by rheology, green circles: obtained by Turbiscan and blues diamonds: obtained by Rheolaser® Master.

Universality of colloidal gels behavior in the linear regime

To compare the viscoelastic behavior of natural rubber latex gels to other ones in the linear regime, we plotted the plateau modulus G'_0, multiplied by their initial particle size (a), dependence to the volume fraction obtained for different colloidal gel systems from literature with our data. We multiplied the plateau modulus to the initial particle size to eliminate the size effect. Our data exhibited a scaling behavior of the elastic modulus G'_0 with a power law exponent of the same order as other colloidal gels as illustrated in Figure 6.3 (de Rooij *et al.* 1994; Yanez *et al.* 1996; Gisler *et al.* 1999; Yanez *et al.* 1999; Pouzot *et al.* 2006; Romer *et al.* 2014). Moreover, the slope of the curve represents the fractal structure and the difference of the absolute values of $G'_0\ a$ is proportional to the bond rigidity (k_0) according the fractal relation $G'_0 = k_0/a\ \Phi_v^A$ (Pantina and Furst 2005). Despite the fact that these colloidal gels present similar global properties, they exhibited significant differences in terms of elastic modulus to a given volume fraction. The differences were explained by differences in the interaction potential between particles composing these different networks. These interactions will vary with the physic-chemical conditions. As described in chapter 4, we did not observe an impact on the viscoelastic properties with the range of temperature (4 to 40° C) and pH (3-5.5).

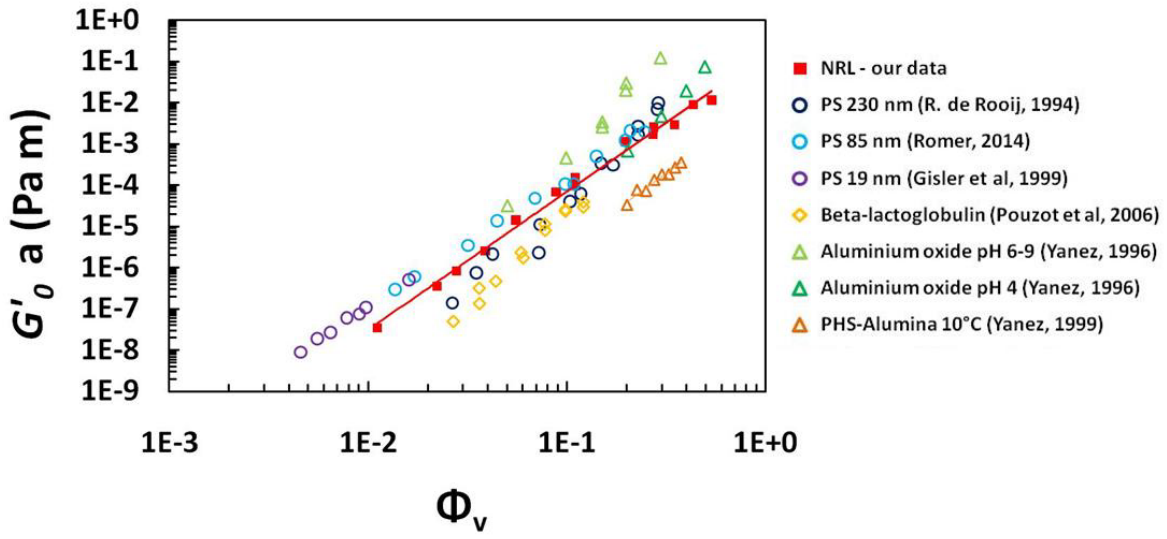

Figure 6.3: $G'_0\ a$ as a function of Φ_v obtained from our data (red squares) and some data estimated from literature: purples circles (Gisler *et al.* 1999), light blue circles (Romer *et al.* 2014), dark blue circles (de Rooij *et al.* 1994), yellow diamond (Pouzot *et al.* 2006), green and light green triangles (Yanez *et al.* 1996) and orange triangles (Yanez *et al.* 1999).

Structuration and destructuration of the gel under stress

In chapter 4, we focused on the characterization of the viscoelastic properties of gels formed at pH 4. The scaling law $G'_0 \sim \Phi_v^{3.35}$ demonstrated in the chapter 3 was confirmed in chapter 4 using different Couette geometries with different surface: sanded, serrated and plastic. The absence of wall-slip during the measurements was thus confirmed. In the non-linear regime, two different behaviors were observed depending on the volume fraction. For fractal gels ($0.01 < \Phi_v < 0.25$), a strain hardening behavior was observed, *i.e.* an increase of G' and G'' with the increase of the stress (or strain). This strain hardening occurred at a strain γ ~10 % and was followed by a destructuration and/or a fracture (γ_f ~10 0%) of gels after passing through maxima viscoelastic moduli (G'_{max}, G''_{max}). For these fractal gels, a scaling behavior between the G'_{max} and the volume fraction, *i.e.* $G'_{max} \sim \Phi_v^{1.67}$ was demonstrated in chapter 4. For non fractal gels, obtained at high volume fraction (> 0.25), the fracture was observed at smaller strain (γ_f ~ 10%) without any strain hardening.

The strain hardening behavior was in good agreement with the fractal colloidal model proposed by Gisler *et al.* (Gisler *et al.* 1999). The origin of this behavior could be attributed to the bending of particles strand. Indeed, the shear induced the formation of new connections between some strands and therefore an increase of the elasticity (Wessel and Ball 1992). Then, for a constant imposed oscillatory strain during the gelation, a critical destructuration strain was observed around 50 %. When this imposed strain was higher than 50 %, a progressive destructuration of the network was observed till the fracture. Interestingly, this value of 50 % was linked to: *i)* the onset of the increase of the fractal backbone dimension (D_b), *ii)* the apparition of troughs during the increase/decrease of stress (both reported in chapter 4) and *iii)* the limit of the hardening obtained during gelation under shear (reported in chapter 5). Recently, the competition between formation and breaking of bonds under shear was recently proposed by Colombo and Del Gado (Colombo and Del Gado 2014). These authors proposed a model of colloidal gel where the stress is heterogeneously located on certain zones of the network. In these zones where the elasticity is higher, the first breaking of connections occurs.

A proposition of a scheme in strain-Φ_v space is presented in Figure 6.4. This scheme is based on the results described in this thesis and hypotheses proposed in literature. This model assumes that strain hardening is due to the integration in the network of particles that were originally not elastically active, *i.e.* dangling chains for examples. Under deformations, such particles might come into contact with others one, with which they will established new irreversible bonds, and therefore contribute to the overall elasticity. For the fractal gels ($\Phi_v <$ 0.25), the beginning of strain hardening, *i.e.* formation of new bonds, was observed around 10 % of strain. Despite the fact that the fracture occurs around 100 % of strain, some connections begin to break when a critical strain of ~50 % was reached. Above this critical strain, both formation and breaking of connections occur up to the fracture when the strain was continuously increased. On the other hands, the non fractal gels ($\Phi_v >$ 0.25) fracture at smaller strain, < 10 %, due to the breaking of connections.

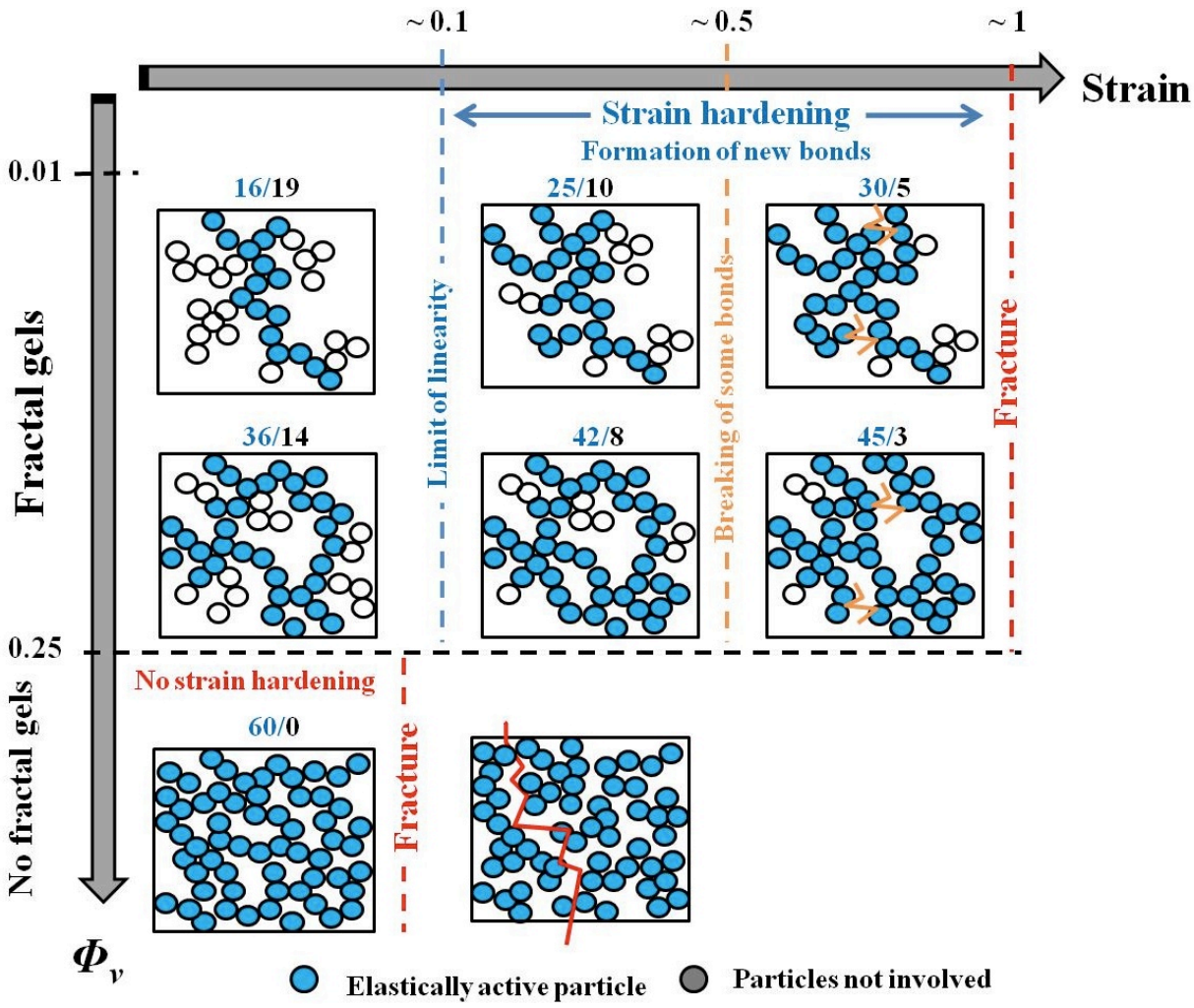

Figure 6.4: Schema of the structure of the NRL gel in the strain-Φ_v space. The limit of fractality (dark dashed line) was observed at Φ_v =0.25, the onset of strain hardening (blue dashed line) at $\gamma \sim 10$ %, the critical strain (orange dashed line) at $\gamma \sim 50$ % and the fractures (red dashed lines) at $\gamma \sim 100$ % for the fractal gels and at $\gamma < 10$ % for the non fractal gels.

The question of the homogeneity of restructuration and destructuration during the deformation was explored using the rheo-ultrasound analysis. In fact, the linear profile of the velocity displacements inside the gel, for all strains applied in a large range of volume fraction, confirms this homogeneity. However, it is important to note that this technique allows to observe the displacements fields inside the gel at a scale around 100-200 µm. So, the structuration and destructuration can be homogenous at this scale but may be heterogeneous at smaller scales. Indeed, these results do not exclude the local heterogeneity proposed by Colombo and Del Gado (Colombo and Del Gado 2014).

In the chapter 5, we studied the impact of the oscillatory strain imposed during the acid-induced gelation of the natural rubber latex on the network structure. Shear forces applied during the gelation induced a reorganization of the network structure of the natural rubber latex gels. For fractal gels with a volume fraction below 0.25, four regimes were observed depending on the initial strain imposed during the gelation. In the regime I, for initial strain

below 10 % imposed during gelation, the viscoelastic properties still unchangeable as expected. In the regime II, the natural rubber latex gels can be hardened during the gelation, with G'_0 that increases with the strain imposed. Interestingly, the elastic properties obtained during the gelation were equivalent to those obtained for a reference gel during a continuous progressive increase of oscillatory strain. In the regimes III and IV, these gels exhibit an over-shoot, *G'* passed through a maximum, and then *G'* decreased continuously during the gelation. Despite this decrease, for a given applied strain, the moduli *G'* remained almost equivalent to those observed for a reference gel (*i.e.* γ =0.5 % imposed during the gelation). These results suggest that, whatever the value of strain applied during the gelation, at the end, when reaching the same strain (after strain sweep), the network structure, on a macroscopic point of view, is quite the same.

For these gels (Φ_v < 0.25) formed under a strain above 50 %, the capacity to exhibit the strain hardening during the stress sweep was lost. Moreover, gels formed in the regime III at very high strain (> 90 %) were macroscopically heterogeneous as visually observed. In the chapter 5, we determined the capacity to control the hardening during the formation of the gel and after the formation of the network by controlling the oscillatory strain applied during the gelation. Interestingly, the strain limit between the regimes II and III corresponded to the same critical strain (~50 %) observed in chapter 4. Above this strain value, the progressive destructuration of the network occurs due to the breaking of some connections as described previously.

Irreversibility of the structuration of NRL gels

Unlike other colloidal gels, the irreversibility of the strain hardening was demonstrated for our system when the stress was increased and decreased several times at large deformation. The strain hardening behavior, observed for our NRL gels, was independent of temperature (4 - 40° C), kinetics of acidification (final pH 3-5) and frequency of measurements (0.01 - 10 Hz). Interestingly, an increase of the fractal backbone dimension was observed as a function of the maximum strain imposed during the irreversible strain hardening. This evolution can be explained by the formation of new irreversible particle-particle interactions due to the restructuration of the network under shear as described previously.

These irreversible interactions between particles were observed since the aggregation process. As described in chapter 3, if particles aggregate the redispersion was no longer possible even at very high pH (~10-12). The irreversibility of these interactions could be attributed to the unique nature of rubber particles. Indeed, the complex membrane surrounding rubber particles exhibited a special complex composition. Though the nature of this membrane is still unclear, it is known about the presence of mainly proteins and lipids. In the case of ammoniated latex, some lipids are hydrolysis in fatty acid soaps (Ho 1989; Blackley 1996; Singh *et al.* 2014). This membrane exhibited a zone of ion permeability (Ho *et al.* 1996; Rochette *et al.* 2013). Recently advances in the studies of the presence and role of REF and SRPP proteins on the membrane could be help to understand these interactions (Hillebrand *et al.* 2012; Berthelot *et al.* 2014). The presence of proteins linked to the polyisoprene chains are related to the original

properties of the raw natural rubber (Tanaka 2001; Tanaka and Tarachiwin 2009; Vaysse *et al.* 2012).

Another possibility is the impact of the polyisoprene chains inside the rubber particles. Today the role of the polyisoprene chains in the adhesion between rubber particles is still unclear but their participation on the irreversibility behavior cannot be excluded. However, despite the high hydrophobic behavior of these polyisoprene chains, the interpenetration betweens the chains could take place at high deformation amplitude.

Impact of the composition of the membrane on the rheological properties

In the line with the last point discussed, an open question is about the impact of the structure composition of the particle membrane on the rheological properties of NRL gels in the non linear regime.

For this, we analyzed the viscoelastic properties of NRL gels obtained from a field natural rubber latex from Thailand (annex II). The composition of the membrane and the state of the polyisoprene chains inside the particles are supposed to be different of those of the NRL used during this thesis. However, the viscoelastic properties in the linear regime of the gels made with fresh field latex were equivalent to those observed from gels made with the commercial latex used in this thesis (Figure 6.5). In the linear regime, the viscoelastic properties of fresh field NRL gels can be described by the scaling law's based on the fractal theory. The G' obtained superposed well on the $G' \sim \Phi_v^{3.35}$ described in chapter 4 (Figure 6.5). However, the strain hardening ($G'_{max} - G'_0$) of this fresh NRL gels was much lower than the one obtained with the commercial latex used during this thesis (Figure 6.5). This suggests that the nature of the connections between particles plays an important role on the properties in the non linear regime. But, the values of the strain and stress at the fracture (γ_f, σ_f) were equivalent to those observed for the commercial NRL gels (annex II). This suggests a different reorganization under shear but the same maximal deformation supported by the network. So, based on the good agreement with the colloidal gel models and from both latex, we suggest that particle-particle interactions are truly at the origin of gel viscoelastic properties.

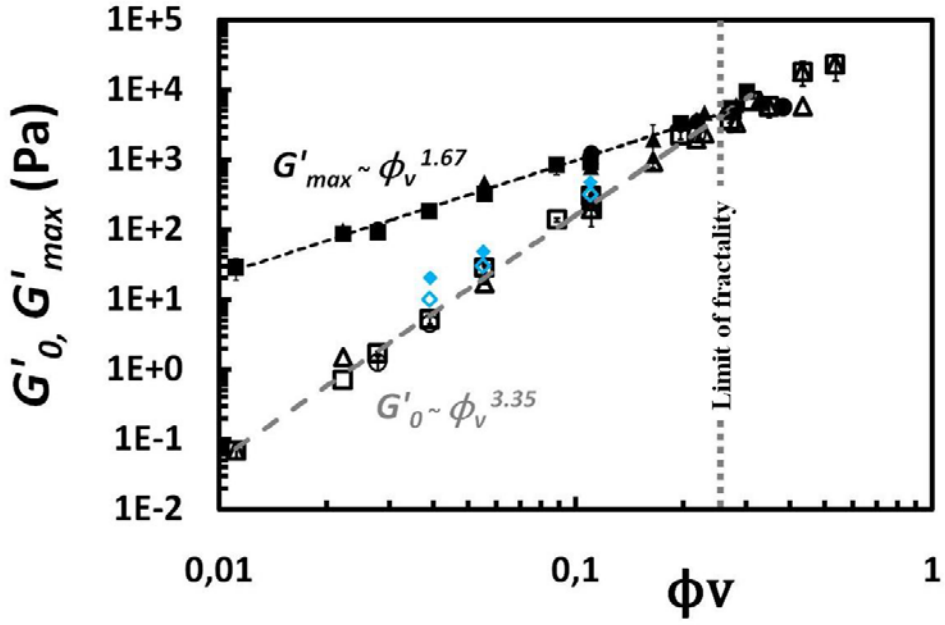

Figure 6.5: G'_{max} (filled symbols) and G'_0 (open symbols) as function of volume fraction for a fresh ammoniac natural rubber latex from Thailand (blues diamonds). The modulis obtained for the commercial natural rubber latex, illustrated in Figure 4.2 (chapter 4), are reproduced by the dark symbols for purposes of comparison. The grey dashed line represents the limit of fractality.

Prospects

In order to understand the structuration of the rubber particles network, different studied could be conducted in the future such as*: i*) the use of a fresh natural rubber latex, *ii*) the utilization of imagery methods coupled to the classic rheometry and *iii*) the studied of the second step of transformation which the colloidal gel collapse into a rubber network.

The utilization of fields natural rubber latex could be interest to compare with the results obtained during this studied. Indeed, the natural rubber latex used during this thesis was a pre-vulcanized natural rubber latex. The pre-vulcanization is supposed to cause sulfur crosslinks between the polyisoprene chains inside the particle (Ho 1989; Blackley 1996). It cannot be rule out also changes in the nature of membrane because of pre-vulcanization. Moreover, the irreversibility of the viscoelastic properties in the non linear regime for these fields NRL gels needs to be studied.

To study the structure of the network formed for the NRL gels, confocal microscopy can be used. For example, the fractal dimension of the network can be estimated by imagery (Hagiwara *et al.* 1997; Thill *et al.* 1998). We started to observe the size and the shape of rubber particles and the formation of the natural rubber latex gels (annex III). For this, we used a Nile Red fluorescent dye to tag the hydrophobic molecules, mostly the lipids, present in the membrane of rubber particles. Figure 6.6 shows the micrographs of the natural rubber latex before and after acidification. The spherical shape, particles size around 1 µm and

aggregates formed by these particles were confirmed by the confocal images. The observation of the formation of the gel of natural rubber latex and their structures need to be completed. A combination of other fluorescent dye and Nile red can be used to identify the proteins and lipids on the membrane. Recently, a confocal rheology method was described in literature (Boitte *et al.* 2013; Dutta *et al.* 2013; Koumakis *et al.* 2015). The use of this method could be a good way to observe the structuration and destructuration during the strain hardening to elucidate the mechanism involved.

Another prospect to study the relation between the acid-induced gelation and the properties of the natural rubber is about the collapse of the colloidal gel (particles network) into a rubber network (polyisoprene "fibers"). Today, little is known about this collapse: at what moment the rubber particles disappear? Are the long rubber chains formed only after the collapse? Or, are them already formed inside the particles? The studied of this collapse by the combination of the imagery and rheological measurements seem to be a good choice to understand this transformation. Indeed, we observed a collapse of the natural rubber latex gel by confocal microscopy if the microscopy slide is pressed with a finger (Figure 6.7). Solution was liberated after the compression and a network was formed. However, the studies about this collapse need to be performed.

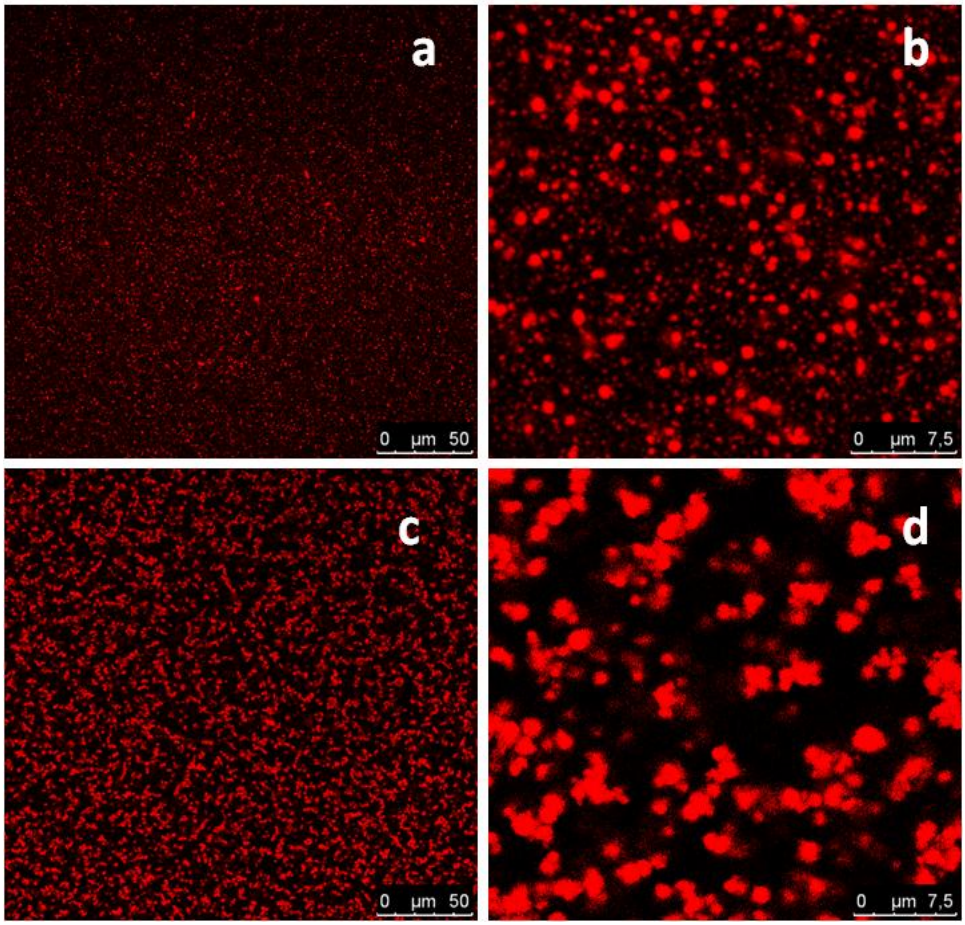

Figure 6.6: Confocal microscopy images of natural rubber latex tagged with the Nile Red at Φ_v= 0.05. In (a) and (b) images of particles taken before gelation and in (c) and (d) images of aggregates taken after the addition of 1 % of GDL. The square scales are 246x246 µm in (a) and (c) and 34x34 µm in (b) and (d).

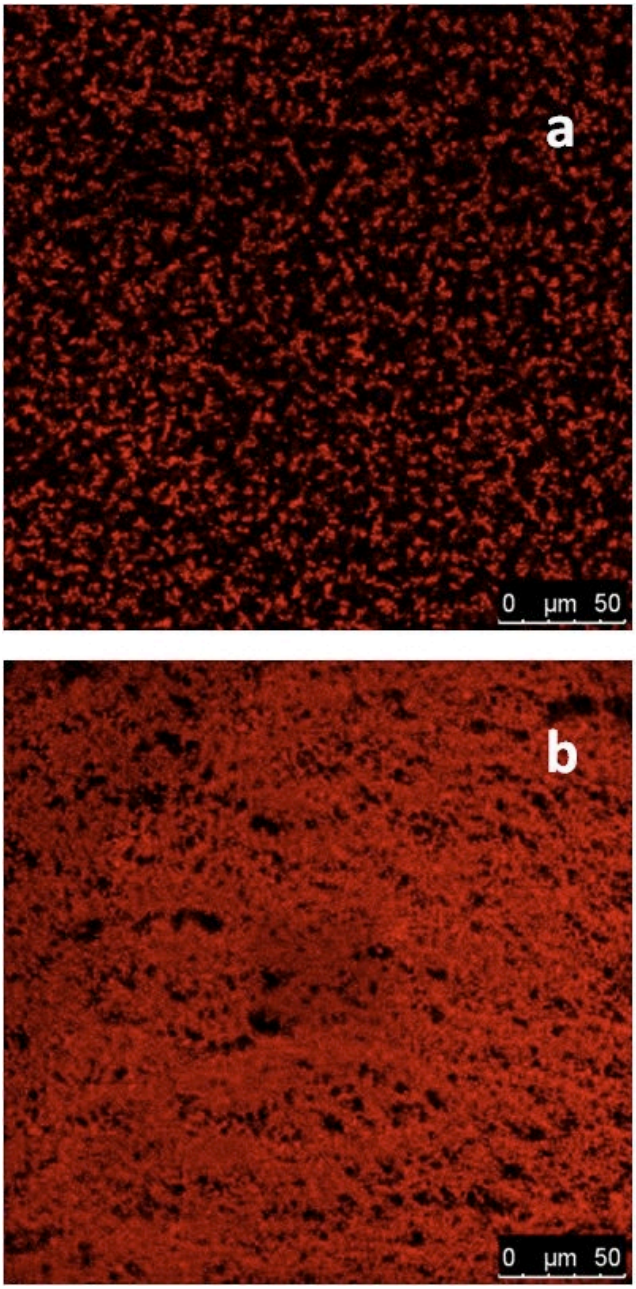

Figure 6.7: Confocal microscopy images for a gel at Φ_v =0.05 acidified with 1 % of GDL. Images of natural rubber gel (a) and a collapsed gel obtained after compression using a finger (b). The square scale is 246.03x246.03 µm.

References

Berthelot, K., *et al.* (2014). "Rubber particle proteins, HbREF and HbSRPP, show different interactions with model membranes." Biochimica et Biophysica Acta (BBA) - Biomembranes **1838**(1, Part B): 287-299.

Blackley, D. C. (1996). Polymer Latices: Science and Technology. London, Chapman & Hall.

Boitte, J.-B., *et al.* (2013). "A novel rheo-optical device for studying complex fluids in a double shear plate geometry." Review of Scientific Instruments **84**(1): 013709.

Colombo, J. and E. Del Gado (2014). "Stress localization, stiffening, and yielding in a model colloidal gel." Journal of Rheology **58**(5): 1089-1116.

de la Fuente, M. A., *et al.* (2002). "Recent advances in the characterisation of heat-induced aggregates and intermediates of whey proteins." Trends in Food Science & Technology **13**(8): 262-274.

de Rooij, R., *et al.* (1994). "Elasticity of weakly aggregating polystyrene latex dispersions." Physical Review E **49**(4): 3038-3049.

Dutta, S. K., *et al.* (2013). "Development of a confocal rheometer for soft and biological materials." Review of Scientific Instruments **84**(6): 063702.

Gisler, T., *et al.* (1999). "Strain Hardening of Fractal Colloidal Gels." Physical Review Letters **82**(5): 1064-1067.

Hagiwara, T., *et al.* (1997). "Fractal Analysis of the Elasticity of BSA and β-Lactoglobulin Gels." Journal of Agricultural and Food Chemistry **45**(10): 3807-3812.

Hillebrand, A., *et al.* (2012). "Down-Regulation of Small Rubber Particle Protein Expression Affects Integrity of Rubber Particles and Rubber Content in Taraxacum brevicorniculatum." Plos One **7**(7).

Ho, C. C. (1989). "Changes in electrokinetic properties of natural rubber latex after surface chemical modifications." Colloid and Polymer Science **267**(7): 643-647.

Ho, C. C., *et al.* (1996). "Surface Structure of Natural Rubber Latex Particles from Electrophoretic Mobility Data." Journal of Colloid and Interface Science **178**(2): 442-445.

Koumakis, N., *et al.* (2015). "Tuning colloidal gels by shear." Soft Matter **11**(23): 4640-4648.

Larsen, T. H. and E. M. Furst (2008). "Microrheology of the liquid-solid transition during gelation." Physical Review Letters **100**(14).

Nicolai, T. and D. Durand (2007). "Protein aggregation and gel formation studied with scattering methods and computer simulations." Current Opinion in Colloid & Interface Science **12**(1): 23-28.

Pouzot, M., *et al.* (2006). "Strain hardening and fracture of heat-set fractal globular protein gels." Journal of Colloid and Interface Science **293**(2): 376-383.

Rochette, C. N., *et al.* (2013). "Shell Structure of Natural Rubber Particles: Evidence of Chemical Stratification by Electrokinetics and Cryo-TEM." Langmuir **29**(47): 14655-14665.

Romer, S., *et al.* (2014). "Rheology and internal dynamics of colloidal gels from the dilute to the concentrated regime." EPL (Europhysics Letters) **108**(4): 48006.

Singh, M., *et al.* (2014). "Influence of hydrophobically modified inulin (INUTEC NRA) on the stability of vulcanized natural rubber latex." Colloids and Surfaces A: Physicochemical and Engineering Aspects **451**(0): 90-100.

Tanaka, Y. (2001). "Structural characterization of natural polyisoprenes: Solve the mystery of natural rubber based on structural study." Rubber Chemistry and Technology **74**(3): 355-375.

Tanaka, Y. and L. Tarachiwin (2009). "Recent Advances in Structural Characterization of Natural Rubber." Rubber Chemistry and Technology **82**(3): 283-314.

Thill, A., *et al.* (1998). "Determination of Structure of Aggregates by Confocal Scanning Laser Microscopy." Journal of Colloid and Interface Science **204**(2): 357-362.

Vaysse, L., *et al.* (2012). Natural rubber in Polymer Science: A Comprehensive Reference. Amsterdam, Elsevier BV.

Wessel, R. and R. C. Ball (1992). "Fractal aggregates abd gels in shear-flow." Physical Review A **46**(6): R3008-R3011.

Winter, H. H. a. F. C. (1986). "Analysis of Linear Viscoelasticity of a Crosslinking Polymer at the Gel Point." J Rheology **30**: 367.

Yanez, J. A., *et al.* (1999). "Viscoelastic Properties of Particle Gels." Journal of Colloid and Interface Science **209**(1): 162-172.

Yanez, J. A., *et al.* (1996). "Shear Modulus and Yield Stress Measurements of Attractive Alumina Particle Networks in Aqueous Slurries." Journal of the American Ceramic Society **79**(11): 2917-2917.

Annexes

Annex I

Determination of the gelation time

By rheology

The gelation time was determined at the cross-over between viscous *G"* and elastic *G'* moduli during acidification. Indeed, for the liquids the *G"* are larger than *G'* and the latter becomes larger than the former after the gelation point. In some measurements of the gelation of the natural rubber latex, the G' was initially larger than *G"*. This can be explained by the low viscosity of the samples which is very closed to the viscosity of the water. Indeed, none of the rheometers used during this work were sensitive enough to detect the first step of aggregation of the natural rubber latex. To verify this, we performed a frequency sweep of the natural rubber latex at different strain which confirmed the lack of sensitivity. In cases where the cross-over between *G'* and *G"* was not observed, the gelation time was determined by the maximum of the first derivate of *G'* as a function of time. However, the determined gelation time is equivalent in both cases (Figure AI.1).

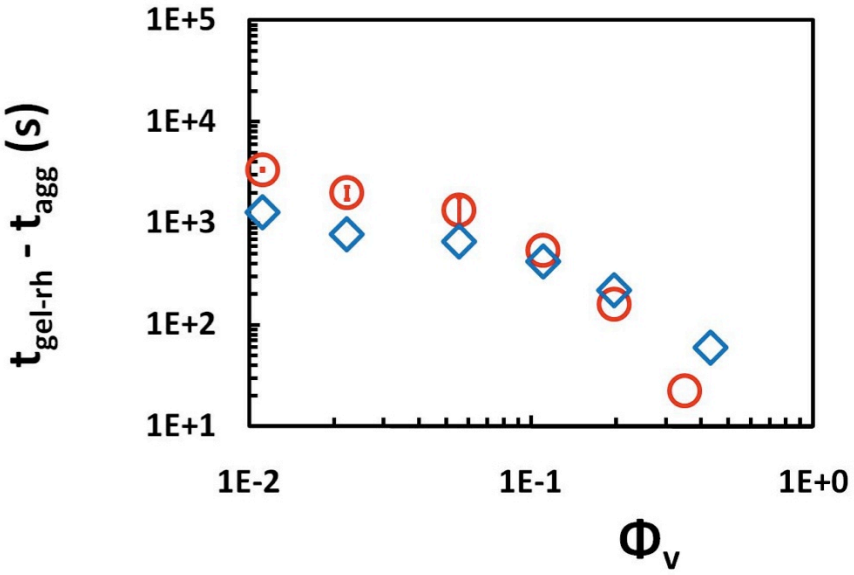

Figure AI.1: Gelation time determined by rheology using two different methods. In red at cross-over between *G'* and *G"* and in blue at maximum of the dG'/dt.

By light scattering

To compare to the gelation time determined by rheology, we used two techniques based on light scattering: the Turbiscan tower and the Rheolaser® Master techniques (Formulaction, France). The Turbiscan Tower is based on the multiple light scattering in both transmission and backscattering mode. Samples were scanned in all height by a laser and two different

detectors are used: a backscattering for opaque suspensions and a transmission detector for non opaque suspensions. To determine the gelation time we used the Turbiscan stability index (TSI). The TSI compare the evolution of the scans function of time (Figure AI.2). The Rheolaser® Master is based on multi-speckle DWS. The gelation time was determined based on the Time-Cure superposition (TCS) (Winter 1986; Larsen and Furst 2008)*. Figure AI.3 shows an example of the raw data where the gelation time was determined on the deep of the curve.

** Winter, H. H. a. F. C. (1986). "Analysis of Linear Viscoelasticity of a Crosslinking Polymer at the Gel Point." J Rheology **30**: 367.*

** Larsen, T. H. and E. M. Furst (2008). "Microrheology of the liquid-solid transition during gelation." Physical Review Letters **100**(14).*

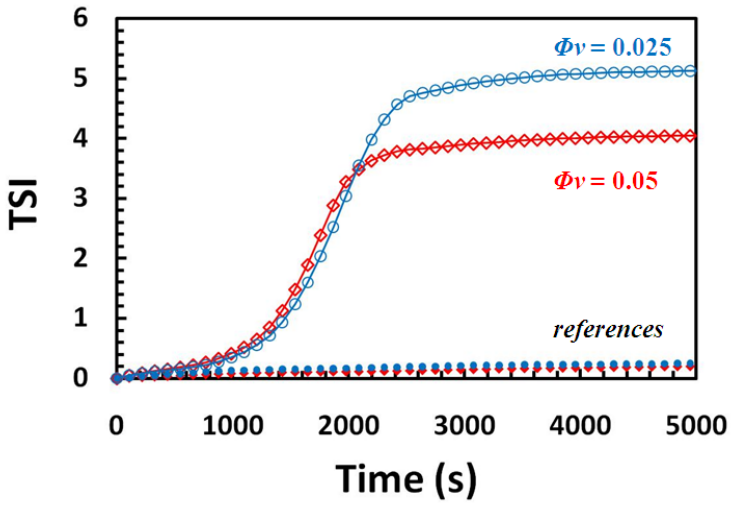

Figure AI.2: Example of the determination of gelation using the TSI parameter. Empty symbols: gels using 1 % of GDL and filled symbols: references. In bleu: Φ_v =0.025 and in red Φ_v =0.05.

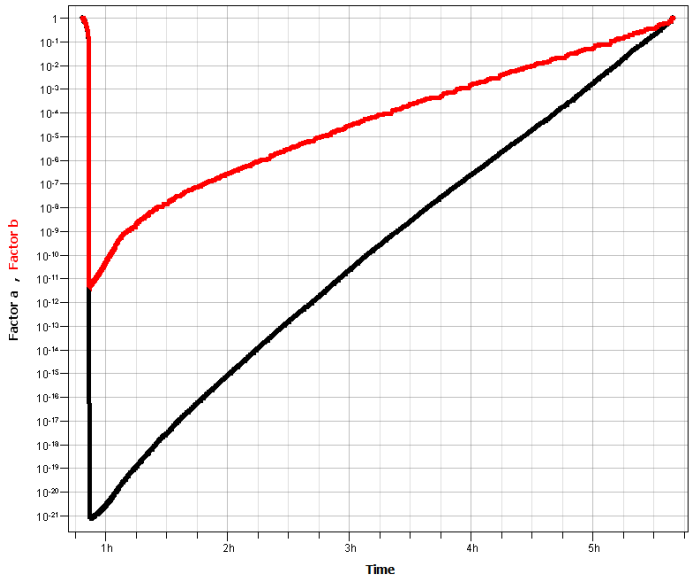

Figure AI.3: Example of raw data of Rheolaser® Master during the gelation of natural rubber latex. Φ_v =0.025 using 1 % of GDL.

Annex II

Rheology of a fresh natural rubber latex from Thailand

We used a fresh natural rubber latex (clone RRIM600) from Thailand. It was stabilized with ammonia (0.6%v/v) at pH 10.5. The dry mass is around 30 %wt. The size distribution is centered around 1 µm using SLS. As described in chapter 2:

- Fresh NRL was dialyzed, without dilution step, against Tris-HCl buffer.

- Volume fraction was adjusted using the Tris-HCl buffer.

- Coagulation takes place *in situ* in the rheometer due to the addition of the GDL

Results of the limit of linearity and at the fracture of strain and stress are illustrated in the Figure AIII-1.

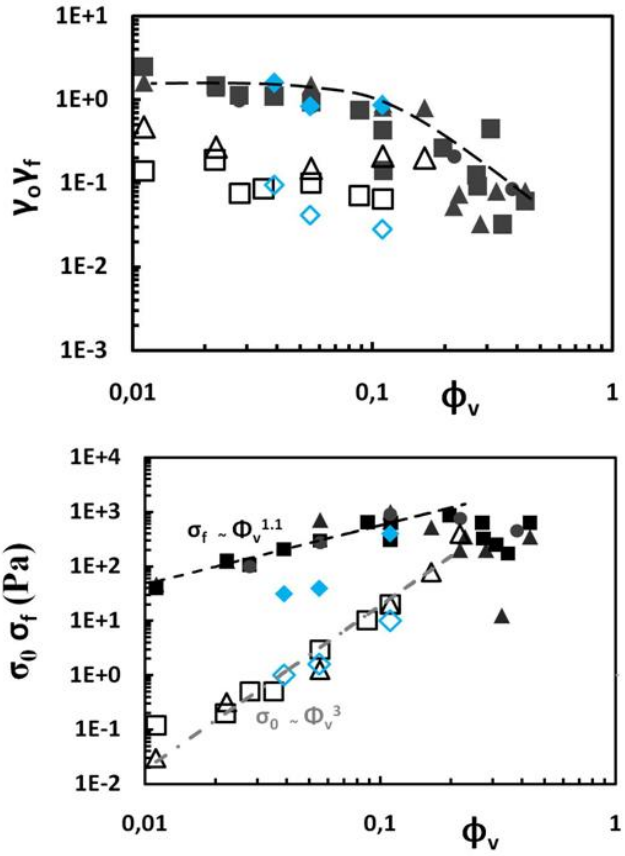

Figure AII.1: In (a) γ_f (filled); γ_0 (empty) and in (b) σ_f (filled); σ_0 (empty) as function of volume fraction. Comparison of parameters obtained for the fresh NRL gels (blues diamonds) and for the commercial NRL gels (represented in dark).

Annex III

Confocal microscopy images

Natural rubber latex gels: observation of aggregates of rubber particles

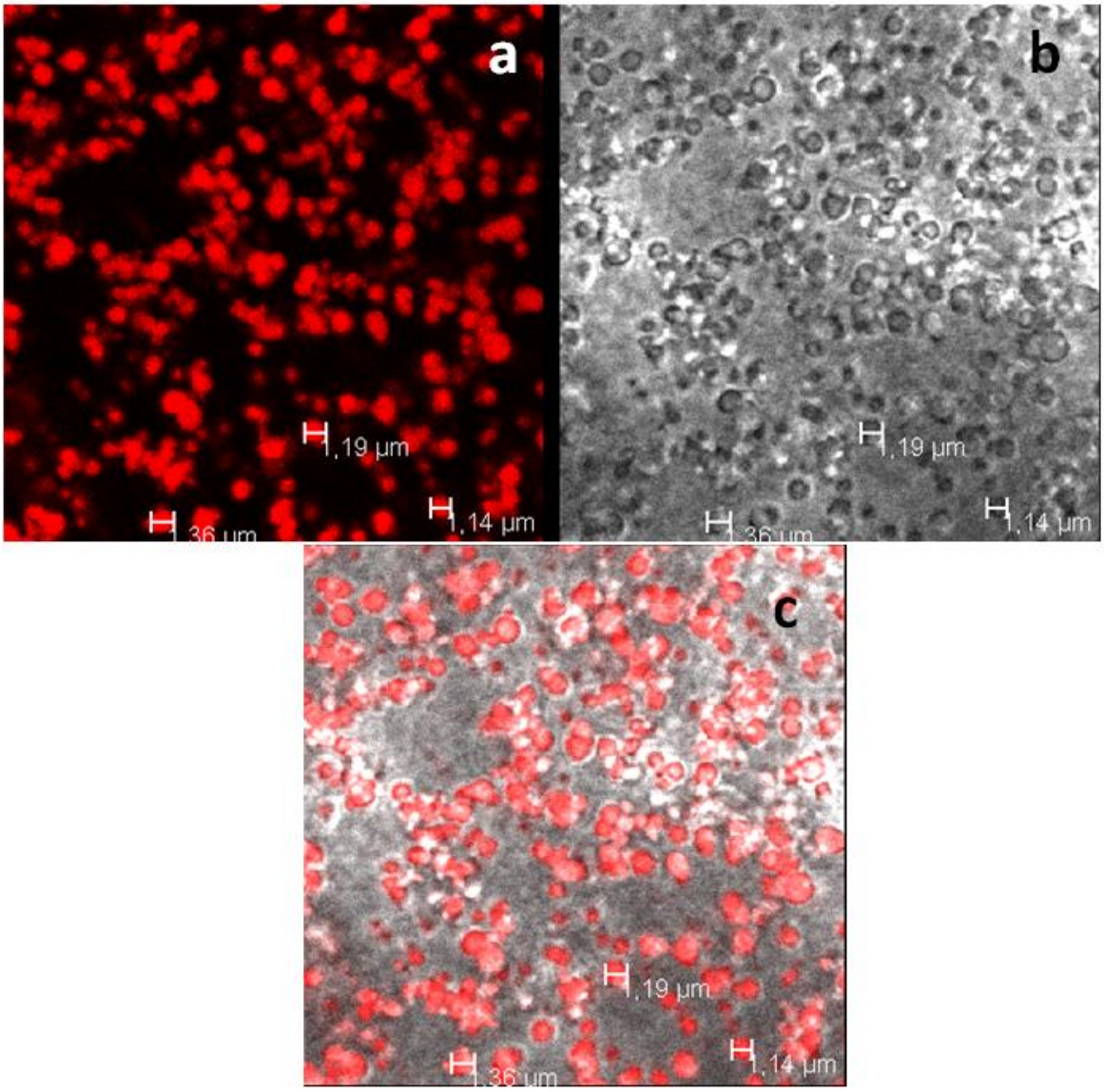

Figure AIII.1: Confocal microscopy images, Φ_v =0.025 with 1 % of GDL.. (a) Fluorescent images, (b) bright light image and (c) superposition (a) in (b). Size: 31.44x31,44 µm.

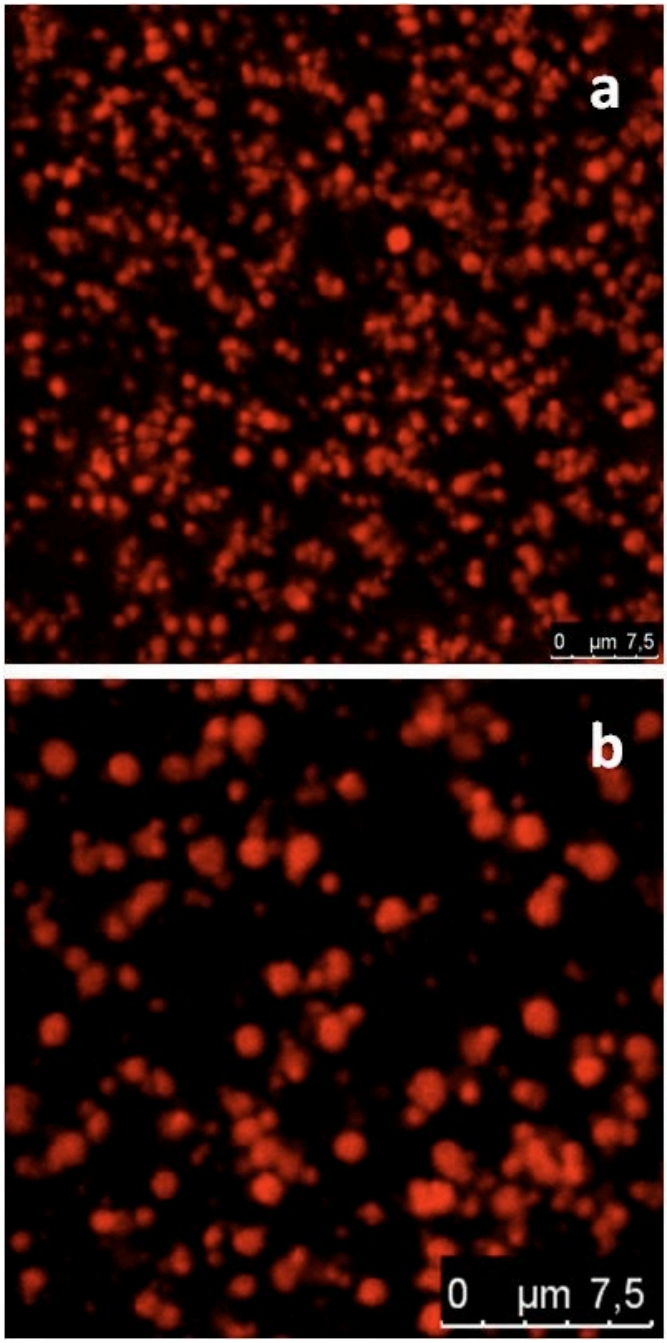

Figure AIII.2: Confocal microscopy images of a NRL gel Φ_v =0.05 with 1 % of GDL. Physical size is (a) 45.61x45.61 µm and (b) 23.07x23.07 µm.

PAS TENIR COMPTER

References

Allain, C., *et al.* (1995). "Aggregation and Sedimentation in Colloidal Suspension." Physical Review Letters **74**(8): 1478-1481.

Allain, C., *et al.* (1995). "Aggregation and Sedimentation in Colloidal Suspensions." Physical Review Letters **74**(8): 1478-1481.

Benítez, E. I., *et al.* (2010). "Fractal Dimension and Mechanism of Aggregation of Apple Juice Particles." Food Science and Technology International **16**(2): 179-186.

Berthelot, K., *et al.* (2014). "Hevea brasiliensis REF (Hev b 1) and SRPP (Hev b 3): An overview on rubber particle proteins." Biochimie **106**(0): 1-9.

Berthelot, K., *et al.* (2014). "Rubber particle proteins, HbREF and HbSRPP, show different interactions with model membranes." Biochimica et Biophysica Acta (BBA) - Biomembranes **1838**(1, Part B): 287-299.

Blackley, D. C. (1996). Polymer Latices: Science and Technology. London, Chapman & Hall.

Boitte, J.-B., *et al.* (2013). "A novel rheo-optical device for studying complex fluids in a double shear plate geometry." Review of Scientific Instruments **84**(1): 013709.

Bonfils, F., *et al.* (2005). "Evolution in the natural rubber native structure and plasticity retention index from the first tapping of clonal trees." Journal of Applied Polymer Science **97**(3): 903-909.

Bowler, W. W. (1953). "Electrophoretic Mobility Study of Fresh Hevea Latex." Industrial and Engineering Chemistry **45**(8): 1790.

Bremer, L. G. B., *et al.* (1993). "Formation, properties and fractal structure of particle gels." Advances in Colloid and Interface Science **46**(0): 117-128.

Bremer, L. G. B., *et al.* (1989). "Theoretical and experimental study of the fractal nature of the structure of casein gels." Journal of the Chemical Society, Faraday Transactions 1: Physical Chemistry in Condensed Phases **85**(10): 3359-3372.

Brenner, T., *et al.* (2009). "Rheology of thermo-reversible fish protein isolate gels." Food Research International **42**(8): 915-924.

Brzozowska-Hanower, J., *et al.* (1978). "Étude du mécanisme de la coagulation du latex d'Heves brasiliensis (Ihnth) Müll. Arg. II. Systèmes enzymatiques impliqués dans le Processus

I . Phénol oxydases." Physiologie Végétale **13**(2).

Buscall, R., *et al.* (1988). "Scaling behavior of the rheology of aggregate networks formed from colloidal particles." Journal of the Chemical Society-Faraday Transactions I **84**: 4249-4260.

Buscall, R., *et al.* (1988). "Scaling behaviour of the rheology of aggregate networks formed from colloidal particles." Journal of the Chemical Society, Faraday Transactions 1: Physical Chemistry in Condensed Phases **84**(12): 4249-4260.

Cao, X. J., *et al.* (2012). "Hydrodynamic and interparticle potential effects on aggregation of colloidal particles." Journal of Colloid and Interface Science **368**(1): 86-96.

Carretero-Gonzalez, J., *et al.* (2010). "Molecular dynamics of natural rubber as revealed by dielectric spectroscopy: The role of natural cross-linking." Soft Matter **6**(15): 3636-3642.

Colombo, J. and E. Del Gado (2014). "Stress localization, stiffening, and yielding in a model colloidal gel." Journal of Rheology **58**(5): 1089-1116.

Cornish, K., *et al.* (1999). "Rubber particles from four different species, examined by transmission electron microscopy and electron-paramagnetic-resonance spin labeling,

are found to consist of a homogeneous rubber core enclosed by a contiguous, monolayer biomembrane." Planta **210**(1): 85-96.
Dai, L. J., *et al.* (2013). "In-depth proteome analysis of the rubber particle of Hevea brasiliensis (para rubber tree)." Plant Molecular Biology **82**(1-2): 155-168.
Dauzac, J., *et al.* (1982). "A plant vacuolar system - the lutoids from Hevea brasiliensis latex." Physiologie Végétale **20**(2): 311-331.
Dawson, H. G. (1949). "Mechanical Stability Test for Hevea Latex." Analytical Chemistry **21**(9): 1066-1071.
de Rooij, R., *et al.* (1994). "Elasticity of weakly aggregating polystyrene latex dispersions." Physical Review E **49**(4): 3038-3049.
Dennis, M. S. and D. R. Light (1989). "Rubber elongation-factor from Hevea brasiliensis - identification, characterization, and role in rubber biosynthesis." Journal of Biological Chemistry **264**(31): 18608-18617.
Dickinson, E. (2013). "Structure and rheology of colloidal particle gels: Insight from computer simulation." Advances in Colloid and Interface Science **199–200**(0): 114-127.
Dinsmore, A. D., *et al.* (2001). "Three-dimensional confocal microscopy of colloids." Applied Optics **40**(24): 4152-4159.
Dukhin, A. S., *et al.* (2007). "Gravity as a factor of aggregative stability and coagulation." Advances in Colloid and Interface Science **134-35**: 35-71.
Dutta, S. K., *et al.* (2013). "Development of a confocal rheometer for soft and biological materials." Review of Scientific Instruments **84**(6): 063702.
Duval, J. F. L. and F. Gaboriaud (2010). "Progress in electrohydrodynamics of soft microbial particle interphases." Current Opinion in Colloid & Interface Science **15**(3): 184-195.
Duval, J. F. L. and H. Ohshima (2006). "Electrophoresis of diffuse soft particles." Langmuir **22**(8): 3533-3546.
Ehabé, E., *et al.* (2005). "Modelling of Mooney viscosity relaxation in natural rubber." Polymer Testing **24**(5): 620-627.
Eric, R. W. and S. Denis (2014). Confocal Microscopy. Encyclopedia of Biomaterials and Biomedical Engineering, Second Edition, Taylor & Francis. **null:** 705-714.
Ewoldt, R. H., *et al.* (2008). "New measures for characterizing nonlinear viscoelasticity in large amplitude oscillatory shear." Journal of Rheology **52**(6): 1427-1458.
Farr, R. S. and R. D. Groot (2009). "Close packing density of polydisperse hard spheres." The Journal of Chemical Physics **131**(24): 244104.
Furukawa, A. and H. Tanaka (2010). "Key Role of Hydrodynamic Interactions in Colloidal Gelation." Physical Review Letters **104**(24): 245702.
Gaboriaud, F., *et al.* (2012). "Unravelling the nanometre-scale stimuli-responsive properties of natural rubber latex particles using atomic force microscopy." Soft Matter **8**(9): 2724-2729.
García, C. P., *et al.* (2013). "Microscopic Analysis of the Interaction of Gold Nanoparticles with Cells of the Innate Immune System." Sci. Rep.
Gibaud, T., *et al.* (2012). "New routes to food gels and glasses." Faraday Discussions **158**(0): 267-284.
Gidrol, X., *et al.* (1994). "Hevein, a lectin-like protein from Hevea brasiliensis (rubber tree) is involved in the coagulation of latex." Journal of Biological Chemistry **269**(12): 9278-9283.
Gidrol, X., *et al.* (1994). "Hevein, a lectin-like protein from Hevea brasiliensis (rubber tree) is involved in the coagulation of latex
" Journal of Biological Chemistry **269**(12): 9278-9283.

Gisler, T., *et al.* (1999). "Strain Hardening of Fractal Colloidal Gels." Physical Review Letters **82**(5): 1064-1067.
Gregory, J. (2009). "Monitoring particle aggregation processes." Advances in Colloid and Interface Science **147–148**(0): 109-123.
Hagiwara, T., *et al.* (1997). "Fractal Analysis of the Elasticity of BSA and β-Lactoglobulin Gels." Journal of Agricultural and Food Chemistry **45**(10): 3807-3812.
Hagiwara, T., *et al.* (1998). "Fractal analysis of aggregates in heat-induced BSA gels." Food Hydrocolloids **12**(1): 29-36.
Hamley, I. W. (2013). Introduction to soft matter: synthetic and biological self-assembling materials, John Wiley & Sons.
Hanower, P., *et al.* (1976). "Étude du mécanisme de la coagulation du latex d'Hevea brasiliensis (Ihnth) Müll. Arg. 1. Facteurs agissant sur la coagulation." Physiologie Végétale **14**(4).
Hasma, H. and A. Subramaniam (1986). "Composition of lipids in latex of Hevea brasiliensis clone RRIM 501 [Malaysia]." Journal of Natural Rubber Research (Malaysia).
Hemar, Y. and D. N. Pinder (2006). "DWS Microrheology of a Linear Polysaccharide." Biomacromolecules **7**(3): 674-676.
Herrmann, H. J., *et al.* (1984). "Backbone and elastic backbone of percolation clusters obtained by the new method of 'burning'." Journal of Physics A: Mathematical and General **17**(5): L261.
Hillebrand, A., *et al.* (2012). "Down-Regulation of Small Rubber Particle Protein Expression Affects Integrity of Rubber Particles and Rubber Content in Taraxacum brevicorniculatum." Plos One **7**(7).
Hilliou, L., *et al.* (2009). "Structural and mechanical characterization of kappa/iota-hybrid carrageenan gels in potassium salt using Fourier Transform rheology." Food Hydrocolloids **23**(8): 2322-2330.
Ho, C. C. (1989). "Changes in electrokinetic properties of natural rubber latex after surface chemical modifications." Colloid and Polymer Science **267**(7): 643-647.
Ho, C. C. (1989). "Changes in eletrokinetic properties of natural-rubber latex after surface chemical modifications." Colloid and Polymer Science **267**(7): 643-647.
Ho, C. C. and M. C. Khew (1999). "Surface Morphology of Prevulcanized Natural Rubber Latex Films by Atomic Force Microscopy: New Insight into the Prevulcanization Mechanism." Langmuir **15**(19): 6208-6219.
Ho, C. C., *et al.* (1996). "Surface Structure of Natural Rubber Latex Particles from Electrophoretic Mobility Data." Journal of Colloid and Interface Science **178**(2): 442-445.
Ho, C. C. and W. L. Ng (1979). "Surface study on the rubber particles in pretreated Hevea latex system." Colloid and Polymer Science **257**(4): 406-412.
Holthoff, H., *et al.* (1996). "Coagulation rate measurements of colloidal particles by simultaneous static and dynamic light scattering." Langmuir **12**(23): 5541-5549.
Honig, E. P., *et al.* (1971). "Effect of hydrodynamic interaction on the coagulation rate of hydrophobic colloids." Journal of Colloid and Interface Science **36**(1): 97-109.
Hsiao, L. C., *et al.* (2014). "Role of shear-induced dynamical heterogeneity in the nonlinear rheology of colloidal gels." Soft Matter **10**(46): 9254-9259.
Hyun, K., *et al.* (2011). "A review of nonlinear oscillatory shear tests: Analysis and application of large amplitude oscillatory shear (LAOS)." Progress in Polymer Science **36**(12): 1697-1753.
Ikeda, S., *et al.* (1999). "Rheological Study on the Fractal Nature of the Protein Gel Structure." Langmuir **15**(25): 8584-8589.

Intapun, J., *et al.* (2010). "Effect of microorganisms during the initial coagulum maturation of Hevea natural rubber." Journal of Applied Polymer Science **118**(3): 1341-1348.
IRSGReport (2015). IRSG Rubber Industry Report.
Jacob, J.-L., *et al.* (1993). "The composition of natural latex fromHevea brasiliensis." Clinical Reviews in Allergy **11**(3): 325-337.
Jacob, J. L., *et al.* (1993). "The composition of natutal latex from Hevea-brasiliensis." Clinical Reviews in Allergy **11**(3): 325-337.
Kim, C., *et al.* (2008). "Characterization of natural rubber using size-exclusion chromatography with online multi-angle light scattering: Study of the phenomenon behind the abnormal elution profile." Journal of Chromatography A **1213**(2): 181-188.
Kim, J. M., *et al.* (2013). "Gel Transition in Adhesive Hard-Sphere Colloidal Dispersions: the Role of Fravitational Effects." Physical Review Letters **110**: 208302(208305).
Klein, C. O., *et al.* (2007). "Separation of the Nonlinear Oscillatory Response into a Superposition of Linear, Strain Hardening, Strain Softening, and Wall Slip Response." Macromolecules **40**(12): 4250-4259.
Kolb, M., *et al.* (1983). "Scaling of Kinetically Growing Clusters." Physical Review Letters **51**(13): 1123-1126.
Koumakis, N., *et al.* (2015). "Tuning colloidal gels by shear." Soft Matter **11**(23): 4640-4648.
Kovalchuk, N. M. and V. M. Starov (2012). "Aggregation in colloidal suspensions: Effect of colloidal forces and hydrodynamic interactions." Advances in Colloid and Interface Science **179**: 99-106.
Krieger, I. M. and T. J. Dougherty (1959). "A Mechanism for Non‐Newtonian Flow in Suspensions of Rigid Spheres." Transactions of The Society of Rheology (1957-1977) **3**(1): 137-152.
Larsen, T. H. and E. M. Furst (2008). "Microrheology of the liquid-solid transition during gelation." Physical Review Letters **100**(14).
Lattuada, M., *et al.* (2003). "Aggregation kinetics of polymer colloids in reaction limited regime: experiments and simulations." Advances in Colloid and Interface Science **103**(1): 33-56.
Lattuada, M., *et al.* (2003). "Estimation of Fractal Dimension in Colloidal Gels." Langmuir **19**(15): 6312-6316.
Laurati, M., *et al.* (2014). "Plastic rearrangements in colloidal gels investigated by LAOS and LS-Echo." Journal of Rheology **58**(5): 1395-1417.
Liao, J., *et al.* (2003). "Linear aggregation of gold nanoparticles in ethanol." Colloids and Surfaces A: Physicochemical and Engineering Aspects **223**(1–3): 177-183.
Licup, A. J., *et al.* (2015). "Stress controls the mechanics of collagen networks." Proceedings of the National Academy of Sciences of the United States of America **112**(31): 9573-9578.
Liengprayoon, S., *et al.* (2011). "Glycolipid composition of Hevea brasiliensis latex." Phytochemistry **72**(14-15): 1902-1913.
Lin, M. Y., *et al.* (1989). "Universality in colloid aggregation." Nature **339**(6223): 360-362.
Lin, M. Y., *et al.* (1990). "Universal reaction-limited colloid aggregation." Physical Review A **41**(4): 2005-2020.
Lin, M. Y., *et al.* (1990). "Universal diffusion-limited colloid aggregation." Journal of Physics: Condensed Matter **2**(13): 3093.
Louie, S. M., *et al.* (2012). "Parameter Identifiability in Application of Soft Particle Electrokinetic Theory To Determine Polymer and Polyelectrolyte Coating Thicknesses on Colloids." Langmuir **28**(28): 10334-10347.
Lu, P. J., *et al.* (2006). "Fluids of clusters in attractive colloids." Physical Review Letters **96**(2): 028306(028304).

Manneville, S., *et al.* (2004). "High-frequency ultrasonic speckle velocimetry in sheared complex fluids." European Physical Journal-Applied Physics **28**(3): 361-373.
Maron, S. H. and P. E. Pierce (1956). "Application of ree-eyring generalized flow theory to suspensions of spherical particles." Journal of Colloid Science **11**(1): 80-95.
Meakin, P. (1983). "Diffusion-controlled cluster formation in 2-6-dimensional space." Physical Review A **27**(3): 1495-1507.
Meakin, P. (1999). "A Historical Introduction to Computer Models for Fractal Aggregates." Journal of Sol-Gel Science and Technology **15**(2): 97-117.
Melito, H. S., *et al.* (2012). "Validation of a large amplitude oscillatory shear protocol." Journal of Food Engineering **113**(1): 124-135.
Mellema, M., *et al.* (2002). "Effects of structural rearrangements on the rheology of rennet-induced casein particle gels." Advances in Colloid and Interface Science **98**(1): 25-50.
Mendoza, C. I. (2011). "Effective static and high-frequency viscosities of concentrated suspensions of soft particles." The Journal of Chemical Physics **135**(5): 054904.
Mendoza, C. I. and I. Santamaría-Holek (2009). "The rheology of hard sphere suspensions at arbitrary volume fractions: An improved differential viscosity model." The Journal of Chemical Physics **130**(4): 044904.
Mezger, T. G. (2006). The rheology handbook : for users of rotational and oscillatory rheometers. Hannover, Vincentz Network.
Mokhtari, T., *et al.* (2008). "The effect of shear on colloidal aggregation and gelation studied using small-angle light scattering." Journal of Colloid and Interface Science **327**(1): 216-223.
Moncho-Jordá, A., *et al.* (2001). "The DLCA-RLCA transition arising in 2D-aggregation: simulations and mean field theory." The European Physical Journal E **5**(4): 471-480.
Montes Ruiz-Cabello, F. J., *et al.* (2015). "Interaction Forces and Aggregation Rates of Colloidal Latex Particles in the Presence of Monovalent Counterions." The Journal of Physical Chemistry B.
Mooibroek, H. and K. Cornish (2000). "Alternative sources of natural rubber." Applied Microbiology and Biotechnology **53**(4): 355-365.
Nawamawat, K., *et al.* (2011). "Surface nanostructure of Hevea brasiliensis natural rubber latex particles." Colloids and Surfaces A: Physicochemical and Engineering Aspects **390**(1–3): 157-166.
Nawamawat, K., *et al.* (2011). "Surface nanostructure of Hevea brasiliensis natural rubber latex particles." Colloids and Surfaces A-Physicochemical and Engineering Aspects **390**(1-3): 157-166.
Ngo Kinh, L. (2013). Natural rubber industry report 2013, Fpt Securities: Vietnam.
Nwadinigwe, C. A. (1988). "Some hitherto uncharacterized latex polyisoprenes." Phytochemistry **27**(7): 2135-2136.
Ohshima, H. (1995). "Electrophoresis of soft particles." Advances in Colloid and Interface Science **62**(2-3): 189-235.
Ohshima, H. (2009). "Theory of electrostatics and electrokinetics of soft particles." Science and Technology of Advanced Materials **10**(6): 063001(063013).
Ohshima, H. (2010). "Effective Viscosity of a Concentrated Suspension of Uncharged Spherical Soft Particles." Langmuir **26**(9): 6287-6294.
Orakdogen, N., *et al.* (2010). "Evidence of Strain Hardening in DNA Gels." Macromolecules **43**(3): 1530-1538.
Ould Eleya, M. M., *et al.* (2004). "Scaling and fractal analysis of viscoelastic properties of heat-induced protein gels." Food Hydrocolloids **18**(2): 315-323.
Pantina, J. P. and E. M. Furst (2005). "Elasticity and critical bending moment of model colloidal aggregates." Physical Review Letters **94**(13).

Pocker, Y. and E. Green (1973). "Hydrolysis of D-glucono-.delta.-lactone. I. General acid-base catalysis, solvent deuterium isotope effects, and transition state characterization." Journal of the American Chemical Society **95**(1): 113-119.

Poon, W. C. K. and M. D. Haw (1997). "Mesoscopic structure formation in colloidal aggregation and gelation." Advances in Colloid and Interface Science **73**: 71-126.

Pouzot, M., *et al.* (2006). "Strain hardening and fracture of heat-set fractal globular protein gels." Journal of Colloid and Interface Science **293**(2): 376-383.

Prasad, V., *et al.* (2007). "Confocal microscopy of colloids." Journal of Physics: Condensed Matter **19**(11): 113102.

Quemada, D. (1977). "Rheology of concentrated disperse systems and minimum energy dissipation principle." Rheologica Acta **16**(1): 82-94.

R.Jullien (1987). "Aggregation phenomena and fractal aggregates." Contemp Phys **28**: 477–493.

Reis, G. D., *et al.* (2015). "Acid-induced aggregation and gelation of natural rubber latex particles." Colloids and Surfaces a-Physicochemical and Engineering Aspects **482**: 9-17.

Rochette, C. N., *et al.* (2013). "Shell Structure of Natural Rubber Particles: Evidence of Chemical Stratification by Electrokinetics and Cryo-TEM." Langmuir **29**(47): 14655-14665.

Rohm, H., *et al.* (2014). "Gelation of Cross-Linked Casein under Small and Large Shear Strain." Journal of Texture Studies **45**(2): 130-137.

Romer, S., *et al.* (2014). "Rheology and internal dynamics of colloidal gels from the dilute to the concentrated regime." EPL (Europhysics Letters) **108**(4): 48006.

Sagis, L. M. C., *et al.* (2001). "Constitutive equations for an elastic material with anisotropic rigid particles." Physical Review E **63**(5).

Sainte Beuve J., V. L., Bonfils F. (2006). Caoutchouc naturel - Maitrise de la variabilité.

Sakdapipanich, J., *et al.* (2015). "Influence of mixed layer of proteins and phospholipids on the unique film formation behavior of Hevea natural rubber latex." Colloids and Surfaces A: Physicochemical and Engineering Aspects **466**(0): 100-106.

Sandkühler, P., *et al.* (2005). "Further insights into the universality of colloidal aggregation." Advances in Colloid and Interface Science **113**(2–3): 65-83.

Sansatsadeekul, J., *et al.* (2011). "Characterization of associated proteins and phospholipids in natural rubber latex." Journal of Bioscience and Bioengineering **111**(6): 628-634.

Shaw, D. (1992). Colloid & Surface chemistry.

Shewan, H. M. and J. R. Stokes (2015). "Analytically predicting the viscosity of hard sphere suspensions from the particle size distribution." Journal of Non-Newtonian Fluid Mechanics(0).

Shewan, H. M. and J. R. Stokes (2015). "Viscosity of soft spherical micro-hydrogel suspensions - Supplementary Material." Journal of Colloid and Interface Science **442**(0): 75-81.

Shih, W.-H., *et al.* (1990). "Scaling behavior of the elastic properties of colloidal gels." Physical Review A **42**(8): 4772-4779.

Singh, A. P., *et al.* (2003). "Simple and rapid methods for SEM observation and TEM immunolabeling of rubber particles." Journal of Histochemistry & Cytochemistry **51**(8): 1105-1108.

Singh, M., *et al.* (2014). "Influence of hydrophobically modified inulin (INUTEC NRA) on the stability of vulcanized natural rubber latex." Colloids and Surfaces A: Physicochemical and Engineering Aspects **451**(0): 90-100.

Sittikijyothin, W., *et al.* (2007). "Heat-induced gelation of beta-lactoglobulin at varying pH: Effect of tara gum on the rheological and structural properties of the gels." Food Hydrocolloids **21**(7): 1046-1055.
Sittikijyothin, W., *et al.* (2007). "Heat-induced gelation of β-lactoglobulin at varying pH: Effect of tara gum on the rheological and structural properties of the gels." Food Hydrocolloids **21**(7): 1046-1055.
Sorensen, C. M. and A. Chakrabarti (2011). "The sol to gel transition in irreversible particulate systems." Soft Matter **7**(6): 2284-2296.
Southorn, W. A. (1960). "Complex Particles in Hevea Latex." Nature **188**(4745): 165-166.
Sridee, J. (2006). Rheological properties of natural rubber latex
Suranaree University of Technology, Thailand. **Thesis**.
Storm, C., *et al.* (2005). "Nonlinear elasticity in biological gels." Nature **435**(7039): 191-194.
Tanaka, Y. (2001). "Structural characterization of natural polyisoprenes: Solve the mystery of natural rubber based on structural study." Rubber Chemistry and Technology **74**(3): 355-375.
Tanaka, Y. and L. Tarachiwin (2009). "Recent Advances in Structural Characterization of Natural Rubber." Rubber Chemistry and Technology **82**(3): 283-314.
Tang, S., *et al.* (2000). "Fractal Morphology and Breakage of DLCA and RLCA Aggregates." Journal of Colloid and Interface Science **221**(1): 114-123.
Tarachiwin, L., *et al.* (2005). "Structural Characterization of α-Terminal Group of Natural Rubber. 1. Decomposition of Branch-Points by Lipase and Phosphatase Treatments." Biomacromolecules **6**(4): 1851-1857.
Thill, A., *et al.* (1998). "Determination of Structure of Aggregates by Confocal Scanning Laser Microscopy." Journal of Colloid and Interface Science **204**(2): 357-362.
Toki, S., *et al.* (2008). "Multi-Scaled Microstructures in Natural Rubber Characterized by Synchrotron X-Ray Scattering and Optical Microscopy." Journal of Polymer Science Part B-Polymer Physics **46**(22): 2456-2464.
Toki, S., *et al.* (2000). "Strain-induced crystallization of natural rubber as detected real-time by wide-angle X-ray diffraction technique." Polymer **41**(14): 5423-5429.
Tokita, M. (1989). "Gelation mechanism and percolation." Food Hydrocolloids **3**(4): 263-274.
Tomilov, A., *et al.* (2013). "Aggregation in Colloidal Suspensions: Evaluation of the Role of Hydrodynamic Interactions by Means of Numerical Simulations." The Journal of Physical Chemistry B **117**(46): 14509-14517.
Tosaka, M., *et al.* (2004). "Orientation and crystallization of natural rubber network as revealed by WAXD using synchrotron radiation." Macromolecules **37**(9): 3299-3309.
Trappe, V. and P. Sandkühler (2004). "Colloidal gels—low-density disordered solid-like states." Current Opinion in Colloid & Interface Science **8**(6): 494-500.
Trappe, V. and D. A. Weitz (2000). "Scaling of the viscoelasticity of weakly attractive particles." Physical Review Letters **85**(2): 449-452.
Vader, D., *et al.* (2009). "Strain-Induced Alignment in Collagen Gels." Plos One **4**(6).
van der Vaart, K., *et al.* (2013). "Rheology of concentrated soft and hard-sphere suspensions." Journal of Rheology **57**(4): 1195-1209.
Vaysse, L., *et al.* (2012). Natural rubber in Polymer Science: A Comprehensive Reference. Amsterdam, Elsevier BV.
Vaysse, L., *et al.* (2009). Natural Rubber in Sustainable Solutions for Modern Economies,Coord. Dr Rainer Höfer, The Royal Society of Chemistry. Cambridge, UK**:** 339-367.
Verheul, M., *et al.* (1998). "Power law behavior of structural properties of protein gels." Langmuir **14**(9): 2263-2268.

Vermant, J. and M. J. Solomon (2005). "Flow-induced structure in colloidal suspensions." Journal of Physics-Condensed Matter **17**(4): R187-R216.
Wales, M. (1962). "Particle size distribution in rubber latex." Journal Phys. Chem **66**(10): 1768–1772.
Weitz, D. A., *et al.* (1985). "Limits of the Fractal Dimension for Irreversible Kinetic Aggregation of Gold Colloids." Physical Review Letters **54**(13): 1416-1419.
Weitz, D. A. and M. Oliveria (1984). "Fractal Structures Formed by Kinetic Aggregation of Aqueous Gold Colloids." Physical Review Letters **52**(16): 1433-1436.
Weitz, D. A., *et al.* (1993). " Diffusing-wave spectroscopy - The technique and some applications ." Physica Scripta **T49B**: 610-621.
Wessel, R. and R. C. Ball (1992). "Fractal aggregates abd gels in shear-flow." Physical Review A **46**(6): R3008-R3011.
Whitmer, J. K. and E. Luijten (2011). "Influence of Hydrodynamics on Cluster Formation in Colloid−Polymer Mixtures." The Journal of Physical Chemistry B **115**(22): 7294-7300.
Wilhelm, M. (2002). "Fourier-Transform Rheology." Macromolecular Materials and Engineering **287**(2): 83-105.
Winter, H. H. a. F. C. (1986). "Analysis of Linear Viscoelasticity of a Crosslinking Polymer at the Gel Point." J Rheology **30**: 367.
Wisunthorn, S., *et al.* (2012). "SEC-MALS study of dynamic structuring of natural rubber: Comparative study of two Hevea brasiliensis genotypes." Journal of Applied Polymer Science **124**(2): 1570-1577.
Wisunthorn, S., *et al.* (2012). "SEC-MALS study of dynamic structuring of natural rubber: Comparative study of two Hevea brasiliensis genotypes." Journal of Applied Polymer Science **124**(2): 1570-1577.
Wititsuwannakul, D. a. W., R. (2001). Biochemistry of Natural Rubber and Structure of Latex. Weiheim, Germany.
Wititsuwannakul, R., *et al.* (2008). "Hevea latex lectin binding protein in C-serum as an anti-latex coagulating factor and its role in a proposed new model for latex coagulation." Phytochemistry **69**(3): 656-662.
Wood, D. F. and K. Cornish (2000). "Microstructure of purified rubber particles." International Journal of Plant Sciences **161**(3): 435-445.
Wu, H. and M. Morbidelli (2001). "A Model Relating Structure of Colloidal Gels to Their Elastic Properties." Langmuir **17**(4): 1030-1036.
Wu, H., *et al.* (2013). "Kinetics of colloidal gelation and scaling of the gelation point." Soft Matter **9**(17): 4437-4443.
Yanez, J. A., *et al.* (1999). "Viscoelastic Properties of Particle Gels." Journal of Colloid and Interface Science **209**(1): 162-172.
Yanez, J. A., *et al.* (1996). "Shear Modulus and Yield Stress Measurements of Attractive Alumina Particle Networks in Aqueous Slurries." Journal of the American Ceramic Society **79**(11): 2917-2917.
Zhong, Q. X., *et al.* (2004). "Cooling effects on a model rennet casein gel system: part I. Rheological characterization." Langmuir **20**(18): 7399-7405.